AWARD NUMBER: W81XWH-13-2-0037

TITLE: Nanoparticle Delivery Of RNAi Therapeutics For Ocular Vesicant Injury

PRINCIPAL INVESTIGATOR: Hai-Quan Mao

CONTRACTING ORGANIZATION: Johns Hopkins University
Baltimore, MD 21218

REPORT DATE: December 2014

TYPE OF REPORT: Final

PREPARED FOR: U.S. Army Medical Research and Materiel Command
Fort Detrick, Maryland 21702-5012

REPORT DOCUMENTATION PAGE

Form Approved
OMB No. 0704-0188

1. REPORT DATE	2. REPORT TYPE	3. DATES COVERED
December 2014	Final Report	04/01/2013—09/30/2014

4. TITLE AND SUBTITLE
Nanoparticle Delivery Of RNAi Therapeutics For Ocular Vesicant Injury

5a. CONTRACT NUMBER

5b. GRANT NUMBER W81XWH-13-2-0037

5c. PROGRAM ELEMENT NUMBER

6. AUTHOR(S)
Hai-Quan Mao

E-Mail: hmao@jhu.edu

5d. PROJECT NUMBER

5e. TASK NUMBER

5f. WORK UNIT NUMBER

7. PERFORMING ORGANIZATION NAME(S) AND ADDRESS(ES)
Johns Hopkins University
3400 N. Charles St.,
W400 Wyman Park Bldg.
Baltimore, MD 21218

8. PERFORMING ORGANIZATION REPORT NUMBER

9. SPONSORING / MONITORING AGENCY NAME(S) AND ADDRESS(ES)
U.S. Army Medical Research and Materiel Command
Fort Detrick, Maryland 21702-5012

10. SPONSOR/MONITOR'S ACRONYM(S)

11. SPONSOR/MONITOR'S REPORT NUMBER(S)

12. DISTRIBUTION / AVAILABILITY STATEMENT
Approved for Public Release; Distribution Unlimited

13. SUPPLEMENTARY NOTES

14. ABSTRACT
This objective of this project is to optimize the nanoparticle delivery system for effective ocular delivery of siRNA in animal models in order to validate the therapeutic targets developed at_USAMRICD. In collaboration with the Target Discovery Core and the *In Vivo* Target Validation Core led by Dr. Albert Ruff at USAMRICD, we have developed new method to control the size and shape of siRNA nanoparticles. More importantly, this method can compact nanoparticles to smaller size with higher stability in physiological media, optimized a protocol to surface-coat nucleic acid nanoparticles with hyaluronic acid and retained the stability of the nanoparticles, and identified the conditions using reversible crosslinking density to stabilize siRNA nanoparticles. In addition, we have demonstrated gene knockdown in several cell lines, and confirmed that disulfide reversible crosslinks are essential to successful transfection and gene knockdown. In a pilot study with Dr. Ruff, we have identified feasible injection parameters and analysis protocols, although initial testing did not show positive gene knockdown with PEGylated spherical nanoparticles following sub-conjunctival injection, we plan to continue test the newer generation of rod and worm-like nanoparticles, which have shown promising results in other animal models.

15. SUBJECT TERMS
None Listed

16. SECURITY CLASSIFICATION OF:			17. LIMITATION OF ABSTRACT	18. NUMBER OF PAGES	19a. NAME OF RESPONSIBLE PERSON
a. REPORT	b. ABSTRACT	c. THIS PAGE			USAMRMC
Unclassified	Unclassified	Unclassified	Unclassified	100	19b. TELEPHONE NUMBER *(include area code)*

Table of Contents

1. Introduction:

This study aimed to optimize the nanoparticle delivery system for effective ocular delivery of siRNA in animal models in order to validate the therapeutic targets developed at USAMRICD. In collaboration with the Target Discovery Core and the *In Vivo* Target Validation Core led by Dr. Albert Ruff at USAMRICD, the team plans to develop potential therapeutic targets for the development of treatments to alleviate the effects of vesicant exposure for the warfighter. The specific tasks include: (1) To optimize nanoparticle tissue retention and cell uptake by conjugating cell adhesion ligand to nanoparticles and by surface coating of hyaluronic acid to improve the muco-adhesive property of the nanoparticles; extend siRNA knockdown duration by tuning the density of reversible crosslinks in nanoparticle core; and confirm that these modifications will not affect the nanoparticle properties; (2) To correlate optimization parameters of the nanoparticles (prepared in Task 1) with the gene knockdown efficiency following ocular delivery; and compare the efficiencies of topical application and subconjunctival injection of the nanoparticles. We had planned to complete the subconjunctival administration of the nanoparticles in Dr. Ruff's Lab at USAMRICD. (3) To confirm and optimize knockdown of therapeutic targets *in vivo*; characterize the expression kinetics; and identify cell types that are transfected by nanoparticles in collaboration with Dr. Ruff.

2. Keywords:

Nanoparticles, non-viral vector, siRNA, gene knockdown, ocular delivery

3. Overall Project Summary:

We have successfully developed an improved protocol to prepare a condensed siRNA nanoparticles with compact and uniform size using PEGylated cationic carriers. Through optimization of the carrier structure, PEG density, and assembly conditions, we have prepared stable siRNA nanoparticles with discrete and compact size of 40 to 60 nm (number average dynamic light scattering measurement in water). We have tested two different cationic polymers, polyphosphoramidate (PPA) and linear polyethyleneimine (PEI) to confirm the applicability of this method to different carriers. In addition, we have tailored the method to effective condense siRNA into both spherical and rod-like particles. These nanoparticles showed much improved stability in buffer with physiological ionic strength. The smaller nanoparticles elicited much higher gene knockdown efficiency in rodent models following a site-specific injection and systematic delivery, suggesting the improved stability in physiological media *in vivo*. These results highlight the effectiveness of our strategy in condensing and stabilizing nanoparticles in promoting their gene knockdown activity *in vivo*. Using a similar protocol, we have also achieved effective condensation of siRNA/PEI-*g*-PEG nanoparticles to an average of 44 nm (Fig. 1). Through molecular dynamics simulation, we revealed the role of solvent quality and PEI–PEG hydrogen bonding in the assembly of lPEI-*g*-PEG/siRNA micelles. The micelle size was preserved after organic solvent removal by means of reversible disulfide crosslinking; we confirmed that the micelles maintained their size in water and physiological media. We have also confirmed size-dependent *in vivo* transfection

efficiency following intravenous injection of the siRNA micelles in rats (Fig. 2). The gene knockdown efficiency in rat liver achieved by the smaller siRNA micelles was significantly higher than for the larger micelles prepared from the same copolymer carrier. The condensation technique introduced here allows a simple and effective way to reduce siRNA particle size and provides a model platform for further study of the effect of particle size on *in vivo* cellular uptake, knockdown efficiency, biodistribution, and pharmacokinetics.

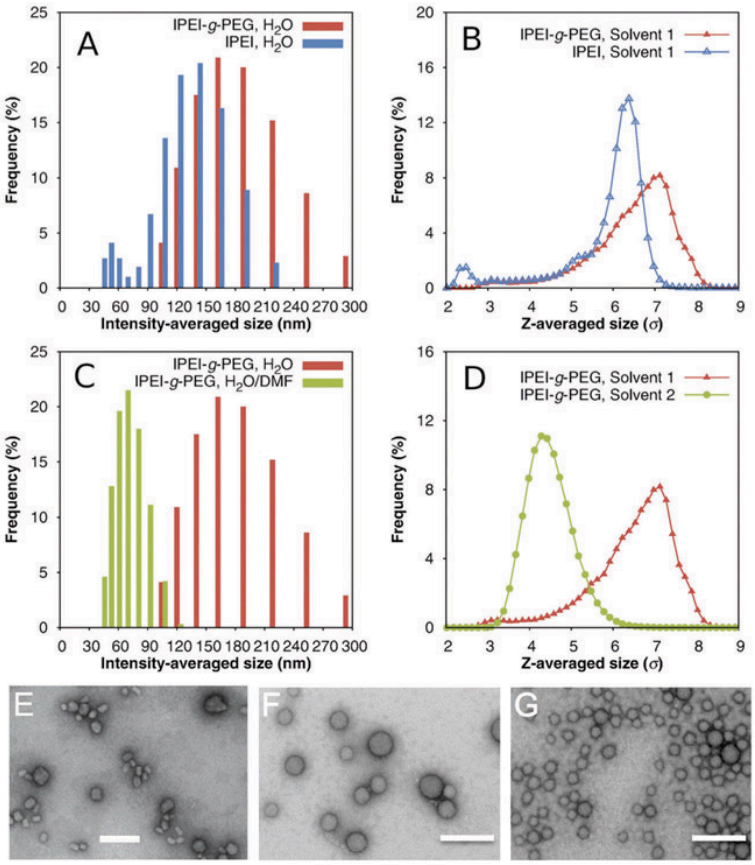

Fig. 1. Size distribution of lPEI-*g*-PEG/siRNA micelles in different solvents. (A) Size distribution of lPEI-*g*-PEG/siRNA micelles and lPEI/siRNA nanoparticles prepared in water, as determined by dynamic light scattering; (B) Simulation results for size distributions of lPEI-*g*-PEG/siRNA micelles and lPEI/siRNA nanoparticles in water; (C) Size distribution of lPEI-*g*-PEG/siRNA micelles prepared in pure water and 7:3 (v/v) DMF–water mixture; (D) Simulation results for size distribution of lPEI-*g*-PEG/siRNA micelles in pure water (labeled "Solvent 1") and 7:3 (v/v) DMF–water mixture (labeled "Solvent 2"); (E–G) TEM images of lPEI/siRNA nanoparticles (E), lPEI-*g*-PEG/siRNA micelles prepared in pure water (F), and lPEI-*g*-PEG/siRNA micelles prepared in DMF–water mixture (G), respectively. All scale bars represent 200 nm.

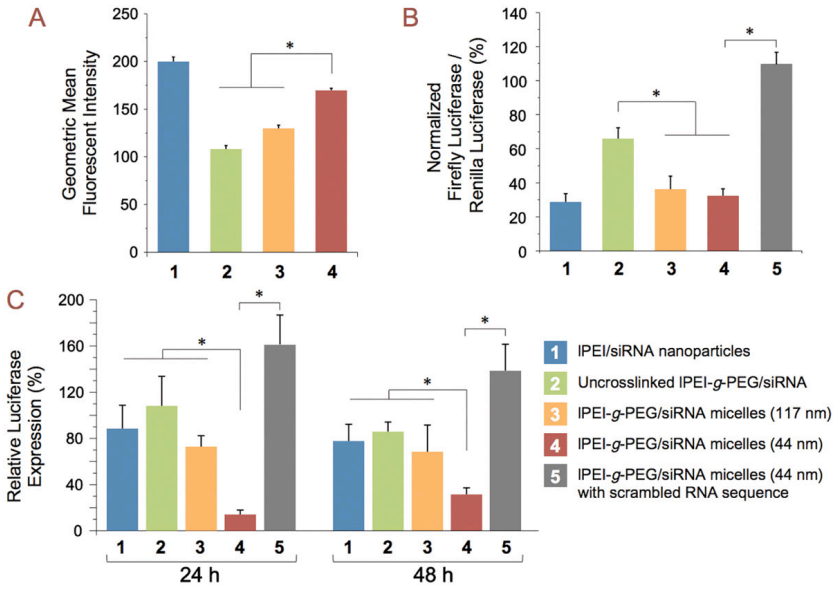

Fig. 2. Size-dependent transfection efficiency of lPEI-*g*-PEG/siRNA micelles. (A) *In vitro* cellular uptake of Alexa Fluor 488-labeled micelles in HepG2 cells. Bars represent mean ± SD (n = 3); (B) *In vitro* gene knockdown efficiency in HepG2 cells following 100 nM equivalent dose of siRNA. Bars represent mean ± SD (n = 3); (C) *In vivo* gene silencing in rat liver at 24 h and 48 h after administration of nanoparticles at a dose equivalent to 80 μg siRNA *via* tail vein injection. Bars indicate mean relative luciferease expression ± SD (n = 4–7). *p <0.05.

In addition, we have recently also developed conditions that allows for shape control over siRNA nanoparticles (Fig. 3). Using a reversible disulfide bond crosslinking method, we have shown these nanoparticles are stable in medium with physiological ionic strength. These nanoparticles also showed significant gene knockdown efficiency *in vitro* and *in vivo* in brain tissue. The results indicate that rod-shaped nanoparticles were most effective for the delivery of siRNAs to the CNS, highlighting the effect of nanoparticle shape on siRNA delivery *in vivo*.

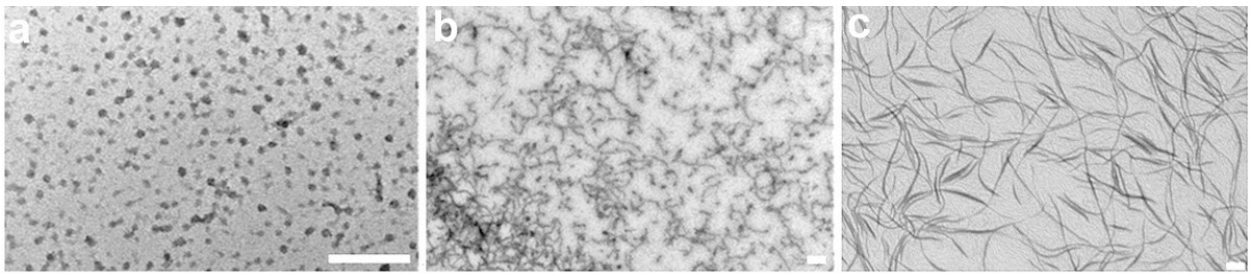

Fig. 3. Tuning the shape of siRNA nanoparticles ranging from spherical $LPEI_{17k}$-8%PEG_{10k}/siRNA nanoparticles (a), rod-like $LPEI_{17k}$-4%PEG_{10k}/siRNA nanoparticles (b), and worm-like $LPEI_{17k}$-2%PEG_{10k}/siRNA nanoparticles (c). Scale bars = 200 nm.

To improve the compatibility of the siRNA nanoparticles with ocular tissue, and improve the retention and uptake of these particles, we adopted a previously developed ionic crosslinking strategy to stabilize the lPEI/siRNA complex prior to HA coating through the incorporation of sodium triphosphate (Fig. 4a). This strategy allows for the formation of stable, discrete spherical particles with average diameters of 100 nm (Fig. 4b). Importantly, HA-coating also significantly improves the knockdown efficiency *in vitro* when tested in two different corneal cell lines, compared to particles without HA coating and without TPP crosslinking (Fig. 4c).

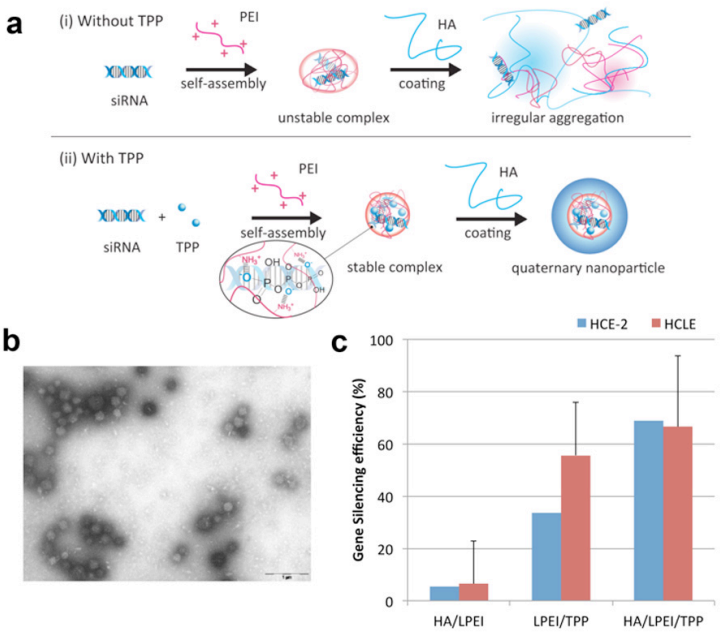

Fig. 4. (a) Preparation of lPEI/siRNA nanoparticles followed by HA-coating leads to irregular aggregation, unless TPP is used to stabilize the complex prior to HA-coating. (b) TEM image of HA-coated lPEI/TPP/siRNA nanoparticles; (c) Luciferase gene silencing efficiency mediated by siRNA nanoparticles in human corneal epithelial (HCE-2) and human corneal limbal epithelial (HCLE) cells with siRNA dose of 100 nM. Values are expressed as mean ± SEM (n=4).

As part of Task 3, we have tested the top three formulations selected based on the above-mentioned experiments, including $lPEI_{22k}$-*g*-PEG_{10k}/siRNA micelles solvent-assembled into 44 nm micelles, $LPEI_{17k}$-8%PEG_{10k}/siRNA spherical nanoparticles, and $LPEI_{17k}$-4%PEG_{10k}/siRNA rod-like nanoparticles. However, all results returned negative failing to show any appreciable gene knockdown effect in the model established in Dr. Ruff's Lab, following subconjuctival injection. For easy deployment of the nanoparticle formulation in the field, we have explored the possibility to deliver nanoparticles through hyaluronic acid (HA) hydrogel, which will significantly extend the duration of nanoparticle delivery in a sustainable manner to the eye.

To assess the delivery via HA hydrogel, crosslinked particles were prepared encompassing fluorescently labeled siRNA (25 bp for enhanced stability- with Alexa 555) and $LPEI_{17k}$-*g*-8%PEG_{10k}. A HA-based hydrogel was made with nanoparticles loaded in it and tuned to have three different stiffness levels (800 Pa, 350 Pa, and 100 Pa). HA solution is currently being used as eye drops to treat dry eyes. It has excellent tissue compatibility. Each formulation was pipetted into a well of 96-well plate. At 30 minutes after the components of the hydrogel and nanoparticles were mixed, we added 50 µl of PBS to each of the wells to test whether the nanoparticles can diffuse out of hydrogel phase. We observed that after 3 h, the hydrogel with the 100-Pa stiffness level gave the highest release of nanoparticles (36.3% as compared to 20.5 % and 18.9% from 350-Pa and 800-Pa stiffness HA hydrogels, respectively (Fig. 5A). However, nanoparticle release after the initial burst (during the next 3 h) were similar for all the hydrogel groups. The PBS samples were run on a gel and free siRNA was not observed, suggesting that siRNA was still encapsulated and the nanoparticles were stable under this condition (data not shown). It is worth noting that the release kinetics following *in vivo* delivery would likely be much faster, due to the clearance of HA hydrogel. The 100-Pa hydrogel lends itself attractively to the concept of building a suitable material that may be applied on the eye with the therapeutic being released over a short time span.

We decided to utilize the hydrogel with a 100-Pa stiffness for an initial *in vivo* evaluation in C57BL/6 mouse. A hydrogel strategy allowed for direct application of our formulation on the surface of the eye so as to be able to mimic a clinically viable delivery strategy. PBS was applied on the left eye (control) and nanoparticles embedded in 100-Pa HA hydrogel were applied to the right eye under anesthesia for a period of 4 h. These nanoparticles contained fluorescently labeled siRNA. As shown in Fig. 5B, the siRNA signal was observable on the epithelial cells. This suggests that the siRNA was able to escape from the hydrogel phase and diffuse onto the surface of the epithelial cell layer. However, too few amount of appreciable siRNA payload co-localized with the cytoplasm of the cells.

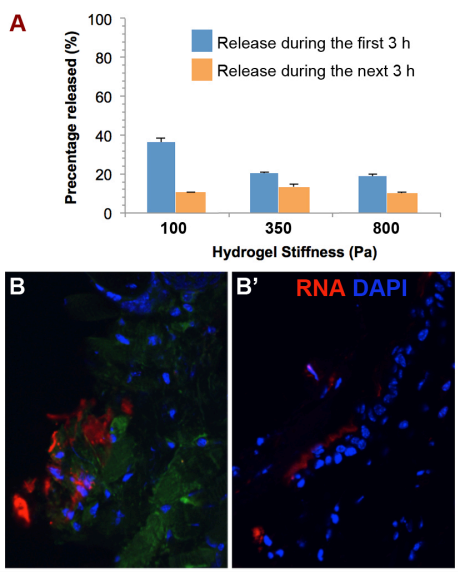

Fig. 5. Nanoparticle release from HA hydrogels. (A). Nanoparticles contained Alexa 555-labeled siRNA were loaded into HA hydrogels with different moduli. Nanoparticle release into the PBS overlying the hydrogel at two different durations were measured by quantifying the amount of fluorescence in supernatant against the total of siRNA encapsulated. (B). Nanoparticles released from 100-Pa HA hydrogel applied on to the surface of the eye in mice. Isoflurane was utilized to anesthetize the mouse for a period of 4 h, following which the eyes were harvested, post-fixed in 4% paraformaldehyde, sectioned, and imaged. The left eye, which is treated with PBS, does not show any background signal.

These results confirm that HA hydrogel delivery is a promising approach for eye surface delivery of siRNA nanoparticles. Cellular entry is a major barrier for effective delivery of siRNA to corneal epithelial cells. Further optimization of nanoparticles to enhance cell uptake, e.g. using targeting ligands tailored for epithelial cells, should be the focus of the next phase study in order to achieve effective delivery of siRNA to the eye.

Although these nanoparticle formulations appeared to be less efficienct in corneal epithelial cells, we had an opportunity to test their potential in treating Alzheimer's Disease (AD) in a mouse model in Dr. Philip Wong's Lab at Johns Hopkins Medicine. AD is a progressive neurodegenerative disease currently lacking effective treatment. Efficient delivery of siRNA *via* nanoparticles may emerge as a viable therapeutic approach. We have used the nanoparticles developed here, particularly linear polyethyleneimine (LPEI)-*g*-polyethylene glycol (PEG) copolymer-based micellar nanoparticles, to deliver siRNA targeting *BACE1* and *APP*, two therapeutic targets of AD. Using LPEI-siRNA nanoparticles against either *BACE1* or *APP* in cultured mouse neuroblastoma (N2a) cells, we observe selective knockdown, respectively, of *BACE1* or *APP*. The encapsulation of siRNA by LPEI-*g*-PEG carriers as those shown in Fig. 3, with different grafting degrees of PEG, leads to the formation of micellar nanoparticles with distinct morphologies, including worm-like, rod-like or spherical nanoparticles. By infusing these shaped nanoparticles into mouse lateral ventricles, we show that rod-shaped nanoparticles achieved the most efficient knockdown of *BACE1* in the brain. Furthermore, such knockdown is evident in spinal cords of these treated mice. Taken together, our findings indicate that the shape of siRNA-encapsulated nanoparticles is an important determinant for their delivery and gene knockdown efficiency in the central nervous system. This proof-of-principle study establishes the potential of

this method for RNAi therapy in CNS. Beyond this model, these nanoparticles may be applicable for targeting other organs or tissues.

4. KEY RESEARCH ACCOMPLISHMENTS:

- We have developed new method to control the size and shape of siRNA nanoparticles. More importantly, this method can compact nanoparticles to smaller size with higher stability in physiological media. Optimized a protocol to surface-coat nucleic acid nanoparticles with hyaluronic acid, and retain the stability of the nanoparticles. Identified the conditions using reversible crosslinking density to stabilize siRNA nanoparticles.

- We have demonstrated gene knockdown in several cell lines, and confirmed that disulfide reversible crosslinks are essential to successful transfection and gene knockdown.

- We have collaborated with Dr. Ruff and tested the first generation of nanoparticles (PEGylated spherical nanoparticles) following sub-conjunctival injection. However, this pilot study did not show positive gene knockdown with the initial nanoparticle formulation and dose. Nonetheless, we have identified the feasible injection parameters and analysis protocols. Part of the challenge is with the small injection volume, which required lyophilization and resuspension of nanoparticles in extremely high concentration (2 – 5 mg/ml). Severe aggregation was observed under this condition.

- We have developed a topical application method based on hyaluronic acid hydrogel delivery, and demonstrated that siRNA-nanoparticles encapsulated in the hydrogel can be successfully release from the hydrogel in vitro and in vivo following application to the surface of the eye. However, we have also concluded that epithelial cell uptake represents a major barrier for nanoparticle-mediated siRNA delivery.

- We have collaborated with Prof. Philip Wong at Johns Hopkins Neuropathology to explore the application of these siRNA nanoparticles for treating Alzheimer's Disease (AD) in a mouse model, and have shown successful gene knockdown of AD-specific target in mouse brain following infusion into mouse lateral ventricles.

5. CONCLUSION:

Vesicant injury has been unaddressed threat for the warfighters for decades. This proposed study is an important component of the VT-CCRP. The long-term goal is this program is to develop therapeutic strategies to effectively minimize injuries to ocular tissue resulting from vesicant exposure. This task of this project is to develop a nanoparticle system for delivery of the identified gene knockdown targets developed at USAMRICD. We have developed tailored siRNA nanoparticles packaging method to yield nanoparticles with controlled shape and size, and showed that surface modification can improve nanoparticle stability.

Subconjunctival injection can be easily achieved in humans; also various types of therapeutics have been effectively delivered via subconjunctival injection. It has also been shown that subconjunctival injection can effectively deliver nanoparticles, drugs or proteins to corneal mucosal cell types with low cytotoxicity. All the top nanoparticle formulations tested at Dr. Ruff's Lab at USAMRICD did not show any appreciable level of gene knockdown following subconjunctival administration.

In addition, we have developed a topical application method based on hyaluronic acid hydrogel delivery and demonstrated that siRNA-nanoparticles encapsulated in the hydrogel can be successfully release from the hydrogel *in vitro* and *in vivo* following application to the surface of the eye. However, we have also concluded that epithelial cell uptake represents a major barrier for nanoparticle-mediated siRNA delivery. We did not observe significant level of nanoparticle transport inside the cytosol of corneal epithelial cells.

Nonetheless, we have collaborated with Prof. Philip Wong at Johns Hopkins Neuropathology to explore the application of these siRNA nanoparticles for treating Alzheimer's Disease (AD) in a mouse model, and have shown successful gene knockdown of AD-specific target in mouse brain following intrathecal delivery.

6. PUBLICATIONS, ABSTRACTS, AND PRESENTATIONS:

Manuscripts published and in review (attached):

- Shyam R, Ren Y, Lee J, Braunstein KE, Mao HQ, Wong PC. (2015). Intraventricular delivery of siRNA nanoparticles to the central nervous system. Mol. Ther. Nucleic Acids. 4: e242.
- Qu W, Wu J, Mao HQ, Luijten E. Solvent induced size reduction of self-assembled siRNA/copolymer nanoparticles. ?bt_lacb Fc_jrfa_pc Materials. (In Review)

Invited reviews (attached):

- Williford JM, Shyam R, Santos JL, Mao HQ. Methods and Applications of Nanoparticle Shape Control in Therapeutic Delivery. Biomaterials Science. (2015).
- Williford JM, Wu J, Ren Y, Archang MM, Leong KW, Mao HQ. Recent Advances in Nanoparticle-Mediated siRNA Delivery. Annual Reviews in Biomedical Engineering. 16 (7): 347-370 (2014). PMID: 24905873.

Conference Presentations:

- Shyam R, Lee J, Ren R, Wong, P, Mao HQ. siRNA delivery mediated by shape-controlled nanoparticles. The 17th Annual Meeting of the American Society of Gene and Cell Therapy, Washington, D.C., May 21-24, 2014. Podium Presentation.
- American Chemical Society National Meeting, Symposium on Biomacromolecules for Therapeutics and Diagnostic Delivery. Indianapolis, IN. September 8–12, 2013. (Invited)

7. INVENTIONS, PATENTS AND LICENSES:

- Shape-Controlled siRNA Nanoparticles for In Vivo Delivery of RNA Therapeutics. US Provisional Patent Application Serial No. 62/000,838 (Filed on 05/20/2014) (Attached).

8. REPORTABLE OUTCOMES:

- A series of nanoparticles for siRNA packaging with small and compact size, and different shapes;
- A method for siRNA packaging and stabilization, and surface modification.
- A hyaluronic acid hydrogel based delivery method for ocular surface delivery of nanoparticles.

9. OTHER ACHIEVEMENTS:

Nothing to report.

10.REFERENCES:

None included.

11.APPENDICES:

- Shyam R, Ren Y, Lee J, Braunstein KE, Mao HQ, Wong PC. (2015). Intraventricular delivery of siRNA nanoparticles to the central nervous system. Mol. Ther. Nucleic Acids. 4: e242.
- Qu W, Wu J, Mao HQ, Luijten E. Solvent induced size reduction of self-assembled siRNA/copolymer nanoparticles.
- Williford JM, Shyam R, Santos JL, Mao HQ. Methods and Applications of Nanoparticle Shape Control in Therapeutic Delivery. Biomaterials Science. (2015).
- Williford JM, Wu J, Ren Y, Archang MM, Leong KW, Mao HQ. Recent Advances in Nanoparticle-Mediated siRNA Delivery. Annual Reviews in Biomedical Engineering. 16 (7): 347-370 (2014). PMID: 24905873.
- Shape-Controlled siRNA Nanoparticles for In Vivo Delivery of RNA Therapeutics. US Provisional Patent Application Serial No. 62/000,838 (Filed on 05/20/2014) (Attached).

Citation: Molecular Therapy—Nucleic Acids (2015) 4, e242; doi:10.1038/mtna.2015.15

www.nature.com/mtna

Intraventricular Delivery of siRNA Nanoparticles to the Central Nervous System

Rishab Shyam[1], Yong Ren[2,3], Jason Lee[1,3], Kerstin E Braunstein[4], Hai-Quan Mao[2,3,5,6] and Philip C Wong[4,7]

Alzheimer's disease (AD) is a progressive neurodegenerative disease currently lacking effective treatment. Efficient delivery of siRNA via nanoparticles may emerge as a viable therapeutic approach to treat AD and other central nervous system disorders. We report here the use of a linear polyethyleneimine (LPEI)-*g*-polyethylene glycol (PEG) copolymer-based micellar nanoparticle system to deliver siRNA targeting *BACE1* and *APP*, two therapeutic targets of AD. Using LPEI-siRNA nanoparticles against either *BACE1* or *APP* in cultured mouse neuroblastoma (N2a) cells, we observe selective knockdown, respectively, of *BACE1* or *APP*. The encapsulation of siRNA by LPEI-*g*-PEG carriers, with different grafting degrees of PEG, leads to the formation of micellar nanoparticles with distinct morphologies, including worm-like, rod-like, or spherical nanoparticles. By infusing these shaped nanoparticles into mouse lateral ventricles, we show that rod-shaped nanoparticles achieved the most efficient knockdown of *BACE1* in the brain. Furthermore, such knockdown is evident in spinal cords of these treated mice. Taken together, our findings indicate that the shape of siRNA-encapsulated nanoparticles is an important determinant for their delivery and gene knockdown efficiency in the central nervous system.

Molecular Therapy—Nucleic Acids (2015) **4**, e242; doi:10.1038/mtna.2015.15; published online 12 May 2015
Subject Category: siRNAs, shRNAs, and miRNAs Nanoparticles

Introduction

Alzheimer's disease (AD) is a progressive neurodegenerative disease that significantly impairs memory and cognitive function and affects close to 35 million people worldwide.[1,2] Pathological hallmarks of AD include the presence of amyloid plaque deposits and neurofibrillary tangles in the affected brain tissue.[3] The continued formation of amyloid-β ($A\beta_{1-40}$ and $A\beta_{1-42}$) species by successive cleavage of the amyloid precursor protein (*APP*) by β-secretase (*BACE1*) and γ-secretase leads to the formation of toxic amyloid plaques in the extracellular space.[4] While BACE1 knockout mice failed to generate amyloid-β, significant behavioral deficits were observed.[5,6] Additional genetic studies have shown that moderate reductions in BACE1 and γ-secretase can effectively reduce amyloidosis.[7] However, clinical trials involving using BACE1 and γ-secretase inhibitors to attenuate amyloidosis have been halted recently, due to toxicities and off-targeting effects.[8,9] Thus, there is an urgent need to develop new methods to specifically modulate these targets of interest, as we are faced with a burgeoning aging population.

RNA interference (RNAi) therapeutics have been actively pursued for selective gene knockdown and currently tested in several clinical trials.[10] RNAi offers promise to selectively knockdown the key players implicated in the AD pathway. To fully realize the potential of RNA therapeutics, including short interfering RNAs (siRNAs), effective cationic carriers can be tailored to package these siRNAs into nanoparticles or complexes, which serve to protect the RNA therapeutics and facilitate the delivery and uptake of the nanoparticles into target cells. This siRNA delivery strategy has been particularly successful through intravascular administration, leading to liver-targeted delivery and cancer-targeted delivery where the enhanced permeation and retention effect can be exploited as a means of selective delivery.[11,12] A recent study showed the use of a gold nanoparticle platform to deliver siRNA to target the antiapototic pathway in glioblastoma multiforme (GBM) *in vivo* mouse models.[13] Significant progress has been made to reduce the immunogenicity of viral carriers for the purposes of gene therapy in the central nervous system (CNS).[14] Here, we focus on delivering siRNA using a nonviral delivery strategy so as to mitigate the safety concerns associated with viral vectors. Nonviral carriers have been shown to have a good safety profile and have been employed for delivery of siRNA in humans.[11,15] More recently antisense therapy, and the development of single stranded optimized siRNA sequences, has emerged as an alternative method that was shown to knockdown proteins implicated in the CNS of Huntington's disease (HD) and Tau proteins in mouse models.[16,17] These RNA sequences will require the same packaging vehicles.

Linear polyethylenimine (LPEI) has been demonstrated to be a versatile carrier for gene therapy applications.[18,19] Studies have highlighted the ability of LPEI-based carriers

[1]Department of Biomedical Engineering, Johns Hopkins University School of Medicine, Baltimore, Maryland, USA; [2]Department of Materials Science and Engineering, Whiting School of Engineering, Johns Hopkins University, Baltimore, Maryland, USA; [3]Institute for NanoBioTechnology, Johns Hopkins University, Baltimore, Maryland, USA; [4]Department of Pathology, Division of Neuropathology, Johns Hopkins University School of Medicine, Baltimore, Maryland, USA; [5]Translational Tissue Engineering Center, Johns Hopkins University School of Medicine, Baltimore, Maryland, USA; [6]Whitaker Biomedical Engineering Institute, Johns Hopkins University, Baltimore, Maryland, USA; [7]Department of Neuroscience, Johns Hopkins University School of Medicine, Baltimore, Maryland, USA. Correspondence: Philip C Wong, Department of Pathology, Division of Neuropathology, Johns Hopkins University School of Medicine, Baltimore, Maryland, USA. E-mail: wong@jhmi.edu or Hai-Quan Mao, Department of Materials Science and Engineering, Whiting School of Engineering, Johns Hopkins University, Baltimore, Maryland, USA. E-mail: hmao@jhu.edu
Keywords: Alzheimer's disease; gene therapy; polymeric carriers; RNAi; siRNA
Received 13 January 2015; accepted 8 April 2015; published online 12 May 2015. doi:10.1038/mtna.2015.15

to complex with DNA and RNA, forming complexes with an average diameter in tens to a couple of hundreds of nanometers, to deliver targets of interest *in vitro* and *in vivo* to modulate gene expression.[19,20] Nanoparticles prepared with LPEI and plasmid DNA have successfully mediated gene expression in the mouse CNS.[21] In this study, we demonstrate specific gene knockdown in mouse neuroblastoma N2a cells using LPEI with an average molecular weight (MW) of 17 kDa ($LPEI_{17k}$) to encapsulate siRNA targeting *BACE1* or *APP*. To improve biocompatibility of LPEI, we grafted polyethylene glycol (PEG, M_n = 10 kDa) to $LPEI_{17k}$ at different grafting densities, and developed a method to package siRNA into micellar nanoparticles with different shapes including worm-like, rod-like, and spherical nanoparticles. Here, we describe methods for varying the shapes of these nanoparticles by varying the structural parameters of the carriers and assembly condition between the copolymer carrier and siRNA, and then compare the *in vivo* efficacy and safety of these shaped nanoparticles in terms of targeting *BACE1* in the CNS of mice.

Results

To improve the biocompatibility of LPEI/siRNA nanoparticles, we grafted PEG_{10k} on to $LPEI_{17k}$ with varying grafting degrees. In most of the reported work, higher N/P ratios (*i.e.*, molar ratio of amines in the LPEI to phosphate groups in the siRNA) have been used to maximize siRNA packaging and transfection.[22] We chose to prepare siRNA nanoparticles with $LPEI_{17K}$ at a relatively lower N/P ratio of 5, so as to limit cytotoxic effects in both *in vitro* and *in vivo* contexts.[23] Under these conditions, siRNA can be effectively condensed. Using transmission electron microscopy (TEM), we observed that nanoparticles made with LPEI-*g*-PEG at increasing PEG grafting density of 0.6, 0.8, or 1.2% displayed a propensity to form respectively worm-like, rod-like, or spherical shaped nanoparticles(**Figure 1a–c**). To prevent relaxation of the complexes and release of siRNA from micelles in physiological media prematurely, and improve delivery efficiency of their payload to the cytoplasm of target cells, we adopted a disulfide crosslinking strategy.[24,25] These stabilized micellar nanoparticles showed high colloidal stability in 150 mmol/l NaCl solution, with no appreciable increase in size after incubation for 4 hours at room temperature (**Figure 1d**). In contrast, $LPEI_{17k}$/siRNA particles exhibited slightly larger size than LPEI-*g*-PEG/siRNA micelles, but were prone to significant aggregation in 150 mmol/l of NaCl (**Figure 1d**). Similarly, the crosslinked $LPEI_{17K}$/siRNA nanoparticles also showed severe aggregation in NaCl solution (**Supplementary Figure S1**). Our findings suggest that the condensation facilitated by the PEG grafts on the LPEI backbone is essential for the stabilization of siRNA-loaded nanoparticles, an important factor that may impact on *in vivo* delivery of the siRNA payload.

It is interesting to note that the shape of the nanoparticles is also dependent on the ratio of copolymer to siRNA in the preparation, effectively measured by the N/P ratio. Using $LPEI_{17k}$-*g*-0.6%-PEG_{10k} as an example, we observed that minor deviations in N/P ratio from 3 to 6 significantly influenced the shape of complex nanoparticles. TEM imaging for all particles that were stabilized with disulfide crosslinking

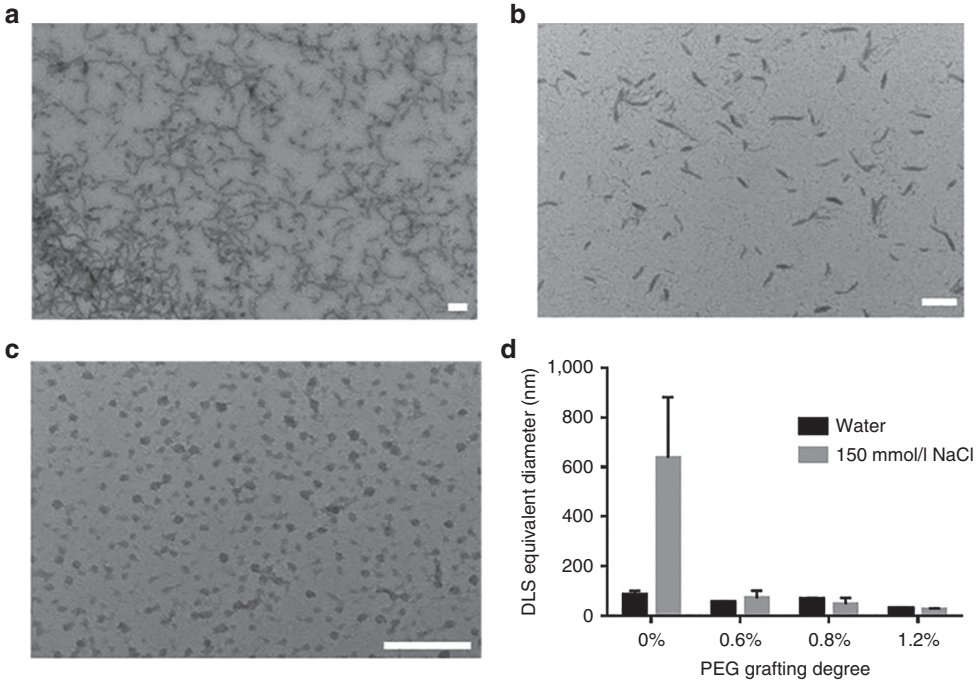

Figure 1 Tuning the shape of LPEI-*g*-PEG/siRNA micellar nanoparticles by varying PEG grafting degree. (**a**) $LPEI_{17k}$-*g*-0.6%PEG_{10k}/siRNA nanoparticles (N/P = 5) showing worm-like morphology. (**b**) $LPEI_{17k}$-*g*-0.8%PEG_{10k}/siRNA nanoparticles (N/P = 5) showing rod-like morphology. (**c**) $LPEI_{17k}$-*g*-1.2%PEG_{10k}/siRNA nanoparticles (N/P = 5) showing spherical morphology. All scale bars = 200 nm. (**d**) Particle size measured by dynamic light scattering in water and 150 mmol/l NaCl after incubation at room temperature for 4 hours ($n \geq 3$, mean ± SD). The $LPEI_{17k}$/siRNA nanoparticles without PEG grafts (0%) were prepared at an N/P ratio of 10 without crosslinking.

confirmed that as the N/P ratio increased from 3 to 6, the nanoparticles transitioned from a worm-like morphology at N/P ratio of 3 to a rod-like morphology at N/P ratio of 6 (**Supplementary Figure S2**). Both the PEG grafting degree and ratio of LPEI to siRNA can be varied to effectively control the shape of siRNA-loaded micellar nanoparticles.

Before assessing the effect of nanoparticle shape on delivery of siRNA to knockdown targets of interest in the CNS, we screened for the appropriate siRNA sequences and evaluated the ability of our siRNA-loaded nanoparticles to knockdown *BACE1* and *APP* in a cell culture model, namely, N2a cells which endogenously express both genes.[26] We first verified that $LPEI_{17k}$ complexed with siRNA against either *BACE1* or *APP*, formed nanoparticles with an average diameter of below 100 nm (**Supplementary Figure S3**). These nanoparticles showed successful delivery of siRNA to the cytoplasm in N2a cells (**Figure 2d**). After screening multiple siRNAs targeting either *BACE1* or *APP* by transfection of N2a cells (data not shown), we selected two top candidates, BACE33 and APP35, for further evaluation. Protein blot analysis revealed that while naked siRNAs were unable to alter the protein levels of their targets, $LPEI_{17k}$/siRNA complexes encapsulating BACE33 or APP35 reduced the level of *BACE1* or *APP*, respectively, by 63.3 ± 25.4% or 75.6 ± 10.2% of nontransfected control (**Figure 2a–c**). Note that the knockdown of *BACE1* by BACE33 did not alter the level of APP, and neither did the knockdown of *APP* by APP35 affect the level of *BACE1*. Moreover, transfections performed with $LPEI_{17k}$/siRNA nanoparticles at a dose of 5 µg of siRNA did not elicit cytotoxicity as judged by the viability of transfected cells (**Figure 2e**). Empirically, we determined that an optimal dose for knockdown of BACE1 is between 3 to 5 µg of siRNA (**Figure 2f**).

Next we assessed the effect of nanoparticle shape on the delivery of siRNAs to cells of the CNS globally. We performed intraventricular infusions of LPEI/siRNA nanoparticles and shaped micellar nanoparticles in awake and freely moving mice (**Figure 3a**), a delivery approach thought capable

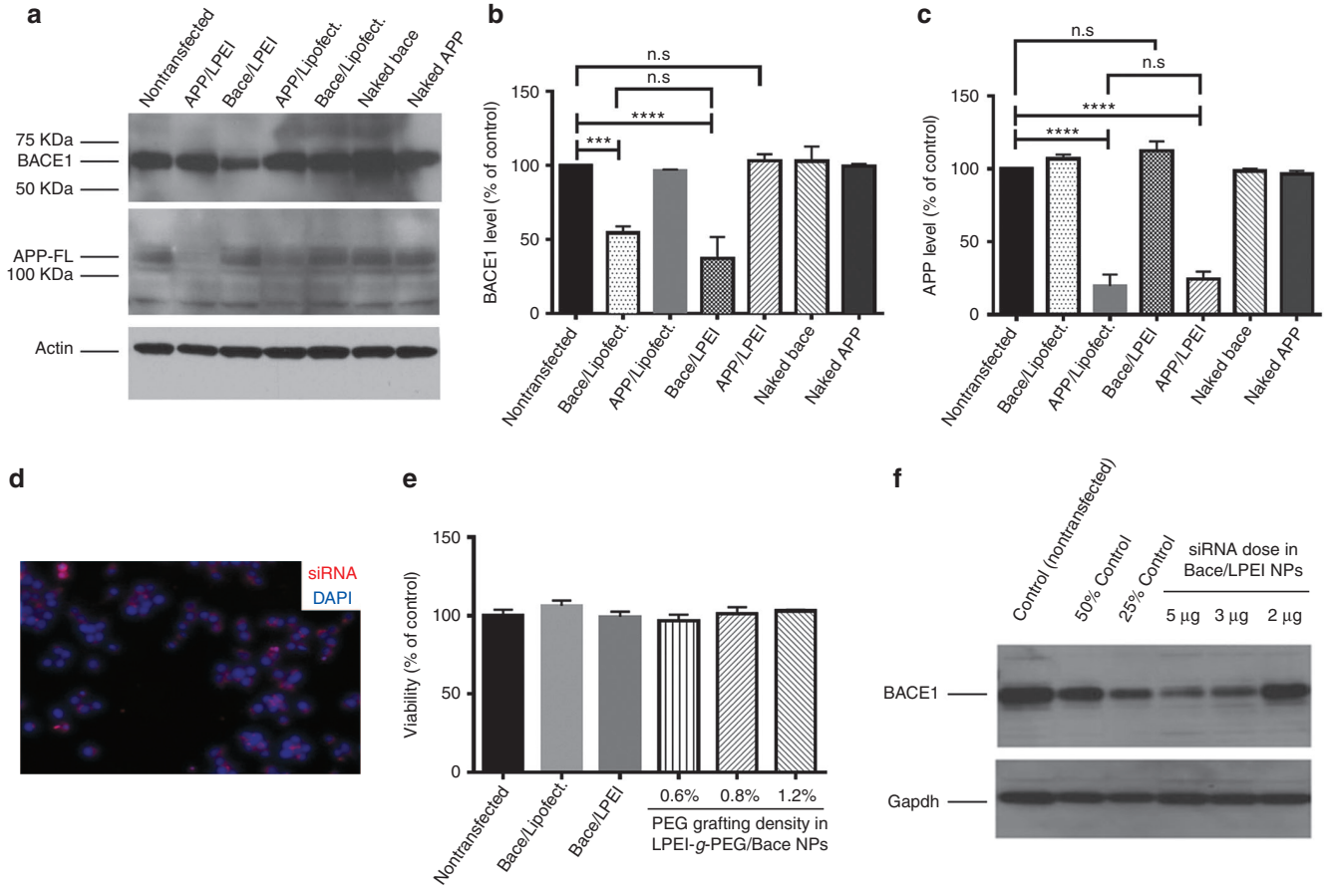

Figure 2 ***In vitro*** **knockdown efficiency of $LPEI_{17k}$/siRNA nanoparticles in N2a cells**. (**a**) Protein blot analysis of *BACE1* and *APP* levels after N2a cells were transfected with nanoparticles prepared with sequences BACE33 and APP35, respectively, or with Lipofectamine (positive control) and naked sequences (negative control). Lipofect: Lipofectamine. (**b,c**) Quantification of protein blot analysis of (**b**) *BACE1* and (**c**) *APP* protein levels as compared to nontransfected N2a cells ($n = 4$, mean ± SEM, analysis of variance (ANOVA), $F = 19.75$, $P < 0.0001$). All *in vitro* studies were performed at an N/P ratio of 10. (**d**) Microscopic analysis of the *in vitro* cell culture model confirmed that fluorescently labeled siRNA (red) was delivered to the cytoplasm of cells using $LPEI_{17K}$ (nuclei-DAPI). We noted the classical pattern of siRNA accumulation in the cell around the nucleus (stained blue). (**e**) MTT assay analysis confirms that over the transfection period of 24 hours, the various formulations built on the $LPEI_{17k}$ platform were not toxic ($n = 5$, mean ± SEM, ANOVA, n.s., not significant). (**f**) Transfection studies in N2a cells with varying amounts of siRNA delivered in the form of nanoparticles with the $LPEI_{17k}$. The first three lanes are a dilution series of protein lysates from untransfected cells.

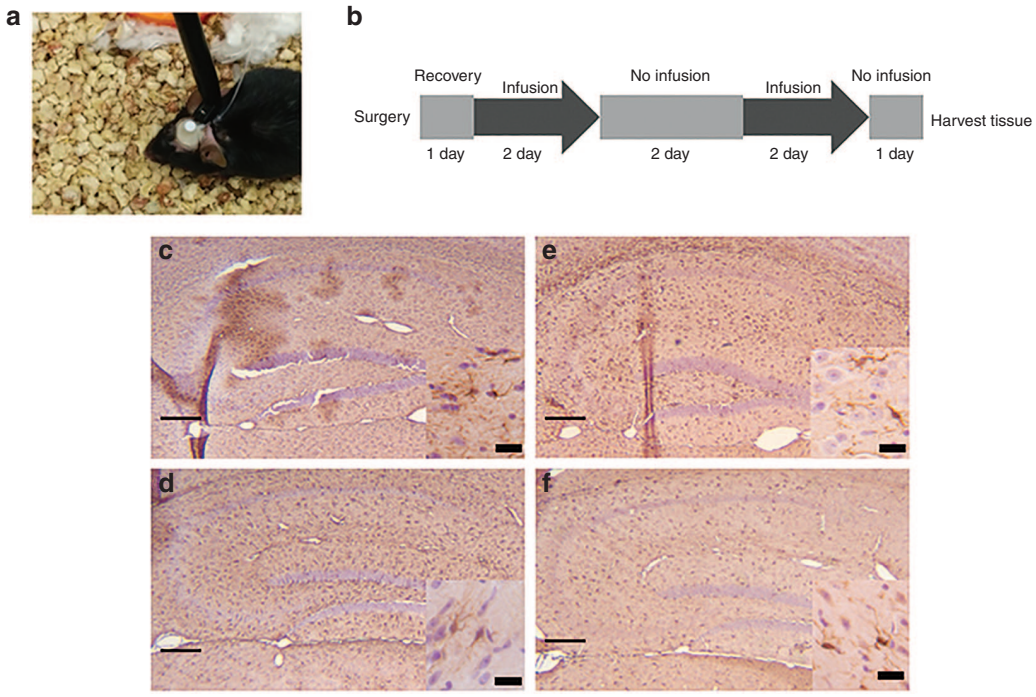

Figure 3 Schematic showing the infusion setup and immunohistochemical (IHC) analysis for astrocytic and microglial activation in the mouse hippocampus infused with micellar nanoparticles. (**a**) Infusion setup allowing for continuous infusion into the lateral ventricle of the brain of a mouse. The tube from the cannula was connected to a slow infusion pump. The animals were awake, freely moving, and had free access to food pellets and water. (**b**) Schematic of infusion regimen. All infusions were performed at 0.1 µl/minute. (**c,d**) IHC staining of tissue sections of the right (ipsilateral) hippocampus showing no significant difference in local recruitment of GFAP+ astrocytes to vehicle (**c**) and siRNA/LPEI$_{17k}$-*g*-0.8%PEG$_{10k}$ nanoparticles (**d**) after the 7-day infusion protocol. (**e,f**) Similarly, no significant difference in microglial cell (Iba-1+) activation following the 7-day infusion protocol for vehicle (**e**) and siRNA/LPEI$_{17k}$-*g*-0.8%PEG$_{10k}$ nanoparticles (**f**). Images of other sections are in **Supplementary Figure S7**. Scale bar = 200 µm. Inset scale bar = 20 µm.

of achieving global distribution of payload in the brain.[17,27] Mice were initially infused with up to 64 µg of siRNA in the right lateral ventricle (referred as the ipsilateral side) over a 7-day period (**Figure 3b**). Unfortunately, such effort of using our optimized formulations from the *in vitro* studies did not lead to reduction in levels of *BACE1* (**Supplementary Figure S4**). Initial *in vivo* pilot studies were performed with LPEI/siRNA nanoparticles at N/P ratios of 10 and 20, reasoning that the knockdown efficiency would be higher for higher N/P ratios. Consistent with other studies,[28] we noticed significant toxicity leading to a high fatality rate in the experimental group, where nanoparticles with an N/P ratio of 20 exhibited a higher level of toxicity than that with an N/P ratio of 10. We therefore used a low N/P ratio of 5 so as to minimize the amount of LPEI in nanoparticles to mitigate toxicity effects in the CNS and focused on evaluating the efficiency of LPEI$_{17K}$-*g*-PEG$_{10k}$/siRNA micellar nanoparticles stabilized with disulfide crosslinking, hypothesizing that PEG corona on micellar nanoparticles could reduce toxicity while providing a better opportunity for siRNA delivery due to higher colloidal and complex stability. For all of the LPEI$_{17k}$-*g*-PEG$_{10k}$/siRNA nanoparticles in N2a cells, the viability was greater than 95% when compared with the untransfected control (**Figure 2e**). However, these LPEI$_{17k}$-*g*-PEG$_{10k}$/siRNA micellar nanoparticles showed minimal transfection and knockdown efficiency *in vitro.* Given that the *in vitro* results do not typically match the *in vivo* transfection efficiency for PEGylated carriers,[20,29] we continued with assessing the *in vivo* delivery efficiency of these micellar nanoparticles with spherical, rod-like and worm-like shapes to the CNS.

To determine whether nanoparticles can be transported into the brain parenchyma, we followed the fate of fluorescently labeled siRNA encapsulated in nanoparticles, in the brain of mice, following an intraventricular infusion for two days. To facilitate identification of neurons in the brain, we used mice genetically encoded with GFP in which neurons are sparsely marked by GFP in the cytoplasm.[30] Proximal to the lateral ventricle, we observed a gradient of fluorescently labeled siRNA emanating from the infusion site toward the brain parenchyma (**Supplementary Figure S5**). The accumulation pattern of the siRNA strongly suggests that these nanoparticles were able to gain access to the cytoplasm of cells in the brain parenchyma.

To assess potential untoward side effects of nanoparticles infused into brains of mice up to one week, we examined glial cells, which are normally activated and migrate to the site of injury in the brain.[31] Since cannulation of the right lateral ventricle would lead to the injury of tissue in the immediate vicinity, we first confirmed that similar activation of glial cells at the injury site occurred for animals infused with vehicle (5% glucose solution) or those with nanoparticles (**Supplementary Figure S6**). Note that in regions away from the site of injury, a decrease in glial cell activation was observed (**Supplementary Figure S6a–f**). No significant

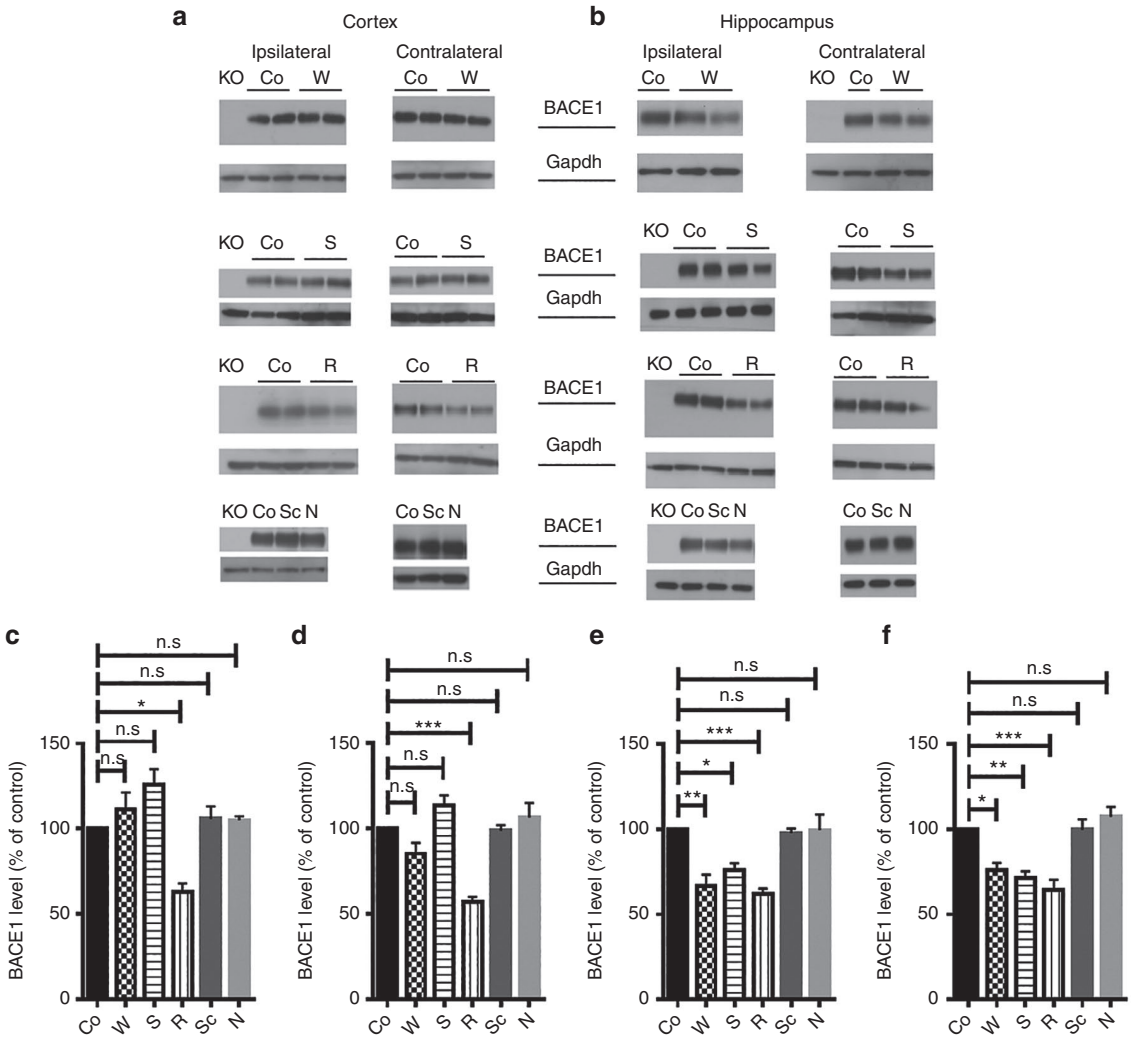

Figure 4 ***In vivo BACE1*** **knockdown in the cortex and hippocampi of mice infused with worm-like, rod-like, and spherical micellar nanoparticles**. All infusions were performed in the right (ipsilateral) lateral ventricle at a dose of 16 µg of siRNA/day with the same dosing regimen for all nanoparticles as show in Figure 3b ($n = 4$ for infusion of worm-like, rod-like, and spherically shaped nanoparticles, scrambled and naked siRNA infusion studies were performed in duplicate). (**a,b**) Protein blot analysis of BACE1 levels in the cortex (**a**) and hippocampus (**b**), in both the right (ipsilateral) and left (contralateral) hemispheres after delivery of sequence BACE33 using worm-like (W), spherical (S), and rod-like (R) nanoparticles. KO, BACE knockout; Co, vehicle infusion; Sc, Scrambled siRNA complexed with $LPEI_{17k}$-*g*-0.8%PEG_{10k}; N, naked siRNA sequence BACE33. (**c–f**) Quantification of *BACE1* levels from protein blot analysis in the (**c**) ipsilateral cortex (mean ± SEM, analysis of variance (ANOVA), $F = 9.133$, $P < 0.05$, Tukey's multiple comparisons test), (**d**) contralateral cortex (mean ± SEM, ANOVA, $F = 17.91$, $P < 0.0001$, Tukey's multiple comparisons test), (**e**) ipsilateral hippocampus (mean ± SEM, ANOVA, $F = 13.45$, $P < 0.0001$, Tukey's multiple comparisons test), and (**f**) contralateral hippocampus (mean ± SEM, ANOVA, $F = 14.04$, $P < 0.0001$, Tukey's multiple comparisons test).

difference in glial cell activation was seen in the contralateral side of brains between both sets of mice (data not shown). While these results confirmed that $LPEI_{17k}$-*g*-PEG_{10k}/siRNA nanoparticles did not elicit an untoward response over a 2-day period, we also examined any potential impact for mice infused for at least 7 days. Using markers of astrocytic and microglial activation, we did not observe any difference in activation of both cell types in the ipsilateral hippocampus of mice infused with rod shaped nanoparticles as compared to control (**Figure 3c–f**). Likewise, no difference was observed for other types of shaped nanoparticles either (**Supplementary Figure S7**). Taken together with the observation that microglial and astrocytic cells continued to maintain their normal morphology, our findings suggest that these micellar nanoparticles do not induce significant inflammation and cytotoxicity in the brain when infused for over 1 week.

Interestingly, while worm-like and spherical nanoparticles did not alter *BACE1* levels, infusion of rod-shaped nanoparticles into the lateral ventricle led to the knockdown of *BACE1* by 36.8 ± 4.8% and 42.8 ± 2.9% within the ipsilateral and contralateral side of the cortex, respectively, as compared to the vehicle infused control (**Figure 4a**,**c**,**d**). In the ipsilateral hippocampus, spherical, rod-like, and worm-like nanoparticles reduced *BACE1* levels by 24.1 ± 4.1%, 38.2 ± 3.4%, and 33.3 ± 6.7%, respectively (**Figure 4b**,**e**,**f**). In the contralateral hippocampus, the corresponding *BACE1* knockdown

efficiencies were 28.9±4.1%, 35.6±5.9%, and 24.2±4.5%, respectively, for spherical, rod-like, and worm-like nanoparticles. Together, these findings suggest that the shape of nanoparticles appears to influence their efficiency for delivery to cells in the CNS, and the rod-like particles are most efficient among this series. To further evaluate how extensive these nanoparticles could distribute throughout the CNS, we examined their ability to knockdown *BACE1* in the brainstem and spinal cord, regions that are farther away from the site of infusion. We too observed that our nanoparticles were able to significantly reduce levels of *BACE1* in the brainstem and spinal cord of mice (**Supplementary Figure S8**). Our findings thus establish that efficient siRNA delivery to the CNS can be achieved by shaped micellar nanoparticles based on the $LPEI_{17k}$-*g*-PEG_{10k}/siRNA nanoparticle platform.

Discussion

Despite the enormous therapeutic potential of siRNAs for treating neurological diseases, delivery of these molecules, either through local or systemic administration, remains a great challenge.[10] Tremendous progress has been made towards developing suitable carriers for siRNA as therapeutics which in the form of nanoparticles have reached clinical trials.[12] Besides particle surface properties, and charge density, nanoparticle shape has been shown to be key parameter towards improving the delivery efficiency.[32] Studies have shown how different shapes utilize differing mechanisms to gain entry into cells.[33,34] While exciting progress has been made in terms of manipulating RNA sequences into a variety of geometries, shape control of the RNA species encapsulated within nanoparticles has been inaccessible.[35–37] A recent study showed that rod shaped particles accumulated to a greater extent in the lung and brain vasculature when infused intravenously as compared to spherically shaped particles.[38]

Our recent work showing that the shape of DNA-encapsulated nanoparticles is an important factor to influence transfection efficiency in a rat liver model supports the notion that the shape of nanoparticles could be an important determinant for their payload delivery efficiency.[39] Pioneering work involving the use of DNA as building blocks have been extended to RNA and more recently to long RNAi (microsponges) that were developed in an effort to overcome challenges of packaging short pieces of siRNA.[35,40] These RNA species when encapsulated by a polycationic carrier typically form spherical particles. While shape control using RNA as a structural building block has been achieved,[37] the control of nanoparticle shape with RNA as the functional payload has not been demonstrated. Our finding on the ability to control siRNA nanoparticle shape using LPEI-*g*-PEG copolymer carriers establishes the first evidence that the shape of polycation/siRNA micellar nanoparticles can be varied in a systematic fashion. This study confirmed that increasing the PEG grafting density leads to more condensed spherical morphology, whereas lower grafting density yields rod- and worm-like micelles. This observation can be explained using the traditional micelle packing models for amphiphilic diblock copolymer micelles assembled in aqueous media.[41] Assuming that the degrees of condensation between the LPEI backbone and siRNA are similar for graft copolymers with different PEG grafting densities under the same N/P ratio, since the grafting densities are relatively low (< 2%), condensation of siRNA with copolymers having a higher PEG grafting density generates micellar nanoparticles with a higher PEG surface density, thus favoring the formation of spherical micelles. This is analogous to micelle assembly, where the shape control is governed by the volume ratio of the hydrophilic (corona) to hydrophobic (core) blocks—higher ratio favors spherical micelle formation and lower ratio yields worm-like micelles.[41] The trend observed by varying N/P ratio is also consistent with this interpretation: a higher N/P ratio leads to higher PEG density on micelle surface, favoring spherical micelle formation, although it is surprising that such a small range of N/P ratio variation from 3 to 6 can lead to significant shape variation.

Using this method, we were able to generate nanoparticles with relatively low N/P ratios compared with higher amount of transfection agents used in nanoparticle formulations.[22] This is advantageous in terms of better biocompatibility and lower cytotoxicity of the nanoparticles prepared for transfection applications.[23] Our overall strategy also relies on stabilization of the shaped nanoparticles using a reversible disulfide crosslinking scheme that has been widely adopted by other DNA and siRNA delivery platforms.[24] This method ensures that the prepared nanoparticles will maintain their size and shape in serum containing medium, important to *in vivo* administration. The availability of a panel of shape-controlled nanoparticles will enable future studies to explore shape-dependent transport *in vivo*. This method relying on the control of copolymer structure and concentrations of the copolymer and siRNA solutions is thus straightforward to scale up for production.

Previous studies have highlighted challenges involved in designing a suitable method to target the key enzymes involved in the *APP* pathway.[42,43] Since mechanism-based toxicities are associated with inhibition of γ-secretase,[44] we focused on developing a suitable delivery vehicle for siRNA targeting *BACE1* and *APP*. Previously, we and others employed RNAi strategies delivered by viral vectors to reduce levels of *BACE1*, which emerged as a powerful tool to deliver short hairpin RNA to decrease protein levels.[45,46] The nonviral siRNA delivery approaches can potentially mitigate putative safety concerns associated with viral vectors, such as insertional mutagenesis and the risk of inflammation.[47] One recent report showed a nanoparticle delivery system using exosomes, with rabies virus glycoprotein (RVG) as a targeting ligand, can reduce the level of *BACE1* when delivered to the brain.[48] Our study here confirms that the series of shape-controlled micellar nanoparticles are nontoxic to brain tissue as judged by the lack of astrocytic or glial cell activation in response to nanoparticle infusion over a 7-day period. After validating in an N2a cell culture model, the ability of nanoparticles to deliver siRNA to modify levels of *BACE1* and *APP*, two different proteins in the *APP* processing pathway of AD, we evaluated their efficacy in the CNS of mice by targeting *BACE1*. Since AD is a neurodegenerative disorder that globally affects the brain, we focused on ensuring that the nanoparticles were distributed throughout the brain as opposed to a local infusion close to the site of interest. In

contrast to several studies focused on inducing RNAi in the CNS of mice,[49,50] our discovery of shaped nanoparticles provides the opportunity to evaluate whether shape of nanoparticles is a major determinant for efficient delivery of siRNA throughout the CNS. Our proof of principle study establishes that rod-liked nanoparticles exhibited higher efficiency in reducing BACE1 levels in the ipsilateral and contralateral side of the brain. Interestingly, the reduction in *BACE1* levels observed in the hippocampus was not significantly different among various shaped nanoparticles. This could be attributed to the proximity of the hippocampus to the lateral ventricles, which mimics a local infusion process. Previous work using mouse models of AD has supported the notion that moderate reductions in BACE1 would prevent potential mechanism-based toxicity while providing beneficial effects in the brain.[7] The modest reduction of *BACE1* afforded by our nanoparticle delivery system in the CNS (35–45%) would be amenable for design of a safe and effective therapeutic strategy to target *BACE1* for AD. Additional carrier optimization may facilitate the duration of gene knockdown, a strategy that should be considered in future design of nanoparticle based therapies. Moreover, our findings of knockdown in the brain stem and spinal cord, regions that are farther away from the infusion site, further support the notion that these shaped nanoparticles achieved broad distribution and delivery of siRNAs in the CNS. Although we did not see significant knockdown in the thoracic spinal cord, future studies using intrathecal infusion of these nanoparticles may clarify differences in the efficiency of knockdown in the spinal cord with this nanoparticle system. Further exploration of attributes of the rod-shaped particles that promote greater efficacy should allow us to design more suitable carriers to enhance CNS delivery.

Although we have shown here that rod-shaped particles work best in this animal model following intraventricular delivery, it remains to be demonstrated as to whether the worm-like and spherical nanoparticles, at varying N/P ratios, would be more suitable for other tissue targets or when administered through a different delivery route. While this study does not address the potential of this micellar nanoparticle system for systemic delivery and crossing the blood–brain barrier, worm-like micellar nanoparticles with longer circulation dynamics in rodent models provide the motivation for future investigation for intravenous delivery.[39,51,52] Decorating nanoparticles with targeting ligands of the insulin or transferrin receptor or cell penetrating peptides have been established as promising approaches to improve delivery of cargo to cells of interest.[53,54] Exploiting these approaches coupled with shape-controlled siRNA nanoparticles will lead to further development of an improved set of carriers. As siRNA and antisense therapeutic strategies continue to mature and move into clinical trials using highly optimized sequences, these shape-controlled nanoparticles and their unique properties may provide new opportunities to optimize RNA therapeutic delivery for a variety of disease targets.

In conclusion, we have shown here that micellar nanoparticles with worm- and rod-like, and spherical shapes can be prepared by self-assembly of the complexes between siRNA and LPEI-*g*-PEG copolymer carriers. The PEG corona and reversibly crosslinked core of the micelles enable these nanoparticles to be stable under physiological conditions. Interestingly, these micellar nanoparticles revealed differences in knockdown capability following infusion into the lateral ventricles in mice with the rod-like micelles showing the most effective and selective knockdown of a key therapeutic target in AD. Future development of siRNA delivery strategies leveraging shape as a tunable parameter would broaden the toolkit we have at our disposal for creating a translatable platform for RNAi therapeutics.

Materials and methods

Synthesis and characterization of LPEI-g-PEG copolymer. Linear polyethyleneimine (LPEI HCl salt, M_n of LPEI = 17 kDa) was a gift from Polymer Chemistry Innovations (Tucson, AZ). N-Hydroxysuccinimidyl ester of methoxy polyethylene glycol hexanoic acid (PEG-NHS, M_n = 10 kDa) was purchased from NOF America Corporation (White Plains, NY). The LPEI·HCl (7.95 mg, 0.1 mmol of amine) was dissolved in 1 ml of DI water. NaOH solution was added to the solution drop-wise to raise the pH to 6. Then 80 mg of PEG-NHS (designed grafting degree of PEG per amine on LPEI = 8%) was added to the solution and the reaction mixture was vortexed. After incubation overnight, the reaction mixture was dialyzed against DI water and lyophilized to yield a white foam-like solid with a 95% yield. The molecular weight of the graft copolymer was characterized by GPC (gel permeation chromatography) using an Agilent 1200 series Isocratic HPLC System equipped with TSKgel G3000PWxl-CP column and TSKgel G5000PWxl-CP column (Tosoh America, Grove City, OH), which was connected with a multi-angle light scattering detector (MiniDawn, Wyatt Technology, Santa Barbara, CA). The $LPEI_{17k}$-*g*-PEG_{10k} polymer was obtained with a PEG grafting degree of 1.2%, which corresponds to an average of 4.6 PEG grafts per LPEI molecule. For two other $LPEI_{17k}$-*g*-PEG_{10k} copolymers with designed grafting degree of 4% and 2%, the actual PEG grafting degrees were 0.8 and 0.6%, respectively.

Particle formulation. $LPEI_{17k}$-*g*-PEG_{10k} was first modified with Trauts reagent (Sigma, St. Louis, MO) in the presence of dithiothreitol (DTT, Thermo Scientific, Rockford, IL). Trauts reagent was dissolved in deionized water (cell culture grade, Corning, Manassas, VA) to a concentration 2 mg/ml, and DTT was dissolved in DI water to a concentration of 20 mg/ml. An aliquot of 9 µl of 50 mmol/l polymer solution was mixed with 18.6 µl of Trauts reagent solution and 13 µl of the DTT solution, and then 59.4 µl of water was added to this mixture, the pH adjusted to 7.3. At the end of this 2.5-hour reaction, the mixture was desalted using an Amicon centrifugal filter (3 KDa MWCO, Sigma-Aldrich) with water three times and reconstituted to a volume of 110 µl. An aliquot of 10 µl of DTT solution was added to this solution and the pH adjusted to ~1.8–2.0. On the other hand, 9.8 µl of 100 µmol/l siRNA (equivalent to 16 µg of siRNA) solution was added to 60 µl of water, and mixed with 60 µl of the polymer solution and vortexed. The nanoparticle solution was then dialyzed against water overnight to remove DTT and other reagents. Crosslinking was carried out for 48 hours with aerial oxidation similar to our previous study.[39] The nanoparticle solution was then dialyzed for 24 hours against water following which the samples were analyzed by dynamic light scattering using a Malvern Zetasizer Nano ZS, which also provided information

about zeta potential, followed by TEM analysis for nanoparticle shapes. The protocols detailed above and in the following section were designed to yield nanoparticles with an N/P ratio of 5. The volume of mixing between the polymer and siRNA was scaled accordingly to achieve additional N/P ratios ranging from 3 to 6.

Transmission electron microscopy. An aliquot of 10 µl of nanoparticle solution was deposited on ionized nickel grid covered by carbon. The excess liquid on the grid was pipetted out after 7 min, and then 6 µl of 2% uranyl acetate solution was deposited on the grid and allowed to incubate for 30 seconds. The excess liquid was once again pipetted out and the grid was allowed to dry at room temperature prior to being examined. The samples were imaged on a Tecnai FEI-12 electron microscope.

Intraventricular infusion in mice. Following anesthetization, the hair above the skull of C57BL/6J mice was removed to expose the scalp. An incision was made along the midline to expose the skull. A hole was drilled through the skull, above the right lateral ventricle (bregma–0.5 mm, 1.0 mm lateral). After drilling, bone fragments were cleaned away. An Alzet apparatus (brain infusion kit# 3, Cupertino, CA) was used as per manufacturer's specifications to place a cannula at a depth of 2.2 mm. The cannula was cemented using dental cement. A sufficiently long tube (FEP-tubing, SCIPRO, Sanborn, NY), so as to allow free head and neck movement of the mice, was used to connect the end of the cannula above the skull to a slow infusion pump (Stoelting, Wood Dale, IL). The animal was then placed in a special enclosure, Raturn Microdialysis Stand-Alone System (with free access to food and water) where the tube going to the slow infusion pump can be secured and the process of infusing the therapeutic agent was begun (0.1 µl/minute during the infusion phase). At any given point, there would be only one mouse present in the Raturn Microdialysis Stand-Alone System undergoing infusion (BASi, West Lafayette, IN). We used a slow infusion pump to facilitate the flexibility of having a system that would be able to deliver reagents from a period varying from 2 to 7 days with the ability to stop infusions as per our staggered infusion protocol (**Supplementary Figure S7e**). Importantly, it allowed us to deliver a specific volume of therapeutic to the targeted area in the brain and monitor the effect in the live animal, which would mimic a clinical setting where the therapeutic can be potentially used. The right and left hemisphere were referred to, respectively, as the ipsilateral or contralateral side of the brain with reference to the side of infusion. All animal studies were performed in compliance with the Johns Hopkins Institutional Animal Care and Use Committee approved protocols.

Immunohistochemical analysis. Mice (controls and those undergoing infusion) were perfused with cold 4% paraformaldehyde in phosphate-buffered saline. The brains were harvested and each hemisphere separated following which they were embedded in paraffin, sectioned sagitally, and processed for immunohistochemical analysis using the peroxidase–antiperoxidase method[46] with antibodies specific to BACE1 (1:500), glial fibrillary acidic protein (GFAP, 1:500, Dako Cytomation, Carpinteria, CA), and Iba-1 (1:500, Wako Chemicals, Richmond, VA). Secondary, biotinylated, goat-anti-rabbit antibodies were purchased from Vectashield (Burlingame, CA). The sections were counter-stained with hematoxylin.

Western blot analysis. Harvested mouse brains (cortex, hippocampus, and brain stem) and spinal cords (cervical, thoracic, and lumbar) were homogenized with radio-immunoprecipitation buffer (Sigma) in the presence of protease inhibitors (Thermo Scientific, Rockford, IL). Following the manufacturer recommended protocol, lysates were centrifuged at 14,000 rpm at 4 °C for 20 minutes, and the supernatant was used for western blotting. The lysates were run on a 4–12% bis-tris gel (Life Technologies, Grand Island, NY) and then transferred on to a polyvinylidene difluoride (PVDF) membrane. For western blot analysis, the membranes were blocked in 5% milk in tris buffered saline-tween 20 - (TBS-T) for an hour and then probed with antibodies specific for BACE1 (1:2,500), glyceraldehyde-3-phosphate dehydrogenase (GAPDH) (1:20,000, Sigma), APP-CTF (1:8,000), and Actin (1:5,000, Sigma). Band densitometry analysis was performed using Image Studio Lite software from LI-COR (Lincoln, NE).

In vitro knockdown and cell viability studies. The siRNAs used in this study are shown in **Table 1**.

Luciferase Stealth control and fluorescently labeled (Alexa-555) sequences were all purchased from Life Technologies. Lipofectamine2000 in Opti-Mem media was used for transfection as per manufacturer recommendations (Life Techonologies). Transfection experiments were performed in a six-well plate with N2a cells maintained in 10% fetal bovine serum (FBS), 1× Glutamax, 1× MEM-NEAA, 1× sodium pyruvate and antibiotic free conditions (Life Technologies). Cells were transfected with siRNA packaged in nanoparticles or Lipofectamine2000. Cell culture medium was replaced after 16 hours with fresh medium and the cells were harvested for further analysis after 24 hours. For harvesting cells, the media was first aspirated from each well. Following which, each well was washed twice with cold (4 °C) phosphate-buffered saline. A cell scraper was used to collect the cells from each well and protein extraction was performed using the radio-immunoprecipitation buffer following a similar protocol as the tissue protein extraction. The prepared lysates were further probed for protein content via western blot analysis. Cell viability was checked via an 3-(4,5-dimethylthiazol-2-yl)-2,5-diphenyltetrazolium bromide (MTT) assay based on the manufacturer

Table 1 siRNA Sequences targeting BACE1 and APP

siRNA	Sequences
BACE33	Sense-5′-GAGCCCUUCUUUGACUCCCUGGUGA; Antisense-5′-UCACCAGGGAGUCAAAGAAGGGCUC
BACE23	Sense-5′-GAGGGAGCAUGAUCAUUGGUGGUAU; Antisense-5′-AUACCACCAAUGAUCAUGCUCCCUC
APP35	Sense-5′-GCGGAUGGAUSUUUGUGAGACCCAU; Antisense-5′-AUGGGUCUCACAAACAUCCAUCCGC
APP34	Sense-5′-GACCAGGUUCUGGGCUGACAAACAU; Antisense-5′-AUGUUUGUCAGCCCAGAACCUGGUC
APP33	Sense-5′-UCAGGAUUUGAAGUCCGCCAUCAAA; Antisense-5′-UUUGAUGGCGGACUUCAAAUCCUGA

recommended protocol (Life Technologies). In a 96-well plate, N2A cells were treated at a scale proportional to that of a transfection in a six-well plate. A similar time scale of incubation for 24 hours was maintained after which time knockdown analysis was performed. The cytotoxicity of the samples was analyzed on an EPOCH BIOTEK (Winooski, VT) plate reader.

Confocal fluorescence imaging. Mice (with neurons sparsely expressing GFP, Thy-1 Promoter, gift from the Richard Huganir lab at Johns Hopkins University) were perfused with cold 4% paraformaldehyde in phosphate-buffered saline 24 hours after undergoing infusion protocol. The brains were harvested and each hemisphere separated. Following which they were postfixed 4% paraformaldehyde for 24 hours. The tissues were then treated for 48 hours with 30% sucrose for cryopreservation following which they were placed in a mold with OCT and prepared for cryosectioning. The tissue samples were sectioned sagitally (16-µm thickness), and collected on superfrost glass and probed with antibodies specific to BACE1 (1:500), GFAP (Dako Cytomation), and Microglia (Wako Chemicals). Mounting media (Life Technologies) preloaded with DAPI was applied prior to application of the coverslip. Microscopic analyses were performed on a Zeiss LSM 510 microscope. In the case of cell culture, cells were grown on a cover slip placed at the bottom of a six-well plate. At the end of the transfection study with fluorescently labeled siRNA over the same conditions as the knockdown studies, the cover slip was washed in phosphate-buffered saline, and 0.2 M acetic acid in 0.5 M sodium chloride solution. Following which the cover slips were treated with 0.4% Trypan blue solution Hanks buffered salt solution to quench extracellular fluorescence.[55] Mounting media (Life Technologies) preloaded with DAPI was applied to a glass slide prior to placing the cover slip on it for further microscopic analysis.

Gel retardation assay. A 2% agarose gel (with ethidium bromide) in a TAE buffer was used to elucidate release of siRNA from micellar nanoparticle formulations. Nanoparticle formulations were incubated with varying concentrations of dextran sulfate, following which 20 µl of each sample was loaded in each well with loading buffer. Samples were run on the gel for 20 minutes at 120 V.

Statistical analysis. Statistical comparisons were performed using ordinary one-way analysis of variance. Comparisons between groups were performed using Tukey's multiple comparisons test using GraphPad Prism Software (La Jolla, CA). Errors bars used in this study were in SD and SEM and noted in the figures.

Supplementary material

Figure S1. Transmission electron microscopy (TEM) images of non-PEGylated crosslinked LPEI17k/siRNA particles at N/P ratio of 5, indicating severe aggregation of complexes in 150 mM NaCl.
Figure S2. TEM images showing effect of N/P ratio on the shape of LPEI17k-g-0.6%PEG10k/siRNA micellar nanoparticles.
Figure S3. Gel retardation and zeta potential analyses of LPEI17k-g-PEG10k/siRNA micellar nanoparticles, and TEM image of LPEI17k/siRNA nanoparticles.
Figure S4. Protein blot analyses detailing examples of initial studies involving siRNA nanoparticles being infused into the brain of mice.
Figure S5. Microscopic analysis of fluorescently labeled siRNA encapsulated in micellar nanoparticles in the brain parenchyma.
Figure S6. Microscopic analysis of astrocytic cells (GFAP+ staining) in response to brain infusion over 2 days.
Figure S7. Microscopic analysis of astrocytic and microglial activation in the hippocampus as assessed by immunohistochemistry after infusion of micellar nanoparticles containing 64 µg of siRNA following a 7-day infusion protocol.
Figure S8. *In vivo* BACE1 knockdown in the brainstem, and cervical, thoracic, and lumbar sections of the spinal cord of mice, using worm- and rod-like, and spherical micellar nanoparticles.

Acknowledgments. We are grateful to Venette Nehus and Frances Davenport for their technical assistance. This work was partially supported by grants from the National Institute of Neurological Disorders and Stroke (NS41438, to P.C.W.), the Alzheimer's Disease Research Center (AG005146, P.C.W.), The Frederick J. Pelda Alzheimer's Research Fund (P.C.W.), the National Institute of Biomedical Imaging and Bioengineering (EB015152, H.Q.M.), and Defense Threat Reduction Agency (W81XWH-13-2-0037, H.Q.M.). We thank Donald Price, Tong Li, and Michele Pucak for their valuable discussions. The authors declare no conflict of interest.

1. Holtzman, DM, Morris, JC and Goate, AM (2011). Alzheimer's disease: the challenge of the second century. *Sci Transl Med* **3**: 77sr71.
2. Ridge, PG, Mukherjee, S, Crane, PK and Kauwe, JS; Alzheimer's Disease Genetics Consortium (2013). Alzheimer's disease: analyzing the missing heritability. *PLoS One* **8**: e79771.
3. Choi, SH, Kim, YH, Hebisch, M, Sliwinski, C, Lee, S, D'Avanzo, C *et al.* (2014). A three-dimensional human neural cell culture model of Alzheimer's disease. *Nature* **515**: 274–278.
4. Koffie, RM, Meyer-Luehmann, M, Hashimoto, T, Adams, KW, Mielke, ML, Garcia-Alloza, M *et al.* (2009). Oligomeric amyloid beta associates with postsynaptic densities and correlates with excitatory synapse loss near senile plaques. *Proc Natl Acad Sci USA* **106**: 4012–4017.
5. Savonenko, AV, Melnikova, T, Laird, FM, Stewart, KA, Price, DL and Wong, PC (2008). Alteration of BACE1-dependent NRG1/ErbB4 signaling and schizophrenia-like phenotypes in BACE1-null mice. *Proc Natl Acad Sci USA* **105**: 5585–5590.
6. Aguzzi, A and O'Connor, T (2010). Protein aggregation diseases: pathogenicity and therapeutic perspectives. *Nat Rev Drug Discov* **9**: 237–248.
7. Chow, VW, Savonenko, AV, Melnikova, T, Kim, H, Price, DL, Li, T *et al.* (2010). Modeling an anti-amyloid combination therapy for Alzheimer's disease. *Sci Transl Med* **2**: 13ra1.
8. Cai, J, Qi, X, Kociok, N, Skosyrski, S, Emilio, A, Ruan, Q *et al.* (2012). β-Secretase (BACE1) inhibition causes retinal pathology by vascular dysregulation and accumulation of age pigment. *EMBO Mol Med* **4**: 980–991.
9. Imbimbo, BP and Giardina, GA (2011). γ-secretase inhibitors and modulators for the treatment of Alzheimer's disease: disappointments and hopes. *Curr Top Med Chem* **11**: 1555–1570.
10. Kanasty, R, Dorkin, JR, Vegas, A and Anderson, D (2013). Delivery materials for siRNA therapeutics. *Nat Mater* **12**: 967–977.
11. Lee, JM, Yoon, TJ and Cho, YS (2013). Recent developments in nanoparticle-based siRNA delivery for cancer therapy. *Biomed Res Int* **2013**: 782041.
12. Coelho, T, Adams, D, Silva, A, Lozeron, P, Hawkins, PN, Mant, T *et al.* (2013). Safety and efficacy of RNAi therapy for transthyretin amyloidosis. *N Engl J Med* **369**: 819–829.
13. Jensen, SA, Day, ES, Ko, CH, Hurley, LA, Luciano, JP, Kouri, FM *et al.* (2013). Spherical nucleic acid nanoparticle conjugates as an RNAi-based therapy for glioblastoma. *Sci Transl Med* **5**: 209ra152.
14. Gray, SJ, Nagabhushan Kalburgi, S, McCown, TJ and Jude Samulski, R (2013). Global CNS gene delivery and evasion of anti-AAV-neutralizing antibodies by intrathecal AAV administration in non-human primates. *Gene Ther* **20**: 450–459.

15. Davis, ME, Zuckerman, JE, Choi, CH, Seligson, D, Tolcher, A, Alabi, CA *et al.* (2010). Evidence of RNAi in humans from systemically administered siRNA via targeted nanoparticles. *Nature* **464**: 1067–1070.
16. DeVos, SL, Goncharoff, DK, Chen, G, Kebodeaux, CS, Yamada, K, Stewart, FR *et al.* (2013). Antisense reduction of tau in adult mice protects against seizures. *J Neurosci* **33**: 12887–12897.
17. Yu, D, Pendergraff, H, Liu, J, Kordasiewicz, HB, Cleveland, DW, Swayze, EE *et al.* (2012). Single-stranded RNAs use RNAi to potently and allele-selectively inhibit mutant huntingtin expression. *Cell* **150**: 895–908.
18. Bonnet, ME, Erbacher, P and Bolcato-Bellemin, AL (2008). Systemic delivery of DNA or siRNA mediated by linear polyethylenimine (L-PEI) does not induce an inflammatory response. *Pharm Res* **25**: 2972–2982.
19. Jäger, M, Schubert, S, Ochrimenko, S, Fischer, D and Schubert, US (2012). Branched and linear poly(ethylene imine)-based conjugates: synthetic modification, characterization, and application. *Chem Soc Rev* **41**: 4755–4767.
20. Höbel, S and Aigner, A (2013). Polyethylenimines for siRNA and miRNA delivery in vivo. *Wiley Interdiscip Rev Nanomed Nanobiotechnol* **5**: 484–501.
21. Goula, D, Remy, JS, Erbacher, P, Wasowicz, M, Levi, G, Abdallah, B *et al.* (1998). Size, diffusibility and transfection performance of linear PEI/DNA complexes in the mouse central nervous system. *Gene Ther* **5**: 712–717.
22. Shim, MS and Kwon, YJ (2009). Acid-responsive linear polyethylenimine for efficient, specific, and biocompatible siRNA delivery. *Bioconjug Chem* **20**: 488–499.
23. Zheng, M, Pavan, GM, Neeb, M, Schaper, AK, Danani, A, Klebe, G *et al.* (2012). Targeting the blind spot of polycationic nanocarrier-based siRNA delivery. *ACS Nano* **6**: 9447–9454.
24. Jiang, X, Zheng, Y, Chen, HH, Leong, KW, Wang, TH and Mao, HQ (2010). Dual-sensitive micellar nanoparticles regulate DNA unpacking and enhance gene-delivery efficiency. *Adv Mater* **22**: 2556–2560.
25. Lee, JS, Green, JJ, Love, KT, Sunshine, J, Langer, R and Anderson, DG (2009). Gold, poly(beta-amino ester) nanoparticles for small interfering RNA delivery. *Nano Lett* **9**: 2402–2406.
26. Li, Y, Zhou, W, Tong, Y, He, G and Song, W (2006). Control of APP processing and Abeta generation level by BACE1 enzymatic activity and transcription. *FASEB J* **20**: 285–292.
27. Wang, H, Ghosh, A, Baigude, H, Yang, CS, Qiu, L, Xia, X *et al.* (2008). Therapeutic gene silencing delivered by a chemically modified small interfering RNA against mutant SOD1 slows amyotrophic lateral sclerosis progression. *J Biol Chem* **283**: 15845–15852.
28. Williford, JM, Wu, J, Ren, Y, Archang, MM, Leong, KW and Mao, HQ (2014). Recent advances in nanoparticle-mediated siRNA delivery. *Annu Rev Biomed Eng* **16**: 347–370.
29. Mishra, S, Webster, P and Davis, ME (2004). PEGylation significantly affects cellular uptake and intracellular trafficking of non-viral gene delivery particles. *Eur J Cell Biol* **83**: 97–111.
30. Feng, G, Mellor, RH, Bernstein, M, Keller-Peck, C, Nguyen, QT, Wallace, M *et al.* (2000). Imaging neuronal subsets in transgenic mice expressing multiple spectral variants of GFP. *Neuron* **28**: 41–51.
31. Holguin, A, Frank, MG, Biedenkapp, JC, Nelson, K, Lippert, D, Watkins, LR *et al.* (2007). Characterization of the temporo-spatial effects of chronic bilateral intrahippocampal cannulae on interleukin-1beta. *J Neurosci Methods* **161**: 265–272.
32. Venkataraman, S, Hedrick, JL, Ong, ZY, Yang, C, Ee, PL, Hammond, PT *et al.* (2011). The effects of polymeric nanostructure shape on drug delivery. *Adv Drug Deliv Rev* **63**: 1228–1246.
33. Gratton, SE, Ropp, PA, Pohlhaus, PD, Luft, JC, Madden, VJ, Napier, ME *et al.* (2008). The effect of particle design on cellular internalization pathways. *Proc Natl Acad Sci U S A* **105**: 11613–11618.
34. Agarwal, R, Singh, V, Jurney, P, Shi, L, Sreenivasan, SV and Roy, K (2013). Mammalian cells preferentially internalize hydrogel nanodiscs over nanorods and use shape-specific uptake mechanisms. *Proc Natl Acad Sci USA* **110**: 17247–17252.
35. Shopsowitz, KE, Roh, YH, Deng, ZJ, Morton, SW and Hammond, PT (2014). RNAi-microsponges form through self-assembly of the organic and inorganic products of transcription. *Small* **10**: 1623–1633.
36. Afonin, KA, Kasprzak, WK, Bindewald, E, Kireeva, M, Viard, M, Kashlev, M *et al.* (2014). In silico design and enzymatic synthesis of functional RNA nanoparticles. *Acc Chem Res* **47**: 1731–1741.
37. Afonin, KA, Kireeva, M, Grabow, WW, Kashlev, M, Jaeger, L and Shapiro, BA (2012). Co-transcriptional assembly of chemically modified RNA nanoparticles functionalized with siRNAs. *Nano Lett* **12**: 5192–5195.
38. Kolhar, P, Anselmo, AC, Gupta, V, Pant, K, Prabhakarpandian, B, Ruoslahti, E *et al.* (2013). Using shape effects to target antibody-coated nanoparticles to lung and brain endothelium. *Proc Natl Acad Sci USA* **110**: 10753–10758.
39. Jiang, X, Qu, W, Pan, D, Ren, Y, Williford, JM, Cui, H *et al.* (2013). Plasmid-templated shape control of condensed DNA-block copolymer nanoparticles. *Adv Mater* **25**: 227–232.
40. Lee, H, Lytton-Jean, AK, Chen, Y, Love, KT, Park, AI, Karagiannis, ED *et al.* (2012). Molecularly self-assembled nucleic acid nanoparticles for targeted *in vivo* siRNA delivery. *Nat Nanotechnol* **7**: 389–393.
41. Israelachvili, JN. *Intermolecular and Surface Forces*. 3rd edition. Academic Press, Burlington, MA, 2011.
42. Menting, KW and Claassen, JA (2014). β-secretase inhibitor; a promising novel therapeutic drug in Alzheimer's disease. *Front Aging Neurosci* **6**: 165.
43. Reiman, EM (2014). Alzheimer's disease and other dementias: advances in 2013. *Lancet Neurol* **13**: 3–5.
44. Li, T, Wen, H, Brayton, C, Laird, FM, Ma, G, Peng, S *et al.* (2007). Moderate reduction of gamma-secretase attenuates amyloid burden and limits mechanism-based liabilities. *J Neurosci* **27**: 10849–10859.
45. Singer, O, Marr, RA, Rockenstein, E, Crews, L, Coufal, NG, Gage, FH *et al.* (2005). Targeting BACE1 with siRNAs ameliorates Alzheimer disease neuropathology in a transgenic model. *Nat Neurosci* **8**: 1343–1349.
46. Laird, FM, Cai, H, Savonenko, AV, Farah, MH, He, K, Melnikova, T *et al.* (2005). BACE1, a major determinant of selective vulnerability of the brain to amyloid-beta amyloidogenesis, is essential for cognitive, emotional, and synaptic functions. *J Neurosci* **25**: 11693–11709.
47. Kamat, CD, Shmueli, RB, Connis, N, Rudin, CM, Green, JJ and Hann, CL (2013). Poly(β-amino ester) nanoparticle delivery of TP53 has activity against small cell lung cancer *in vitro* and in vivo. *Mol Cancer Ther* **12**: 405–415.
48. Alvarez-Erviti, L, Seow, Y, Yin, H, Betts, C, Lakhal, S and Wood, MJ (2011). Delivery of siRNA to the mouse brain by systemic injection of targeted exosomes. *Nat Biotechnol* **29**: 341–345.
49. Passini, MA, Bu, J, Richards, AM, Kinnecom, C, Sardi, SP, Stanek, LM *et al.* (2011). Antisense oligonucleotides delivered to the mouse CNS ameliorate symptoms of severe spinal muscular atrophy. *Sci Transl Med* **3**: 72ra18.
50. Lima, WF, Prakash, TP, Murray, HM, Kinberger, GA, Li, W, Chappell, AE *et al.* (2012). Single-stranded siRNAs activate RNAi in animals. *Cell* **150**: 883–894.
51. Geng, Y, Dalhaimer, P, Cai, S, Tsai, R, Tewari, M, Minko, T *et al.* (2007). Shape effects of filaments versus spherical particles in flow and drug delivery. *Nat Nanotechnol* **2**: 249–255.
52. Osada, K, Shiotani, T, Tockary, TA, Kobayashi, D, Oshima, H, Ikeda, S *et al.* (2012). Enhanced gene expression promoted by the quantized folding of pDNA within polyplex micelles. *Biomaterials* **33**: 325–332.
53. Kamide, K, Nakakubo, H, Uno, S and Fukamizu, A (2010). Isolation of novel cell-penetrating peptides from a random peptide library using *in vitro* virus and their modifications. *Int J Mol Med* **25**: 41–51.
54. Atwal, JK, Chen, Y, Chiu, C, Mortensen, DL, Meilandt, WJ, Liu, Y *et al.* (2011). A therapeutic antibody targeting BACE1 inhibits amyloid-β production in vivo. *Sci Transl Med* **3**: 84ra43.
55. Rejman, J, Oberle, V, Zuhorn, IS and Hoekstra, D (2004). Size-dependent internalization of particles via the pathways of clathrin- and caveolae-mediated endocytosis. *Biochem J* **377**(Pt 1): 159–169.

Supplementary Information accompanies this paper on the Molecular Therapy–Nucleic Acids website (http://www.nature.com/mtna)

Submitted to ADVANCED HEALTHCARE MATERIALS

DOI: 10.1002/adhm.((please add manuscript number))

Article type: Communication

Reduction of Micellar Nanoparticle Size *via* Solvent-Induced Condensation Improves siRNA Delivery Efficiency *In Vivo*

Juan Wu†, Wei Qu†, John-Michael Williford†, Yong Ren, Xuesong Jiang, Xuan Jiang, Deng Pan, Erik Luijten, and Hai-Quan Mao**

Dr. Juan Wu, Department of Materials Science and Engineering, Johns Hopkins University, Baltimore, MD 21218, USA

Wei Qu, Department of Materials Science and Engineering, Northwestern University, Evanston, Illinois 60208, USA

John-Michael Williford, Department of Biomedical Engineering, Johns Hopkins School of Medicine, Baltimore, Maryland 21205, USA

Dr. Yong Ren, Department of Materials Science and Engineering, Johns Hopkins University, Baltimore, MD 21218, USA

Dr. Xuesong Jiang, Translational Tissue Engineering Center, Whitaker Biomedical Engineering Institute, Johns Hopkins School of Medicine, Baltimore, MD 21287, USA

Dr. Xuan Jiang, Department of Materials Science and Engineering, Johns Hopkins University, Baltimore, MD 21218, USA

Deng Pan, Department of Biomedical Engineering, Johns Hopkins School of Medicine, Baltimore, Maryland 21205, USA

Professor Erik Luijten, Department of Materials Science and Engineering, Northwestern University, Evanston, Illinois 60208; Department of Engineering Sciences and Applied Mathematics, Northwestern University, Evanston, Illinois 60208, USA

Email: luijten@northwestern.edu

Professor Hai-Quan Mao, Department of Materials Science and Engineering, Whiting School of Engineering, Johns Hopkins University, Baltimore, Maryland 21218; Translational Tissue Engineering Center and Whitaker Biomedical Engineering Institute, Johns Hopkins School of Medicine, Baltimore, Maryland 21287, USA

Email: hmao@jhu.edu

†These authors contributed equally to this work.

*Corresponding authors.

Keywords: gene therapy, siRNA delivery, nanoparticle, solvent polarity, size control

PEGylated polycationic carriers have been widely used for the condensation of DNA and RNA molecules into complex core micelles.[1] The PEG corona of these nanoparticles can significantly improve their *colloidal* stability in serum.[2] However, PEGylation of the carriers reduces their condensation capacity,[3] hindering the generation of micellar particles with sufficient *complex* stability. This presents a particularly significant challenge for packaging siRNA into complex micelles, as it has a much smaller size and more rigid chain structure than DNA plasmids. Here, we report a new method to enhance the condensation of siRNA with PEGylated linear polyethylenimine (lPEI) using organic solvent and to prepare smaller siRNA nanoparticles with a more extended PEG corona and higher stability. We have demonstrated the improved gene knockdown efficiency resulting from the reduced siRNA micelle size in mouse liver following intravenous administration.

RNA interference (RNAi) has been demonstrated to be a potent and highly specific post-translational gene regulation process.[4] Through the use of exogenously produced short interfering RNA (siRNA) specifically targeting the gene of interest, RNAi has demonstrated potential as an important therapeutic agent for the treatment of numerous disorders.[5] Delivery of naked siRNA molecules through intravenous injection, however, has failed to yield significant gene knockdown due to their poor pharmacokinetic profile resulting from high susceptibility to nuclease degradation and rapid renal clearance.[5b] Thus, the critical challenge in realizing the full therapeutic potential of siRNA-mediated gene knockdown centers on the development of a safe and effective delivery system. Among the currently explored delivery strategies,[6] polycationic nanoparticles have gained significant attention owing to their versatility and ease of formulation.[7] PEI is the most commonly used polycationic carrier, because of its high buffering capacity that facilitates endosomal escape of nanoparticles and siRNA into the cytoplasm.[8] PEI/siRNA nanoparticles typically carry

positive residual charges on their surface, which lead to significant aggregation in the presence of serum proteins, greatly reducing their efficacy *in vivo*.[9] In addition, they often elicit a high degree of inflammatory responses and toxicity, and are prone to clearance by macrophages following systemic administration, particularly for branched PEI.[10]

Decorating the particle surface with hydrophilic polyethylene glycol (PEG) has often been employed as an effective strategy to alleviate aggregation, reduce opsonization and inflammation response, and prolong nanoparticle circulation time.[11] PEGylation can be achieved by grafting PEG chains onto the polycation backbone. The resulting PEGylated polycations are able to complex with siRNA, forming micellar nanoparticles with a polycation/siRNA core and a PEG corona, where the steric shielding effect of the corona has been demonstrated to lessen aggregation of PEI-*g*-PEG/siRNA nanoparticles.[2] However, whereas a higher degree of PEG grafting density favors the colloidal stability and biocompatibility of the micelles, it reduces the RNA condensation capacity of the PEI-*g*-PEG carrier. Thus, it is a significant challenge to balance PEI-*g*-PEG/siRNA complex stability with colloidal stability and compatibility.

Our new approach employs a PEGylated linear PEI (lPEI) carrier, lPEI-*g*-PEG, which was synthesized by grafting PEG (M_n = 10 kDa) to the backbone of lPEI (M_n = 17 kDa; see *Supporting Information* for copolymer synthesis and characterization). We prepared an lPEI-*g*-PEG copolymer with an average of 4.6 PEG grafts per lPEI, and identified a minimal N/P ratio of 20 for complete siRNA condensation by agarose gel retardation assay (Figure S1). For all following experiments, we prepared siRNA micelles by mixing equal volumes of 200 μg/mL of lPEI-*g*-PEG solution and 20 μg/mL of siRNA solution (corresponding to an N/P ratio of 20) at room temperature. The intensity-averaged diameter of these lPEI-*g*-PEG/siRNA micelles prepared in water was 117 ± 2.3 nm, as measured by dynamic light scattering (DLS; **Figure 1**A, F). On the other hand, lPEI/siRNA nanoparticles exhibited a

slightly smaller diameter of 96.8 ± 10.3 nm (Figure 1A, E). Whereas this size difference may be attributed to the PEG corona, it is nevertheless remarkable given our observations for plasmid DNA, where condensation with block copolymers significantly *reduced* the size of the micelles compared to condensation with polyelectrolytes alone.[12]

To understand this apparent discrepancy, we performed molecular (MD) dynamics simulations of complexation between siRNA and lPEI-*g*-PEG copolymer. We emphasize that both the time scale and the number of particles involved in the complexation processes make coarse-graining (as described in the *Supporting Information*) imperative. However, prior work has shown this approach to be highly suitable for providing meaningful insight into the underlying mechanisms.[12] In addition to the electrostatic interactions between siRNA and lPEI (taken into account via Ewald summation[13]), and the lPEI–solvent and PEG–solvent interactions,[12] we also incorporated the interaction between lPEI and PEG arising from direct hydrogen bonding and from hydrogen bond bridges with water molecules, as lPEI is known to form strong inter- and intra-molecular hydrogen bonds in water.[14] Given that PEG not only has a molecular structure similar to lPEI, but also has a hydrogen bond acceptor in its repeat unit, we adopted the same effective interaction strength for PEG–lPEI as for lPEI–lPEI.[14] To compare to the intensity-averaged distribution of the hydrodynamic diameter measured by DLS, we report the *Z*-averaged[15] radius of gyration of the lPEI-*g*-PEG/siRNA nanoparticles calculated in simulation (Figure 1B). The modeling results indeed matched the experimental observation that the complexation of siRNA with lPEI-*g*-PEG copolymer results in a slight *increase* in particle size. This increase did not arise merely from the physical extent of the PEG corona: the average number of siRNA particles per micelle increased from 7.1 ± 1.3 to 9.4 ± 1.3. We hypothesized that this size increase can be attributed to the lPEI–PEG interaction. To test this conjecture, we performed a second set of simulations of the complexation of siRNA with lPEI-*g*-PEG copolymer, in which we artificially decreased the

attractive interaction between lPEI and PEG (Figure S4). We indeed observed that a weakening of the PEG–lPEI interaction significantly reduces the particle size.

Prompted by this observation, we aimed to condense lPEI-*g*-PEG/siRNA micelles into smaller nanoparticles by disrupting the interaction between lPEI and PEG mediated by hydrogen bonding with water molecules. We added dimethylformamide (DMF), a water-miscible solvent that has been shown to effectively reduce intermolecular hydrogen bonding in other polymeric micelle systems,[16] to siRNA and lPEI-*g*-PEG solutions prior to micelle assembly. In a 7:3 (v/v) DMF–water mixture, we indeed observed a far smaller average particle size of 44.2 ± 6.6 nm (Figure 1C, G). This size reduction of micelles in response to a decrease in solvent polarity was confirmed by MD simulations (Figure 1D). Arguably, the polarity reduction also leads to a decrease in siRNA solubility,[17] which in turn could have resulted in stronger condensation and a growth in aggregate size.[12] We conclude that this effect is overshadowed by the reduction of PEG–lPEI and lPEI–lPEI hydrogen bonding which in turn permits the PEG corona to provide steric shielding.

Whereas DMF as a co-solvent can significantly reduce particle size, it needs to be removed prior to nanoparticle transfection experiments *in vitro* or *in vivo*. However, DMF removal by dialysis resulted in nanoparticle swelling (data not shown). To preserve the nanoparticle size in aqueous media upon DMF removal, we employed a reversible disulfide crosslinking scheme previously tested in DNA/polymer nanoparticles.[12] We introduced thiol groups to the lPEI block and used the purified thiolated lPEI-*g*-PEG to condense siRNA using the protocol described above. Crosslinking was initiated by aerial oxidation over a 48-h incubation at room temperature followed by dialysis to remove the DMF. TEM micrographs in **Figure 2**A-B confirm that no appreciable change in particle size or morphology occurred following solvent removal. The crosslinking was verified by gel electrophoresis (Figure 2C): without disulfide crosslinks, nanoparticles released siRNA upon challenge with an excess amount of dextran

sulfate, a polyanion that can effectively compete with siRNA to complex with lPEI. On the other hand, crosslinked micelles released siRNA under the same conditions only after the disulfide bonds were reduced.

The PEG corona of lPEI-*g*-PEG/siRNA micelles significantly reduced the nanoparticle zeta potential from +30 mV to about +5 mV when condensed in water. Condensation in DMF–water (7:3, v/v) mixture followed by crosslinking and removal of solvent, reduced the zeta potential even further to –8 mV (Figure S2), likely due to the increase of the PEG density at the surface and reduction of imines on the complex core that reacted with the crosslinkers. The near-neutral surface charge on these micelles enhances their colloidal stability in physiological media through suppression of serum protein-mediated agglomeration. Indeed, these crosslinked micelles showed no significant change in particle size in 10% serum (Figure 2D–E). Owing to the covalent crosslinks, these micelles also exhibited high complex stability; they did not show any size change when incubated in the presence of 150 mM sodium chloride (Figure 2F). On the other hand, uncrosslinked lPEI-*g*-PEG/siRNA micelles were destabilized within 30 min of salt challenge.

We anticipated a smaller average particle size to result in more efficient cellular uptake and transfection. To confirm, we first measured the cellular uptake efficiency and gene knockdown efficiency *in vitro*. We also prepared 117-nm micelles that were crosslinked similarly to the 44-nm micelles to exclude differences resulting from the crosslinking. The crosslinked 44-nm micelles displayed 30% and 57% increase of uptake in a hepatocellular carcinoma cell line (HepG2) compared to the crosslinked and uncrosslinked 117-nm micelles, respectively (**Figure 3**A). *In vitro* gene knockdown experiments showed that both the crosslinked 117-nm and 44-nm micelles achieved about 60% decrease in targeted protein expression, an efficiency similar to that of lPEI/siRNA nanoparticles. The uncrosslinked micelles only showed 30% knockdown efficiency, likely due to their limited stability in cell

culture media. In addition, all tested particles maintained a high cell metabolic activity (>80% compared to untreated cells, Figure S3). As an *in vivo* proof of concept, we assessed the effect of reduced nanoparticle size on gene knockdown efficiency in the rat liver following intravenous administration (Figure 3C). We first established high luciferase expression in the liver *via* hydrodynamic infusion of luciferase plasmid DNA.[18] After the transgene expression level stabilized at 5 d post-infusion, lPEI-*g*-PEG/siRNA micelles or lPEI/siRNA nanoparticles containing 80 μg luciferase siRNA were administered *via* tail vein injection. The 44-nm micelles displayed 85% and 70% efficiencies of transgene knockdown in the liver at 24 h and 48 h after injection, respectively. In contrast, the 117-nm micelles only showed ~30% knockdown at both 24 h and 48 h ($p < 0.05$). This significant increase in gene knockdown efficiency for the smaller nanoparticles may be attributed to improved nanoparticle deposition and increased cellular uptake of the smaller nanoparticles. On the other hand, the uncrosslinked micelles and lPEI/siRNA nanoparticles did not show significant knockdown at 24 h and yielded a low level (~15%) of transgene knockdown at 48 h after injection, suggesting that nanoparticle stability in medium is crucial to siRNA delivery *in vivo*. It is important to note that the gene knockdown activity mediated by the 44-nm siRNA nanoparticles is among the highest obtained *via* intravenous injection at such a relatively low siRNA dose (~0.4 mg/kg body weight), without employing any active targeting strategy.[19]

In conclusion, this study provides the first evidence of solvent-assisted condensation of lPEI-*g*-PEG/siRNA micelles to decrease nanoparticle size. By reducing solvent polarity, we decreased the average size of lPEI-*g*-PEG/siRNA micelles from 117 nm in water to 44 nm. Through molecular dynamics simulation we revealed the role of solvent quality and PEI–PEG hydrogen bonding in the assembly of lPEI-*g*-PEG/siRNA micelles. The micelle size was preserved after organic solvent removal by means of reversible disulfide crosslinking; we confirmed that the micelles maintained their size in water and physiological media. More

importantly, our results have demonstrated size-dependent *in vivo* transfection efficiency following intravenous injection of the siRNA micelles in rats. The gene knockdown efficiency in rat liver achieved by the smaller siRNA micelles was significantly higher than for the larger micelles prepared from the same copolymer carrier. The condensation technique introduced here allows a simple and effective way to reduce siRNA particle size and provides a model platform for further study of the effect of particle size on *in vivo* cellular uptake, knockdown efficiency, biodistribution, and pharmacokinetics. As such, it can form the starting point for the development of an effective delivery system that harnesses the therapeutic potential of siRNA.

Experimental Section

Preparation of lPEI-g-PEG/siRNA micelles: 1.33 μg siRNA (Qiagen, Valencia, CA) was first dissolved in 50 μL DI water or 7:3 (v/v) DMF–water mixture and then added to an equal volume of lPEI-*g*-PEG polymer solution at an N/P ratio of 20 prepared in the same mixing solvent. The mixture was vortexed and then incubated for 30 min at room temperature before further characterization. Crosslinked micelles were prepared according to a protocol that we established previously.[12] Micelle characterization methods can be found in the *Supplementary Information*.

Modeling of lPEI-g-PEG/siRNA micelles: Molecular dynamics simulations were performed using coarse-grained models. lPEI-*g*-PEG was represented as a bead–spring polymer model with bead size 7.35 Å and charge density 35%. The siRNA molecule was coarse-grained as a 24-bead rigid body using the VMD Shape-Based Coarse-Graining (SBCG) tool,[20] based on a 22 bp RNA molecule isolated from the Protein Data Bank file 2F8S.[21] To increase the computational efficiency, we scaled down each coarse-grained model to one fourth of its original length. The solvent was simulated implicitly using a Langevin thermostat, and

different solvent compositions were represented through variation of the attractive strength of a Lennard-Jones potential. Monovalent counterions were included to maintain system charge neutrality, and electrostatic interactions were computed using the Ewald method. To accelerate the disassociation and reformation of aggregates, we employed the parallel tempering method,[22] in which 24 copies of the same system were simulated in parallel, at closely spaced temperatures. This approach exploits the larger degree of fluctuations at higher temperatures to provide pathways that permit the simulation at the original temperature to transition between different states of low free energy.

In vitro cell uptake and gene silencing of lPEI-g-PEG/siRNA micelles: HepG2 cells were maintained in Dulbecco's Modified Eagle's Medium (DMEM) supplemented with 10% fetal bovine serum (FBS) and 100 U/mL Penicillin / 100 μg/mL Streptomycin at 37°C and 5% CO_2. At 24 h prior to the experiment, cells were seeded in 24-well plates at a density of 5×10^4 cells/well. For cell uptake studies, micelles were prepared with Alexa Fluor 488-modified siRNA (Qiagen, Valencia, CA). An aliquot of 50 μL micelles equivalent to 100 nM siRNA was added to each well followed by 4 h incubation at 37°C, after which the cells were washed with PBS, trypsinized, and fixed with 2% paraformaldehyde. Fluorescence associated with individual cells was analyzed with a BD FACSCalibur flow cytometer (BD Biosciences) fitted with a 488-nm excitation source and detected using a 515–545 nm filter. A minimum of 10,000 events per sample were collected for analysis. Gene silencing studies were performed using a previously reported protocol.[23]

In vivo gene knockdown efficiency of siRNA micelles via intravenous administration: Animal studies were conducted under a protocol that was approved by the Johns Hopkins School of Medicine Institutional Animal Care and Use Committee (IACUC # RA09A447). A liver-specific gene knockdown model was developed by modification of previously published

protocols.[24] Wistar rats (female, 6–8 weeks, 200–300 g) were transfected with a firefly luciferase plasmid DNA (20 μg DNA in PBS with a volume corresponding to 9 vol/wt% of the rat's body weight) *via* hydrodynamic infusion administered through the tail vein over 15 s according to a published procedure.[25] After 5 days, micelles containing 80 μg siRNA in 1 mL PBS were injected *via* the tail vein. At 24 and 48 h, rats were anesthetized and given 1 mL of D-luciferin solution (*i.p.* 30 mg/mL). The rat was then imaged on an IVIS Spectrum Imaging System. The bioluminescence signal was collected for 1 min, and the level of luciferase expression was expressed as the total photon count per section in the region of interest and was normalized to PBS control to determine knockdown efficiency.

Statistical Analysis: All data were expressed as mean ± SD unless otherwise noted. Statistical comparisons were carried out using a one-way analysis of variance (ANOVA) followed by Turkey's post-hoc test for groups with equal variance or Games–Howell test for groups with unequal variance (SPSS software, version 21, SPSS Inc.). All data were considered to be significant at $p < 0.05$.

Supporting Information

Supporting Information is available from the Wiley Online Library or from the author.

Acknowledgements

Funding for this study was provided by NIH grants R21EB015152, R21EB013274-01A1, and U54CA151838 and NSF grant DMR-1006430, as well as a pilot grant for the Institute of NanoBioTechnology at Johns Hopkins University. We acknowledge computing resources provided by the Quest High-Performance Computing Facility at Northwestern University. J. Wu, W. Qu, and J.-M. Williford contributed equally to this work.

Received: ((will be filled in by the editorial staff))

Revised: ((will be filled in by the editorial staff))

Published online: ((will be filled in by the editorial staff))

References:

[1] K. Osada, R. J. Christie, K. Kataoka, *J. R. Soc. Interface* **2009**, *6 Suppl. 3*, S325.

[2] S. Mao, M. Neu, O. Germershaus, O. Merkel, J. Sitterberg, U. Bakowsky, T. Kissel, *Bioconjug. Chem.* **2006**, *17*, 1209.

[3] O. M. Merkel, A. Beyerle, D. Librizzi, A. Pfestroff, T. M. Behr, B. Sproat, P. J. Barth, T. Kissel, *Mol. Pharm.* **2009**, *6*, 1246.

[4] A. Fire, S. Q. Xu, M. K. Montgomery, S. A. Kostas, S. E. Driver, C. C. Mello, *Nature* **1998**, *391*, 806.

[5] a.) D. Bumcrot, M. Manoharan, V. Koteliansky, D. W. Y. Sah, *Nat. Chem. Biol.* **2006**, *2*, 711; b.) D. Castanotto, J. J. Rossi, *Nature* **2009**, *457*, 426.

[6] B. Khurana, A. K. Goyal, A. Budhiraja, D. Arora, S. P. Vyas, *Curr. Gene Ther.* **2010**, *10*, 139.

[7] K. A. Howard, *Adv. Drug Deliv. Rev.* **2009**, *61*, 710.

[8] A. Akinc, M. Thomas, A. M. Klibanov, R. Langer, *J. Gene Med.* **2005**, *7*, 657.

[9] T. Nomoto, Y. Matsumoto, K. Miyata, M. Oba, S. Fukushima, N. Nishiyama, T. Yamasoba, K. Kataoka, *J. Control. Release* **2011**, *151*, 104.

[10] a.) D. E. Owens, N. A. Peppas, *Int. J. Pharm.* **2006**, *307*, 93; b.) O. M. Merkel, R. Urbanics, P. Bedocs, Z. Rozsnyay, L. Rosivall, M. Toth, T. Kissel, J. Szebeni, *Biomaterials* **2011**, *32*, 4936.

[11] J. V. Jokerst, T. Lobovkina, R. N. Zare, S. S. Gambhir, *Nanomedicine* **2011**, *6*, 715.

[12] X. Jiang, W. Qu, D. Pan, Y. Ren, J. Williford, H. Cui, E. Luijten, H. Q. Mao, *Adv. Mater.* **2013**, *25*, 227.

[13] a.) C. Guáqueta, E. Luijten, *Phys. Rev. Lett.* **2007**, *99*, 138302; b.) P.-Y. Hsiao, E. Luijten, *Phys. Rev. Lett.* **2006**, *97*, 148301; c.) L. K. Sanders, W. Xian, C. Guáqueta,

M. J. Strohman, C. R. Vrasich, E. Luijten, G. C. L. Wong, *Proc. Natl. Acad. Sci. USA* **2007**, *104*, 15994.

[14] P. A. Gembitskii, N. A. Kleshcheva, A. I. Chmarin, D. S. Zhuk, *Polymer Science U.S.S.R.* **1978**, *20*, 2932.

[15] F. R. Hallett, J. Watton, P. Krygsman, *Biophys. J.* **1991**, *59*, 357.

[16] D. Chen, M. Jiang, *Acc. Chem. Res.* **2005**, *38*, 494.

[17] G. B. Jacobson, R. Shinde, R. L. McCullough, N. J. Cheng, A. Creasman, A. Beyene, R. P. Hickerson, C. Quan, C. Turner, R. L. Kaspar, C. H. Contag, R. N. Zare, *J. Pharm. Sci.* **2010**, *99*, 2750.

[18] H. Herweijer, J. A. Wolff, *Gene Ther.* **2007**, *14*, 99.

[19] a.) A. Akinc, M. Goldberg, J. Qin, J. R. Dorkin, C. Gamba-Vitalo, M. Maier, K. N. Jayaprakash, M. Jayaraman, K. G. Rajeev, M. Manoharan, V. Koteliansky, I. Roehl, E. S. Leshchiner, R. Langer, D. G. Anderson, *Mol. Ther.* **2009**, *17*, 872; b.) D. J. Siegwart, K. A. Whitehead, L. Nuhn, G. Sahay, H. Cheng, S. Jiang, M. Ma, A. Lytton-Jean, A. Vegas, P. Fenton, C. G. Levins, K. T. Love, H. Lee, C. Cortez, S. P. Collins, Y. F. Li, J. Jang, W. Querbes, C. Zurenko, T. Novobrantseva, R. Langer, D. G. Anderson, *Proc. Natl. Acad. Sci. USA* **2011**, *108*, 12996; c.) H.-X. Wang, M.-H. Xiong, Y.-C. Wang, J. Zhu, J. Wang, *J. Control. Release* **2013**, *166*, 106.

[20] a.) A. Arkhipov, P. L. Freddolino, K. Schulten, *Structure* **2006**, *14*, 1767; b.) A. Arkhipov, Y. Yin, K. Schulten, *Biophys. J.* **2008**, *95*, 2806.

[21] Y.-R. Yuan, Y. Pei, H.-Y. Chen, T. Tuschl, D. J. Patel, *Structure* **2006**, *14*, 1557.

[22] D. Frenkel, B. Smit, *Understanding Molecular Simulations*, Academic Press, San Diego, USA **2002**.

[23] M. Nakanishi, R. Patil, Y. Ren, R. Shyam, P. Wong, H. Q. Mao, *Pharm. Res.* **2011**, *28*, 1723.

[24] a.) S. E. L. Andaloussi, T. Lehto, I. Mager, K. Rosenthal-Aizman, Oprea, II, O. E. Simonson, H. Sork, K. Ezzat, D. M. Copolovici, K. Kurrikoff, J. R. Viola, E. M. Zaghloul, R. Sillard, H. J. Johansson, F. S. Hassane, P. Guterstam, J. Suhorutsenko, P. M. D. Moreno, N. Oskolkov, J. Halldin, U. Tedebark, A. Metspalu, B. Lebleu, J. Lehtio, C. I. E. Smith, U. Langel, *Nucleic Acids Res.* **2011**, *39*, 3972; b.) S. I. Kim, D. Shin, T. H. Choi, J. C. Lee, G. J. Cheon, K. Y. Kim, M. Park, M. Kim, *Mol. Ther.* **2007**, *15*, 1145.

[25] H. Maruyama, N. Higuchi, Y. Nishikawa, S. Kameda, N. Iino, J. J. Kazama, N. Takahashi, M. Sugawa, H. Hanawa, N. Tada, J. Miyazaki, F. Gejyo, *J. Gene Med.* **2002**, *4*, 333.

Figures

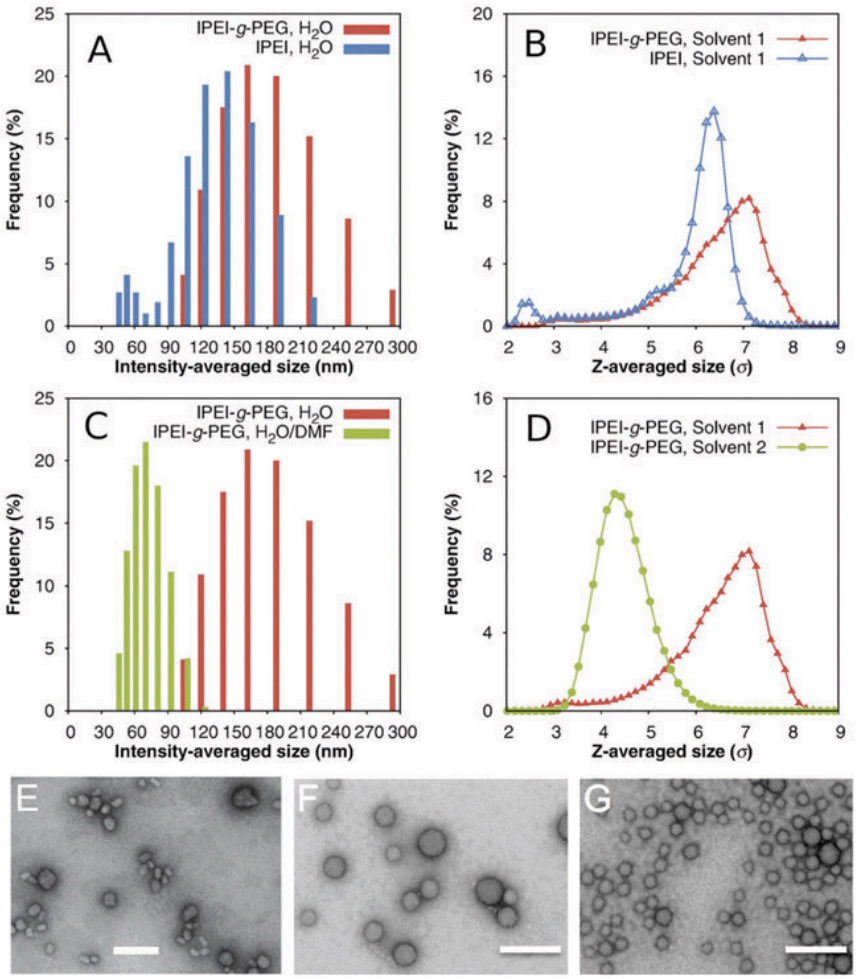

Figure 1. Size distribution of lPEI-*g*-PEG/siRNA micelles in different solvents. (A) Size distribution of lPEI-*g*-PEG/siRNA micelles and lPEI/siRNA nanoparticles prepared in water, as determined by dynamic light scattering; (B) Simulation results for size distributions of lPEI-*g*-PEG/siRNA micelles and lPEI/siRNA nanoparticles in water; (C) Size distribution of lPEI-*g*-PEG/siRNA micelles prepared in pure water and 7:3 (v/v) DMF–water mixture; (D) Simulation results for size distribution of lPEI-*g*-PEG/siRNA micelles in pure water (labeled "Solvent 1") and 7:3 (v/v) DMF–water mixture (labeled "Solvent 2"); (E–G) TEM images of lPEI/siRNA nanoparticles (E), lPEI-*g*-PEG/siRNA micelles prepared in pure water (F), and lPEI-*g*-PEG/siRNA micelles prepared in DMF–water mixture (G), respectively. All scale bars represent 200 nm.

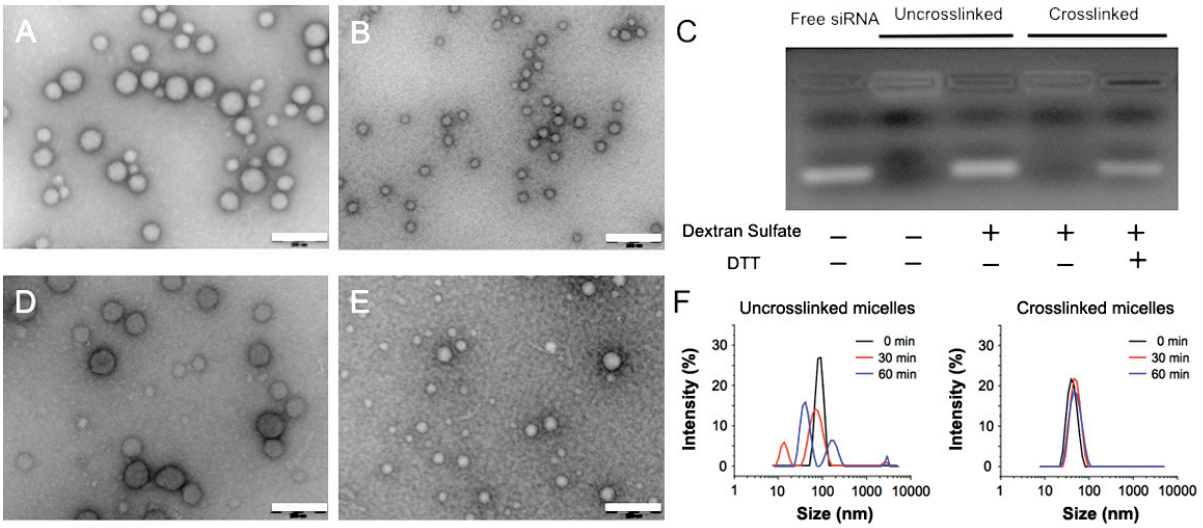

Figure 2. Preservation of size of lPEI-*g*-PEG/siRNA micelles *via* reversible disulfide crosslinking. (A–B) TEM images of crosslinked nanoparticles initially prepared in pure water (A) and in 7:3 (v/v) DMF–water mixture (imaged after removal of solvent) (B); (C) siRNA release from uncrosslinked and crosslinked lPEI-*g*-PEG/siRNA micelles in the presence of dextran sulfate and 50 mM dithiothreitol (DTT) in water; (D–E) TEM images of crosslinked micelles initially prepared in pure water (D) and 7:3 (v/v) DMF–water mixture (E), respectively, following 1 h incubation with 10% (v/v) FBS. (F) Size distributions of uncrosslinked and crosslinked lPEI-*g*-PEG/siRNA micelles following incubation with 0.15 M NaCl for 1 h. All scale bars represent 200 nm.

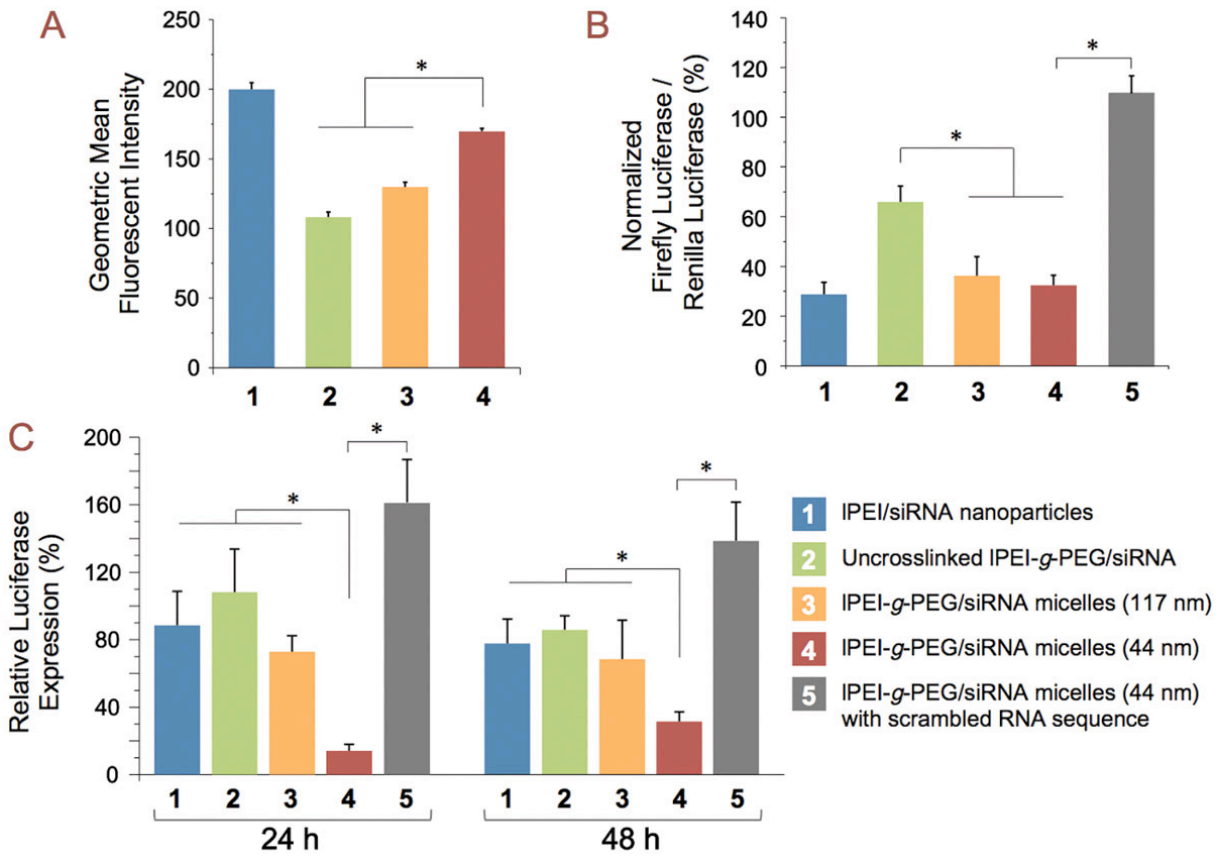

Figure 3. Size-dependent transfection efficiency of lPEI-*g*-PEG/siRNA micelles. (A) *In vitro* cellular uptake of Alexa Fluor 488-labeled micelles in HepG2 cells. Bars represent mean ± SD (n = 3); (B) *In vitro* gene knockdown efficiency in HepG2 cells following 100 nM equivalent dose of siRNA. Bars represent mean ± SD (n = 3); (C) *In vivo* gene silencing in rat liver at 24 h and 48 h after administration of nanoparticles at a dose equivalent to 80 μg siRNA *via* tail vein injection. Bars indicate mean relative luciferease expression ± SD (n = 4–7). *p <0.05.

Submitted to ADVANCED HEALTHCARE MATERIALS

Supporting Information

for ***Adv. Healthcare Mater.***, DOI: 10.1002/adhm.

Reduction of Micellar Nanoparticle Size via Solvent-Induced Condensation Improves siRNA Delivery Efficiency *In Vivo*

Juan Wu[†]*, Wei Qu*[†]*, John-Michael Williford*[†]*, Yong Ren, Xuesong Jiang, Xuan Jiang, Deng Pan, Erik Luijten*[*]*, and Hai-Quan Mao*[*]

[†]These authors contributed equally to this work.

[*]Corresponding authors.

1. Experimental Methods

1.1. Synthesis and characterization of lPEI-g-PEG copolymer

A PEGylated linear PEI (lPEI) copolymer, lPEI-g-PEG, was synthesized by grafting 10 kDa PEG to lPEI with an average M_n of 17 kDa. We chose lPEI owing to its lower cytotoxicity compared to branched PEI,[1] and selected lPEI of relatively high M_n for its higher siRNA condensation capacity and transfection efficiency compared to lPEI of lower molecular weight.[2] The 10 kDa PEG grafts were chosen based upon their ability to provide more effective resistance to protein adsorption and better protection against nuclease degradation than PEG of lower molecular weight.[3]

Linear polyethyleneimine HCl salt (lPEI·HCl, M_n = 17 kDa) was purchased from Polymer Chemistry Innovations, Inc. (Tucson, AZ). N-hydroxysuccinimidyl ester of methoxy polyethylene glycol hexanoic acid (PEG-NHS, M_n = 10 kDa) was purchased from NOF America Corporation (White Plains, NY). The lPEI·HCl (7.95 mg, 0.1 mmol of amine) was dissolved in 1 mL of DI water. The pH of the solution was adjusted to 6 through drop-wise addition of 1 M NaOH solution. The solution was then mixed with 80 mg of PEG-NHS and incubated overnight. The reaction mixture was dialyzed against DI water and lyophilized to yield a white foam-like solid with a 95% yield. The molecular weight of the graft copolymer was characterized by gel permeation chromatography using an Agilent 1200 series Isocratic HPLC System equipped with TSKgel G3000PWxl-CP column and TSKgel G5000PWxl-CP column (Tosoh America, Inc., Grove City, OH), which was connected with a multi-angle light scattering detector (MiniDawn, Wyatt Technology, Santa Barbara, CA). The grafting degree of PEG on lPEI was found to be 1.2%, which corresponds to an average of 4.6 PEG grafts per lPEI.

1.2. Gel electrophoresis analysis of polycation/siRNA nanoparticles

To investigate polycation/siRNA condensation, equal volumes of polymer and siRNA solution were mixed at increasing N/P ratios (molar ratio of amine in lPEI to phosphate in RNA) followed by electrophoresis at 90 V for 40 min on a 1.2 wt% agarose gel. To determine siRNA release from uncrosslinked and crosslinked particles, 20 μM sodium dextran sulfate (M_n =

200 kDa) in 10 mM Tris-HCl (pH 7.4) buffer was added to equal volume of nanoparticle solution containing 1 μM siRNA. The mixed solution was further incubated in the presence or absence of 50 mM DTT overnight at 37°C. An aliquot of each sample was then subjected to electrophoresis as above. The siRNA bands were visualized under a UV transilluminator. **Figure S1** displays the gel retardation analysis, confirming that a minimum N/P ratio of 20 is needed to completely condense siRNA under the tested conditions.

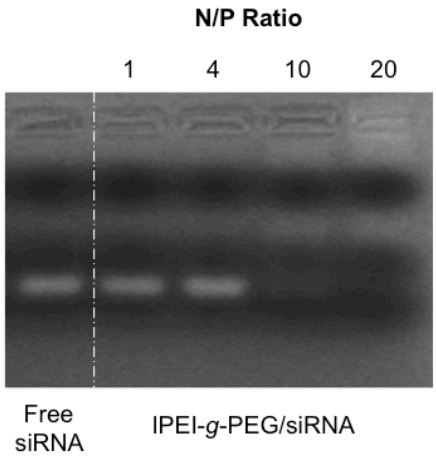

Figure S1. Gel retardation assay of complexation between lPEI-*g*-PEG and siRNA at increasing N/P ratios. Note the faint siRNA band for an N/P ratio of 10.

1.3. Transmission electron microscopy (TEM)

Samples were prepared by depositing 10 μL nanoparticle solution on a freshly ionized nickel grid covered by a carbon film. After 10 min, excess liquid was removed by pipetting. A drop of 2% uranyl acetate solution (~5 μL) was then deposited on the grid for 10 s and subsequently removed. After drying at room temperature, the samples were examined on a Tecnai FEI-12 electron microscope.

1.4. Preparation of crosslinked lPEI-g-PEG/siRNA nanoparticles

lPEI-*g*-PEG copolymer was thiolated with Traut's reagent at a 20% grafting degree of the total amino groups for 2 h at room temperature. The thiolated polymer solution was mixed with siRNA, and the micelle solution was transferred to a dialysis membrane with MWCO of 3.5 kDa

and then subjected to aerial oxidation for 48 h with stirring. The solution was further dialyzed against water for an additional 24 h to remove DMF.

1.5. Nanoparticle size and zeta potential measurements

Particle size and zeta potential were measured by photon correlation spectroscopy and laser Doppler anemometry, respectively, using a Zetasizer Nano ZS90 (Malvern Instruments, Southborough, MA). Size measurement was performed at 25°C at a 90° scattering angle. The mean hydrodynamic diameter was determined by cumulative analysis. The zeta potential measurements were performed using a DTS1060-folded capillary cell in the automatic mode. **Figure S2** reveals the average zeta potential of lPEI-*g*-PEG/siRNA micelles before and after crosslinking, revealing a decrease in particle zeta potential from +5 mV to –5 and –8 mV for 117 nm and 44 nm particles, respectively.

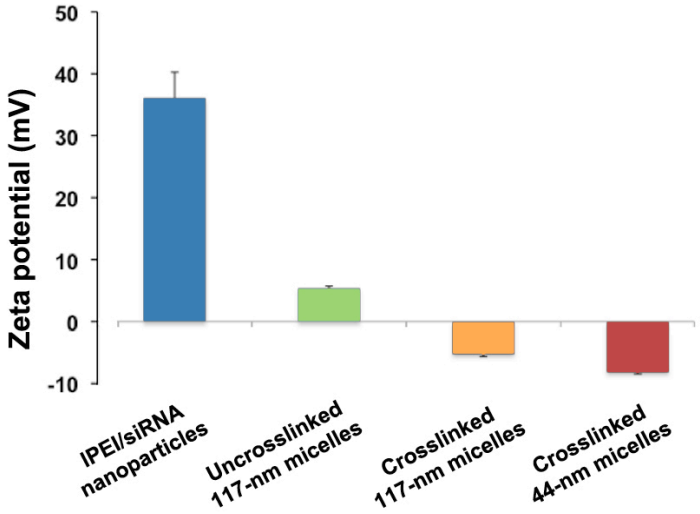

Figure S2. Zeta potential of lPEI-*g*-PEG/siRNA micelles before crosslinking and after crosslinking in both DI water and 7:3 (v/v) DMF–water mixture. Bars show mean ± SD (*n* = 3).

1.6. Characterization of in vitro gene knockdown efficiency

For gene silencing *in vitro*, cells were pre-transfected with 720 ng/well pGL3 DNA, encoding for firefly luciferase, and 80 ng/well pRL-CMV, encoding for Renilla luciferase, using Lipofectamine 2000 according to our previously published protocol. After 4 h, cells were transfected with nanoparticles carrying GL3 siRNA (sense strand

5'-CUUACGCUGAGUACUUCGAdTdT-3', antisense strand 5'-UCGAAGUACUCAGCGUAAGdTdT-3'), or a negative control sequence (AllStars Neg. siRNA, Qiagen, Valencia, CA) at a dose equivalent to 100 nM siRNA. After 48 h, cells were rinsed with PBS and assayed for luciferase expression using a dual luciferase reporter assay kit (Promega, WI). For each well, firefly and Renilla luciferase luminescence was measured using a FLUOstar OPTIMA plate reader (BMG Labtech, Germany). Firefly readings were normalized against Renilla readings, and values were expressed as a ratio to the untreated control.

1.7. Characterization of cytotoxicity of polycation/siRNA nanoparticles

Cytotoxicity of siRNA nanoparticles was determined by a WST-1 dye reduction assay. HepG2 cells were seeded in a 96-well plate 24 h before assay at a density of 20,000 cells/well. The cells were incubated for 4 h with 100 μL complete medium containing nanoparticles at a dose equivalent to 100 nM of siRNA. The medium in each well was then replaced with 100 μL fresh medium containing 10 μL WST-1 reagent (Roche, Mannheim, Germany). The cells were incubated for 1 h at 37°C. The absorbance of the supernatant at 450 nm, using 600 nm as a reference wavelength, was measured on a microplate reader (Infinite M200, TECAN, Männedorf, Switzerland). **Figure S3** illustrates the metabolic activity of HepG2 cells that were treated with different formulations of lPEI-*g*-PEG/siRNA micelles. All formulations maintained >80% cell viability at the tested concentrations.

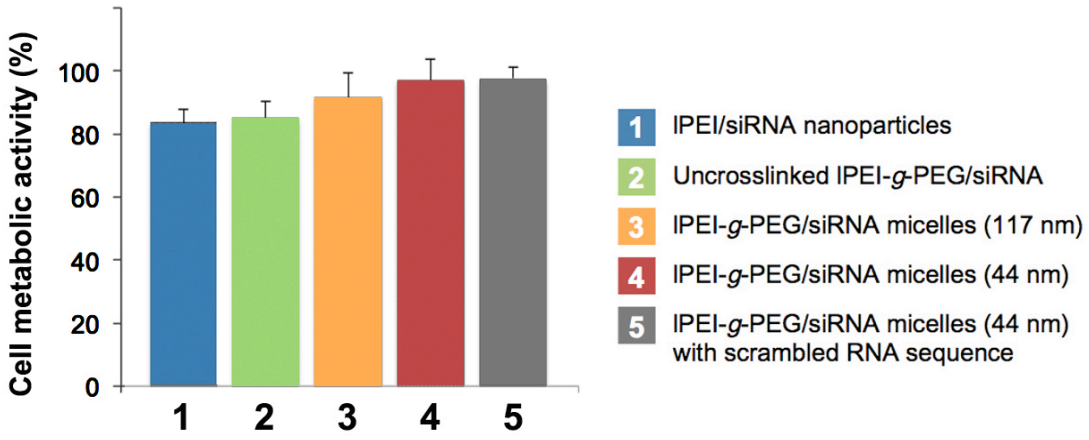

Figure S3. Metabolic activities of HepG2 cells treated with lPEI-*g*-PEG/siRNA micelles at a dose equivalent to 100 nM siRNA. Bars show mean ± SD (n = 4).

2. Computational Methods

2.1. Simulation model and coarse-graining procedure

Molecular dynamics simulations were performed using the LAMMPS package.[4] The large length and time scales involved in micelle formation make it essential to employ coarse-grained models of lPEI, lPEI-*g*-PEG copolymer, and siRNA. The Bjerrum length in water is 7.1 Å, which was chosen as the Lennard-Jones (LJ) unit of distance σ in our simulations. Since lPEI and PEG share a similar molecular structure, we treated them equivalently in the coarse-graining procedure and adopted the same monomer length of 3.5 Å and intrinsic persistence length of 3.8 Å.[5] Three persistence length units were represented as one bead in the model. Based on the blob concept, each bead has a size of approximately 1σ (size of blob ≈ $3^{0.6}$ × 3.8 Å = 7.35 Å ≈ σ). Clearly, for such short segments, the scaling behavior of a long self-avoiding polymer does not fully apply. Nonetheless, this coarse-graining procedure provides a consistent approach to estimate the length of the coarse-grained polymer models for our simulation (*cf.* **Table S1**).

Structural Parameter	PEG	lPEI
Molecular weight (g/mol)	9,500	17,000
Number of monomers	225	386
Number of persistence length segments*	207	356
Number of beads in coarse-grained model*	69	119

Table S1. Molecular weights of PEG and lPEI used in experiments and number of beads in coarse-grained PEG and lPEI models used in simulations. (*Assuming lPEI and PEG have the same persistence length and the same monomer size.)

For lPEI, we used a charge density of approximately 35%[6], corresponding to a pH of 6–7, as used in the experiments. The charges were evenly distributed along the model beads and each bead carried a charge of 1.12*e* (this includes a factor 3.8/3.5 to account for the ratio between persistence length and monomer size). The siRNA molecule was coarse-grained using the VMD

Shape-Based Coarse-Graining (SBCG) tool[7], which approximates the shape of a molecule using a specified number of beads, and outputs the positions of each bead, the equilibrium bond length between beads, and the charge on each bead. Although the SBCG tool produces a (narrow) distribution of bead sizes, we opted for beads of uniform size σ (7.1 Å) to avoid inhomogeneous short-range and electrostatic interactions (the LJ radius of beads affects the contact strength of their electrostatic interaction as well as the range of their LJ interaction). This uniformity was achieved by adjusting the number of coarse-grained beads until the average bead size was close to 7.1 Å, and then setting all beads to this uniform size. For the coarse graining of siRNA, we isolated a 22 bp RNA molecule from the Protein Data Bank file 2F8S[8] and coarse-grained it into a 24-bead rigid body.

In the coarse-grained models, all harmonic interactions were represented by

$$U_{\text{bond}} = 200\varepsilon\left(r - r_0\right)^2 , \quad (1)$$

where r is the center-to-center distance between two bonded beads and r_0 is the equilibrium bond length, with ε the LJ unit of energy. For lPEI and PEG, r_0 was set to 1.12σ; for siRNA r_0 was determined by the SBCG coarse-graining procedure. The electrostatic energies and forces were computed using the Particle–Particle Particle–Mesh Ewald algorithm, with a relative accuracy of 10^{-4}.

Even when these coarse-grained models are employed, it was still impractical to efficiently simulate the experimental system, owing to the strong multi-chain aggregation and the slow conformational decorrelation of long polymer chains. To overcome these limitations, it was necessary to decrease the length of the polymer chains. We therefore scaled down each original coarse-grained model to one fourth of its original length, using 30 beads to represent lPEI, 15 beads to represent a PEG block, and 6 beads (4 carrying a charge $-1.8e$ and 2 carrying a charge $-1.9e$) to represent siRNA. As an additional benefit, this made it possible to simulate a system with a larger number of constituent particles, namely 32 lPEI or lPEI-*g*-PEG polymers and 96 siRNA, thus permitting a better resolution of the aggregate size distribution function. In addition, 1056 positive and 1075 negative monovalent counterions were included to maintain system charge neutrality (1 additional counterion with charge $-0.2e$ was added to ensure precise electoral neutrality).

We employed a Langevin thermostat to simulate the implicit solvent and control the temperature, imposing a damping time 100τ, where τ is the LJ unit of time,

$$\tau = \sqrt{\frac{m\sigma^2}{\varepsilon}}\ , \qquad (2)$$

with m is the LJ unit of mass. The equations of motion were integrated using the velocity-Verlet algorithm. The temperature was set to $T = 1.0\ \varepsilon/k_B$, where k_B is Boltzmann's constant. When the solvent is changed from pure water to DMF–water mixtures at different proportions, the dielectric constant increases, while the charge density of siRNA and lPEI polymers decreases. Following our previous paper[9], we exploited the cancellation of these effects in the electrostatic interaction strength and assumed a constant Bjerrum length and constant charge density in our model.

2.2. Parameter choices to represent solvent quality and hydrogen bonding

Linear PEI forms a crystal hydrate in pure water due to strong inter- and intra-molecular hydrogen bonding[10]. DMF was observed in experiments to be a good solvent for lPEI[11]. On the other hand, as the solvent changes from pure water to water–DMF mixture, the solvent quality for siRNA decreases. Since we employed an implicit solvent, the change from a good to a poor solvent was represented by an increase in the effective attraction between siRNA beads and between lPEI beads. Since the lPEI and siRNA already experience a strong electrostatic interaction, no additional solvent-induced effective attraction between lPEI and siRNA was imposed. Both water and DMF and their mixtures are good solvents for PEG[12], therefore, following our earlier study[9], we did not incorporate PEG solubility variations within the range of DMF/water ratios in our model, but instead represented the uniformly good solvent conditions for PEG *via* a purely repulsive shifted-truncated LJ potential with a cutoff $2^{1/6}\sigma$.

In the coarse-grained modeling, we aimed to elucidate the effect of variation of the solvent quality and the degree of hydrogen bonding on the experimental system, rather than to realize a precise mapping between different solvent conditions onto attractive pair potentials. Thus, we opted to describe the pair potential *via* a LJ potential with two different strengths: $1.0\ k_BT$ and $0.314\ k_BT$. A potential strength of $1.0\ k_BT$ represented a poor-solvent condition and a higher level

of polymer–polymer hydrogen bonding (which includes both direct hydrogen bonding between two monomers and hydrogen bond bridging between two monomers by water molecules); a LJ attraction of 0.314 k_BT (corresponding to the theta solvent condition for the bead–spring model employed[13]) indicated a relatively good solvent condition and a lower level of polymer–polymer hydrogen bonding. This approach allowed us to identify the relative effect of each of the interactions during the solvent change. Given our choice for the temperature, this yielded the parameter combinations listed in **Table S2**. The pair potential was cut off at 2.5σ and shifted at the cutoff to eliminate a discontinuity in the interaction. All other nonbonded short-range interactions were modeled with a purely repulsive shifted-truncated LJ potential with a cutoff $2^{1/6}\sigma$.

Solvent Condition	ε_{LJ} / ε (siRNA)	ε_{LJ} / ε (PEI)	ε_{LJ} / ε (PEI–PEG)
Solvent 1 (Water)	0.314	1.000	1.000
Solvent 2 (Water–DMF mixture)	1.000	0.314	0.314
Solvent 1*	0.314	1.000	0.314

Table S2. Effective attraction strength ε_{LJ} (in units of the LJ energy parameter ε) between siRNA beads, PEI beads, and between lPEI and PEG beads for different solvent conditions.

To test the effect of hydrogen bonding between lPEI and PEG on micelle size, we artificially weakened the interaction strength between lPEI and PEG in water (cf. main text), and labeled this solvent condition Solvent 1*. The size distribution of lPEI-*g*-PEG nanoparticles in Solvent 1* is shown in **Figure S4**, along with the size distribution of the same system in Solvent 1 as a comparison. Figure S4 clearly shows that without strong hydrogen bonding between lPEI and PEG, the micelles decrease in size.

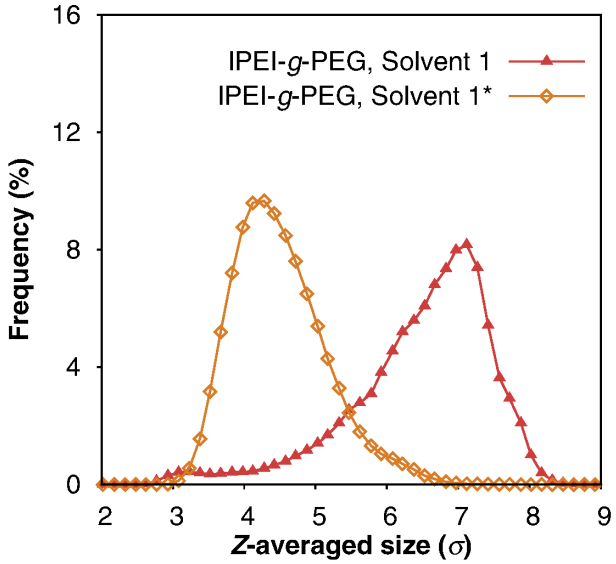

Figure S4. Size distributions of lPEI-*g*-PEG nanoparticles in Solvent 1, with strong lPEI–PEG hydrogen bonding (Solvent 1) and artificially weakened lPEI–PEG hydrogen bonding (Solvent 1*). See Table S2 for simulation parameters.

To confirm the qualitative validity of our parameter choices we also compared the experimental and computational results for the effect of solvent composition on lPEI/siRNA nanoparticles. **Figure S5** shows that for lPEI/siRNA systems, the proposed simulation model with the two-state solvent parameters successfully captured the experimentally observed size variation. As the solvent changes from pure water to a 70:30 (v/v) water–DMF mixture, the solvent quality for lPEI increases and that for siRNA decreases. Although the two solvent effects change in the opposite directions, the lPEI solubility dominates in the complexation of lPEI/siRNA, as demonstrated by the larger particle size in water and the smaller particle size in water–DMF mixture (*cf.* Figure S5). This behavior can be ascribed to the more flexible backbone and the larger contour length of lPEI, which leads to more lPEI–solvent contacts, whereas the siRNA predominantly aggregates *via* lPEI-mediated contacts.

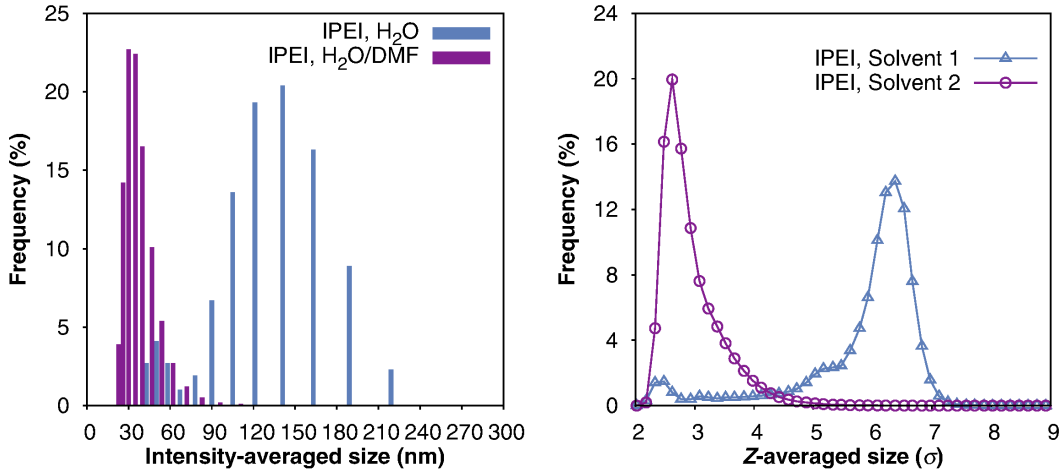

Figure S5. Size distributions of lPEI/siRNA nanoparticles in water and in 70:30 (v/v) water–DMF mixture in experiment (left) and in Solvent 1 and Solvent 2, respectively, in simulations (right).

2.3. Equilibration in the simulations and the use of parallel tempering

The siRNA molecules, the lPEI-*g*-PEG copolymers/lPEI polymers and the counterions were initially placed in a cubic, periodically replicated simulation box with linear size 100σ. To achieve a random initial configuration, a shifted and truncated LJ interaction with cutoff $2^{1/6}\,\sigma$ was used as the only pairwise interaction between any two particles. After an equilibration period of $3 \times 10^3\,\tau$ with time step 0.01τ, the proper LJ interactions (as described above) and all electrostatic interactions were switched on, followed by a second equilibration period of 1200τ. Due to the strong multi-chain attractions, in a typical simulation aggregates only seldom broke up and reformed, making it difficult to obtain an accurate frequency distribution of the aggregate size. To accelerate the disassociation and reformation of aggregates, we therefore employed the parallel tempering method[14]. In this approach, 24 copies of the same system were simulated in parallel, at different temperatures that were logarithmically distributed between $1.0\,k_BT$ and $2.0\,k_BT$. An exchange between configurations simulated at adjacent temperatures was attempted every 200 steps. This approach exploits the larger degree of fluctuations at higher temperatures to provide a pathway for the simulations at the original temperature to transition between states that are separated by high free-energy barriers. Four to eight parallel tempering runs were performed for each solvent condition, each for a period of $4.8 \times 10^5\,\tau$ (corresponding to 10 – 20 days of CPU

time for each of the 24 parallel copies, depending on solvent condition). Following the first two equilibration stages, complexation was permitted to proceed for $6 \times 10^4 \tau$ before sampling was started.

2.4. Determination of the aggregate composition and size distribution in simulation

The nanoparticles or micelles are aggregates of siRNA and lPEI or lPEI-*g*-PEG predominantly bound by electrostatic interactions. To determine the composition of one aggregate, we first determined all the RNA molecules associated with an lPEI or lPEI-*g*-PEG polymer. If one of the siRNA beads (which were all negatively charged) was within a distance 2σ from an lPEI bead (which were all positively charged), the siRNA was considered to be associated with that lPEI or lPEI-*g*-PEG chain. We then identified all the lPEI or lPEI-*g*-PEG polymers that were sharing at least one siRNA, and assigned all the polymers and siRNA molecules associated with each of the polymers to one aggregate.

Experimentally, the particle size distribution was determined by DLS, and reported as the intensity-averaged distribution of the hydrodynamic diameter of the particles. The hydrodynamic diameter obtained by DLS is calculated based on the diffusion coefficient of the particle in the solvent. For lPEI-*g*-PEG/siRNA nanoparticles, the PEG blocks are able to affect the diffusion behavior of the particles and therefore contribute to the hydrodynamic diameter of the particles. Therefore, in simulation, we included the contribution from PEG blocks in the particle-size calculation. As the intensity-averaged size distribution can be approximated by the *Z*-averaged size distribution when the single-particle scattering factor is set to unity[15], we calculated the *Z*-averaged radius of gyration R_Z,

$$R_Z = \frac{\sum_i N_i M_i^2 R_i}{\sum_i N_i M_i^2} , \qquad (3)$$

in which N_i is the number of micelles of radius of gyration R_i and mass M_i.

Although the PEG blocks are included in this size calculation, one advantage of simulation lies in the flexibility of data analysis. In **Figure S6**, we re-analyzed the size distribution data shown in Figure 1D, and compared the particle size with and without taking into account the PEG blocks. For Solvent 1, the PEG blocks were seen to only contribute to a small increase in the size

of lPEI-*g*-PEG/siRNA nanoparticles. If the PEG blocks were not included, the calculated size of the nanoparticles decreased to an average similar to that of the lPEI/siRNA nanoparticles (Figure S5), but with a different distribution, suggesting that the size increase in Figures 1A and 1B should not be ascribed to the inclusion of PEG blocks alone. On the other hand, for Solvent 2 the PEG blocks contributed greatly to the calculated size increase of lPEI-*g*-PEG/siRNA micelles, due to the fact that the higher solubility of lPEI yielded a less compact core with a more diffuse PEG corona.

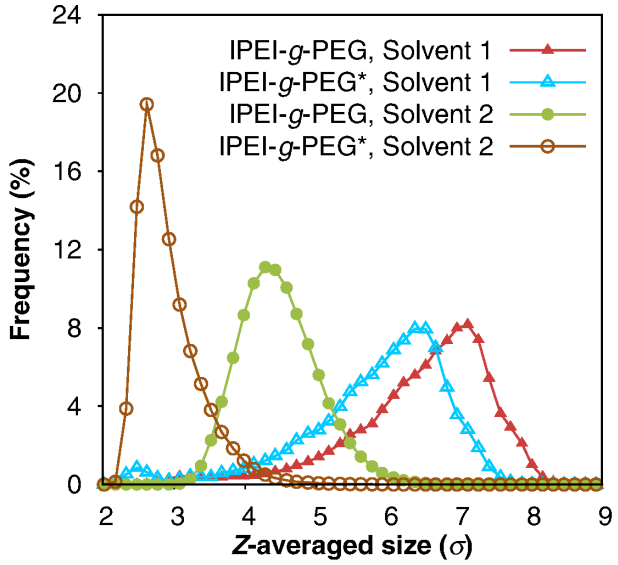

Figure S6. Size distributions of nanoparticles in Solvent 1 and Solvent 2 from simulations. In addition to the distributions of Figure 1D, two size distributions for lPEI-*g*-PEG/siRNA nanoparticles in Solvent 1 and Solvent 2 are included, for which PEG blocks are not included in the size calculation (labeled by lPEI-*g*-PEG*).

Supporting References:

[1] D. Jere, H. L. Jiang, R. Arote, Y. K. Kim, Y. J. Choi, M. H. Cho, T. Akaike, C. S. Cho, *Expert Opin. Drug Deliv.* **2009**, *6*, 827.

[2] A. C. R. Grayson, A. M. Doody, D. Putnam, *Pharm. Res.* **2006**, *23*, 1868.

[3] a.) R. Gref, M. Luck, P. Quellec, M. Marchand, E. Dellacherie, S. Harnisch, T. Blunk, R. H. Muller, *Colloids Surf. B Biointerfaces* **2000**, *18*, 301; b.) S. Mao, M. Neu, O. Germershaus, O. Merkel, J. Sitterberg, U. Bakowsky, T. Kissel, *Bioconjug. Chem.* **2006**, *17*, 1209.

[4] S. Plimpton, *J. Comput. Phys.* **1995**, *117*, 1.

[5] a.) P. L. Hansen, J. A. Cohen, R. Podgornik, V. A. Parsegian, *Biophys. J.* **2003**, *84*, 350; b.) F. Kienberger, V. P. Pastushenko, G. Kada, H. J. Gruber, C. Riener, H. Schindler, P. Hinterdorfer, *Single Molecules* **2000**, *1*, 123.

[6] G. M. Lindquist, R. A. Stratton, *J. Colloid Interface Sci.* **1976**, *55*, 45.

[7] a.) A. Arkhipov, P. L. Freddolino, K. Schulten, *Structure* **2006**, *14*, 1767; b.) A. Arkhipov, Y. Yin, K. Schulten, *Biophys. J.* **2008**, *95*, 2806.

[8] Y.-R. Yuan, Y. Pei, H.-Y. Chen, T. Tuschl, D. J. Patel, *Structure* **2006**, *14*, 1557.

[9] X. Jiang, W. Qu, D. Pan, Y. Ren, J. Williford, H. Cui, E. Luijten, H. Q. Mao, *Adv. Mater.* **2013**, *25*, 227.

[10] P. A. Gembitskii, N. A. Kleshcheva, A. I. Chmarin, D. S. Zhuk, *Polymer Science U.S.S.R.* **1978**, *20*, 2932.

[11] L. Tauhardt, K. Kempe, K. Knop, E. Altuntaş, M. Jäger, S. Schubert, D. Fischer, U. S. Schubert, *Macromol. Chem. Phys.* **2011**, *212*, 1918.

[12] F. E. Bailey, J. V. Koleske, *Poly(ethylene Oxide)*, Academic Press, New York, USA **1976**.

[13] W. W. Graessley, G. S. Grest, R. C. Hayward, *Macromolecules* **1999**, *32*, 3510.

[14] D. Frenkel, B. Smit, *Understanding Molecular Simulations*, Academic Press, San Diego, USA **2002**.

[15] F. R. Hallett, J. Watton, P. Krygsman, *Biophys. J.* **1991**, *59*, 357.

Biomaterials Science

REVIEW

View Article Online
View Journal

CrossMark click for updates

Cite this: DOI: 10.1039/c5bm00006h

Shape control in engineering of polymeric nanoparticles for therapeutic delivery

John-Michael Williford,[a,b,c] Jose Luis Santos,[b,c,d] Rishab Shyam[a,b,c] and Hai-Quan Mao*[b,c,d,e]

Received 7th January 2015,
Accepted 23rd February 2015

DOI: 10.1039/c5bm00006h

www.rsc.org/biomaterialsscience

Nanoparticle-mediated delivery of therapeutics holds great potential for the diagnosis and treatment of a wide range of diseases. Significant advances have been made in the design of new polymeric nanoparticle carriers through modulation of their physical and chemical structures and biophysical properties. Nanoparticle shape has been increasingly proposed as an important attribute dictating their transport properties in biological milieu. In this review, we highlight three major methods for preparing polymeric nanoparticles that allow for exquisite control of particle shape. Special attention is given to various approaches to controlling nanoparticle shape by tuning copolymer structural parameters and assembly conditions. This review also provides comparisons of these methods in terms of their unique capabilities, materials choices, and specific delivery cargos, and summarizes the biological effects of nanoparticle shape on transport properties at the tissue and cellular levels.

[a]*Department of Biomedical Engineering, Johns Hopkins School of Medicine, Baltimore, Maryland 21205, USA*
[b]*Institute for NanoBioTechnology, Johns Hopkins University, Baltimore, Maryland 21218, USA*
[c]*Translational Tissue Engineering Center, Johns Hopkins School of Medicine, Baltimore, MD 21287, USA*
[d]*Department of Materials Science and Engineering, Johns Hopkins University, Baltimore, MD 21218, USA*
[e]*Whitaker Biomedical Engineering Institute, Johns Hopkins University, Baltimore, MD 21218, USA. E-mail: hmao@jhu.edu; Fax: +410-516-5293; Tel: +410-516-8792*

Introduction

Therapeutic delivery using polymeric nanoparticles has received considerable attention for a wide range of biological applications, including drug and gene delivery, tissue engineering and regenerative medicine, and the detection of biomarkers and diagnosis of disease states.[1–4] The potential cargo delivered by nanoparticles is vast: some of the most common include small molecular weight compounds, chemotherapeu-

John-Michael Williford

John-Michael Williford is a Ph.D. candidate in the Biomedical Engineering Program at Johns Hopkins University School of Medicine. His thesis research in Prof. Hai-Quan Mao's Lab involves developing methods and mechanism of shape control of polymer/DNA nanoparticles and engineering shape tunability in DNA nanoparticles for gene delivery applications. John-Michael received his B.S. in biomedical engineering from The University of Akron in 2010.

Jose Luis Santos

Dr Jose Luis Santos completed his Ph.D. in Materials Chemistry at the University of Madeira in Portugal in 2009. His graduate research focused on the development of dendrimers to deliver nucleic acids to stem cells for regenerative medicine applications. He conducted his post-doctoral research on dynamic self-assembly of block copolymers for nanoparticle engineering with Prof. Margarita Herrera-Alonso in the Department of Materials Science and Engineering at Johns Hopkins University from 2010 to 2014. Currently, Dr Santos is a research associate in Prof. Hai-Quan Mao's Lab at the Institute for NanoBioTechnology developing polyelectrolyte nanoparticles for therapeutic delivery.

tics, proteins, nucleic acids, and imaging and diagnostic agents.[5–9] While new systems continue to be developed, success of nanoparticle delivery *in vivo* is often limited, particularly following systemic administration where less than 5% of the total dose successfully reaches the target site.[10,11] Improving the delivery efficiency of nanoparticles is paramount to fully harness their potential as both a research tool and as a potential pharmaceutical agent. For these reasons, renewed focus has been given to engineering nanoparticles through modulation of a specific physical characteristic, nanoparticle shape. Natural pathogens, such as viruses, often display unique shapes, ranging from spherical Heptatitis A virons to micron-sized, worm-shaped Ebola virons.[12,13] While shape is not the only factor that guides the tissue tropism of the virus, applying it to nanoparticle engineering, particularly for polymeric nanoparticles, holds great potential for therapeutic delivery applications. In this review, we highlight the key methods and materials used to generate polymeric nanoparticles with controlled shapes. Using these tools, studies have begun to reveal the biological responses to nanoparticles with controlled shapes, leading to significant differences at the cellular level, tissue level, and systemic level.

Methods of preparing polymeric nanoparticles with controlled shapes

Lithography-based methods

Particle replication in nonwetting template (PRINT) method. PRINT is the most popular among several photolithography techniques that have been developed to prepare polymeric nanoparticles with controlled sizes. It is a top-down approach that utilizes highly fluorinated surfaces, which are nonwetting to the materials being used to generate nanoparticles.[14] Because of this, it is much easier to shape and harvest particles using PRINT, particularly in the nanometer scale, whereas other lithography techniques develop a residual film between the desired object and the mold due to interactions at the interface[15] (Fig. 1a). This method allows for the formation of polymeric nanoparticles in the micro- and nano-scale size ranges with a high degree of uniformity.[15,16] The range of shapes that can be produced through PRINT fabrication is also very wide; particles can range from cubic/cylindrical with an aspect ratio of 1, to worm-like with an aspect ratio as high as 60.[17–19] A variety of materials can also be used to formulate these particles, including hydrogels comprised of crosslinked poly(ethylene glycol) (PEG),[15,18–20] solid particles formulated with poly(lactic acid) (PLA) and poly(lactic acid-*co*-glycolic acid) PLGA,[17,21,22] as well as biopolymer-based particles formulated with serum albumin and insulin.[23,24] Incorporation of various cargos for therapeutics and diagnostics have been achieved, including chemotherapy drugs,[17,22] siRNA,[20,21] RNA replicons,[24] and contrast agents.[25] Recent advances in PRINT technology also allow for the fabrication of Janus particles and end-labeled particles.[26] A study by Morton *et al.* demonstrated a spray method to incorporate layer-by-layer (L*b*L) coatings onto the surface of PRINT fabricated nanoparticles, providing a method for particle synthesis with precise control of nanoparticle size, shape, and surface characteristics.[27] Importantly, the PRINT process can be performed in small batches as well as a continuous, automated roll-to-roll system, providing a large-scale production system for potential clinical applications.[14]

Step and flash imprint lithography (S-FIL). S-FIL method has also been used to generate polymeric nanoparticles with controlled sizes.[28–31] S-FIL is a commercially available lithography technique that utilizes a patterned quartz template to mold photocrosslinkable solutions into defined patterns on a silicon surface.[28] Compared to the PRINT method, S-FIL offers advantages in ease of particle harvesting through the use of a

Rishab Shyam

Rishab Shyam is a Ph.D. candidate in the Department of Biomedical Engineering at Johns Hopkins University School of Medicine under the mentorship of Prof. Philip Wong and Prof. Hai-Quan Mao. His thesis research focuses on the development of polymer-based siRNA nanoparticles for gene knockdown in the central nervous system for therapeutic targets implicated in the Alzheimer's Disease. He received his B.S. in chemical engineering from Purdue University in 2006.

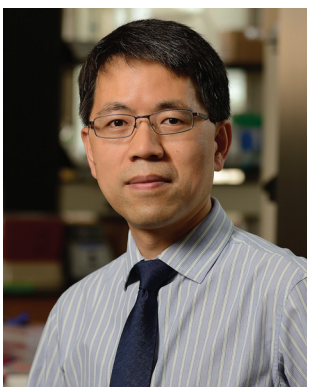

Hai-Quan Mao

Dr Hai-Quan Mao is a professor at the Department of Materials Science and Engineering and the Whitaker Biomedical Engineering Institute at Johns Hopkins University and is a member of the Translational Tissue Engineering Center and the Institute for NanoBioTechnology at Johns Hopkins University. Dr Mao's research focuses on engineering nanomaterials for therapeutic delivery and regenerative medicine applications. Dr Mao received his B.S. in chemistry in 1988 and Ph.D. in polymer chemistry in 1993 from Wuhan University in China and completed his postdoctoral training in the Department of Biomedical Engineering at Johns Hopkins University School of Medicine in 1998.

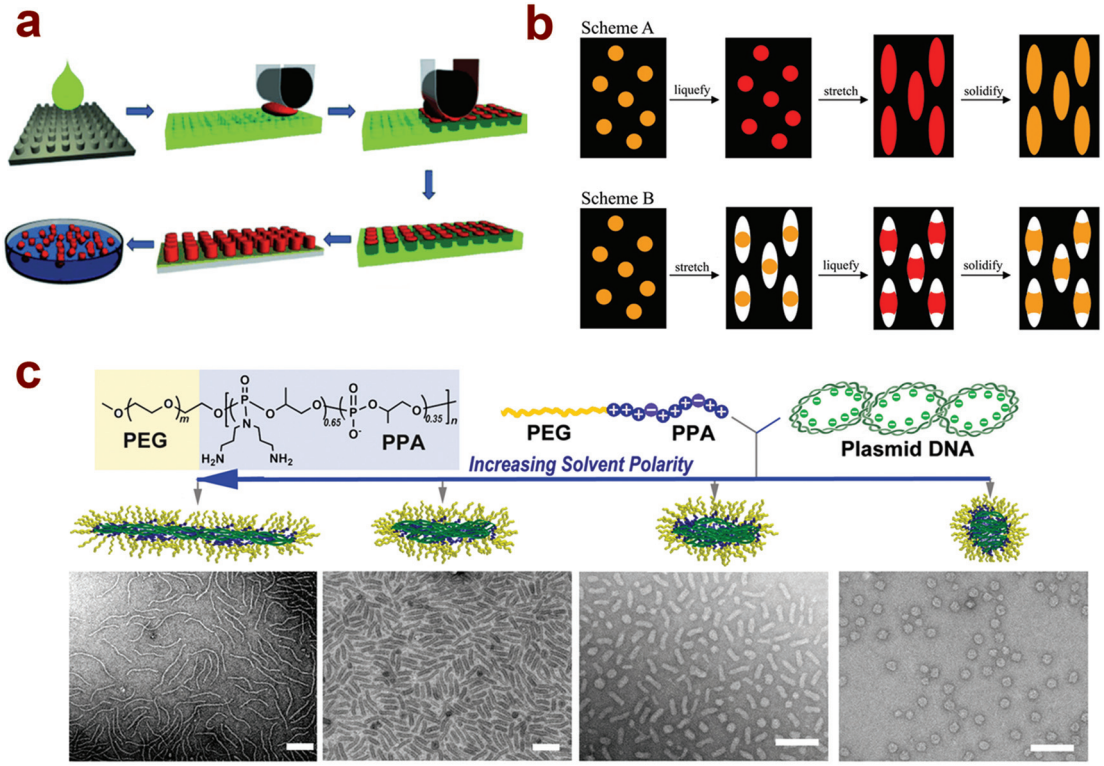

Fig. 1 Several methods have been developed to control the shape of polymeric nanoparticles for therapeutic delivery applications. (A) PRINT technology allows for the generation of particles with controlled shapes and surface chemistries through harvesting from polymer molds with low surface energy;[14] (reprinted with permission, ©2013 Wiley-VCH Verlag GmbH & Co. KGaA, Weinheim) (B) Two distinct methods for generating nanoparticles with nonspherical shapes through stretching and liquefication of precursor films, leading to the formation of rod shaped and barrel shaped particles;[32] (©2007 National Academy of Sciences, USA) (C) Self-assembly of PEG-polycation/DNA nanoparticles in solutions with varying solvent polarity leads to the formation of different shapes, including spheres, rod-like, and worm-like particles.[125] (reprinted with permission, ©2013 Wiley-VCH Verlag GmbH & Co. KGaA, Weinheim.)

water-soluble PVA release layer,[28,30] whereas PRINT requires surgical blades or shear forces to release the particles.[28] S-FIL still allows for precise control of particle size and shape, with feature sizes down to 50 nm. S-FIL has primarily been used to generate PEG hydrogel-based nanoparticles, which have been loaded with biomolecules including antibodies, nucleic acids, and anticancer drugs.[29] In addition, this method has been used to incorporate stimuli-sensitive materials into the nanoparticle matrix, allowing for the release of cargo under physiological conditions through enzyme-mediated cleavage of the carrier materials.[28]

Membrane stretching methods

Another method for generating polymeric nanoparticles with different shapes involves the stretching of spherical particles into complex shapes (Fig. 1b).[32–38] Spherical particles, typically polystyrene (PS) with diameters ranging from 60 nm to 10 μm, are suspended in a solution of poly(vinyl alcohol) (PVA) and generated into films, liquefied in solvent or heated above the glass transition temperature, and stretched in one or two dimensions to generate aspherical shapes, typically rods or elliptical disks, with aspect ratios ranging from 2 to 15.[32] A second method involves stretching the PVA film first, followed by liquefying the spherical particles to fill the void left in the PVA film. This method can be used to generate barrel and lens-shaped objects.[32] In addition to PS, PLGA has also been used to generate stretched particles.[33,34] Conjugation of antibodies for tissue-specific targeting, including anti-ICAM-1 and anti-transferrin for lung and brain delivery, respectively, has been successfully demonstrated.[38]

Self-assembly methods

Self-assembly of amphiphilic copolymers. Self-assembly of amphiphilic copolymers in aqueous or organic media has been widely used to generate nanoparticles. This bottom-up approach relies on the spontaneous assembly of single or multiple block copolymers to generate micellar nanoparticles with well-defined shapes. These amphiphilic copolymers are composed of two or more blocks with distinct polarities, and when placed in selected solvents can form supramolecular assemblies as a result of the thermodynamic incompatibility between the different blocks.[39–42] The final aggregate morphology is dependent on the hydrodynamic volume fraction of one block with respect to the other; the interfacial tension between the aggregate and the solvent mixture, and the kinetics of phase separation, which is dictated by the method used

to trigger the self-assembly of copolymers. The typical structures formed by these amphiphilic macromolecules comprise spherical micelles, cylindrical or worm-like micelles and bilayer structures (*i.e.* polymersomes). In addition, more complex aggregate morphologies including toroidal, disc-like, and compartmentalized particles have been engineered by fine-tuning the block lengths or molecular weights, polymer architecture, and chemical composition.[43–45] Aside from the molecular characteristics of block copolymers, the method used to trigger the self-assembly of copolymers is crucial to the generated micelle morphology.

Conventional methods for synthesizing block copolymer nanoparticles involve the slow addition of a block copolymer dissolved in water-miscible organic solvent into a larger quantity of water, resulting in the formation of aggregates at near thermodynamically equilibrated state. This method has frequently been used to study the kinetics of copolymer nanoparticle formation and to isolate aggregates of unique morphologies.[44,45] Although nanoparticles with various sizes and shapes have been prepared using this method as drug delivery carriers and diagnostic devices,[46,47] the slow mixing kinetics (occurs typically at a time scale of seconds) in comparison with the aggregation events, and the highly heterogeneous nature of the mixing conditions yield nanoparticle preparations with poorly controlled size and with broad distribution, poor colloidal stability, and low drug encapsulation efficiency.

To address these challenges, methods to improve the uniformity of mixing and phase-separation kinetics and to accelerate the mixing rates have been developed recently. For example, microfluidic mixing devices have been developed to yield more uniform mixing; and preparations based on confined impinging jets and multi-inlet vortex mixers rely on rapid mixing in a time scale of milliseconds. Compared to conventional methods, these new techniques allow for the formation of smaller and uniform aggregates in a continuous process, which is amenable for easier scale-up. They also offer a higher degree of versatility and control over particle size and distribution, higher drug encapsulation efficiency, and improved colloidal stability.[48,49]

These methods have predominantly been adopted for preparing spherical-like nanoparticles from block copolymers. Only recently, the Moffitt's group has established conditions to tune aggregate shape using microfluidic devices.[50–53] They employed a gas-liquid multiphase microfluidic reactor, in which argon gas is introduced into the merged liquid streams, compartmentalizing the colaminar flow into segmented liquid plugs. The chaotic advection observed within the liquid plugs enables fast mixing (~1 s) between water and polystyrene-*b*-poly(acrylic acid) copolymer solution triggering the formation of aggregates. The aggregates are subsequently exposed to strong and localized shear forces through the processing channel resulting in the formation of a myriad of aggregate structures including Y-Junctions, cylinders, vesicles and networks. The interplay between the chemical conditions (copolymer concentration, solvent polarity, and ionic strength) and flow kinetics enables the control over the size and the shape of the final aggregate.[50–52] Another interesting example by Förster *et al.* shows that one can also prepare size-controlled unilamellar copolymer vesicles in a fast, continuous and reproducible fashion using perpendicular hydrodynamic flow focusing in a microfluidic device.[54]

Another approach to improve micelle stability and drug release kinetics is to directly conjugate hydrophobic drugs to the polymer block forming the core of the micelles.[55–63] The ability to create multiple aggregate morphologies from a single copolymer is particularly attractive for investigating the effect of shape on aggregate stability, cellular internalization, trafficking, and drug delivery. In a recent example, Hu *et al.* synthesized polyprodrug amphiphiles consisting of polyethylene glycol (PEG) and a reduction-responsive camptothecin prodrug block to prepare particles of different shape including spheres, smooth disks, flower-like large compound vesicles (LCVs), and staggered lamellae with spiked periphery.[64] The self-assembled nanostructures were prepared under highly controlled mixing rate and concentrations; and particles with various shapes were prepared depending on the water addition rate and the organic solvent polarity. The study has shown that particle shape plays a critical role in particle-cell interaction and *in vivo* biodistribution. The staggered lamellae nanoparticles exhibited the fastest cellular uptake and highest stability in biological media. In addition, the blood circulation half-life of these nanoparticles was nearly 15-fold higher than their spherical analogue. In another study, Geng *et al.* found that self-assembly of PEG-*b*-polycaprolactone (PCL) copolymers in water led to the formation of long, filamentous particles, which they termed filomicelles.[65] The filomicelles in aqueous medium displayed lengths ranging from 2 microns up to 20 microns, and filomicelles loaded with paclitaxel were also successfully prepared for anticancer applications.

Conventional copolymer micelles as drug delivery carriers, however, may exhibit limited stability following the extreme dilution upon systemic delivery or as a result of serum protein-copolymer interaction and blood flow stress.[66] Additionally, the rapid dissociation of drug-loaded copolymer micelles in the bloodstream leads to deficient drug accumulation in the tumor and undesired side effects. To suppress these limitations, several research groups have introduced crosslinkable copolymer micelles that present both prolonged circulation *in vivo* and a better control over their drug-release properties.[67–69] Traditionally, crosslinkable copolymer micelles can be prepared through the addition of crosslinking agents that will react with functional domains present in the block copolymer micelle. Three main strategies have been pursued: (i) core-crosslinked stabilized copolymer micelles, where crosslinking occurs either at the hydrophobic chain-end or along the hydrophobic chain; (ii) core–shell interface stabilized copolymer micelles; and (iii) shell-crosslinked stabilized micelles. The location at which the crosslinking occurs as well as the extent of crosslinking significantly impaacts the physicochemical properties of the final aggregate structures. Furthermore, stimuli-responsive crosslinked copolymer micelles can be

prepare by introducing bifunctional crosslinking agents that respond to external stimuli such as temperature, light, pH and redox agents.[67,70–75] The Wooley group has developed several shell crosslinked copolymer micelles for the delivery of therapeutics or as theranostic devices.[71,76,77] In an elegant example, they prepared crosslinked copolymer micelles of different shape, spheres and cylinders with different aspect ratios, to which a cell penetrating peptide (HIV Tat PTD) was conjugated. Both the aggregate shape and the amount of peptide conjugated were found to play a role in the endocytosis and exocytosis of the aggregates evaluated.[78]

Unimolecular micelles prepared from molecular amphiphilic brush-like polymers (MABPs) are an attractive alternative since their covalent nature ensures micellar stability without compromising the drug release profile or biodegradability.[79–81] MABPs are macromolecules comprised of a linear polymer backbone and densely grafted polymer side chains.[82,83] Trigger-sensitive unimolecular micelles can be prepared to achieve on-demand release of encapsulated drugs. For example, aggregates resembling unimolecular micelles of size ranging from 6 to 50 nm containing 10–400 doxorubicin or camptothecin molecules per brush have been prepared. In this micelle system, drug molecules were fully protected by the dense PEG chains and released in its free form upon irradiation with UV light.[84,85] Incorporation of pH- and redox-cleavable linkers in a similar manner can expand the utility of MABPs for the delivery of anticancer drugs.[86] Johnson *et al.* have synthesized nanoparticles with stimuli-responsive dual MRI and NIR optical fluorescence imaging capabilities.[81] The brush polymers contained nitroxide radicals that in the native state partially quench the fluorescence intensity of the NIR dye. Upon exposure to ascorbate or ascorbate/glutathione in cancer cells, nitroxide radicals are reduced, resulting in a significant decrease of the MRI contrast and concomitant increase of the fluorescence intensity. The high *in vivo* stability, long circulation time, and the easy to conjugate cellular targeting moieties to these MABP micelles make them appealing as theranostic devices for tumor imaging and treatment.

Negatively charge polymers, such as polyacrylate and nucleic acid, can also be used as the hydrophilic block instead of PEG to construct amphiphilic micelles. For example, poly(acrylic acid)-*b*-polystyrene (PAA-*b*-PS) block copolymers can self assemble into micelles with different shapes either by changing the block lengths of PAA and PS, or by varying solvent polarity. Furthermore, the micelle shape can be reversibly transformed from spheres to rods to vesicles through modulation of solvent polarity even after micelles are formed.[87,88] More relevant to biomedical application, self-assembly of nucleic acid–based amphiphiles is highlighted in a recent review by Kwak and Herrmann.[89] In these assemblies, the oligonucleotide chain, mostly DNA, is conjugated to a hydrophobic polymer chain, forming either linear block copolymer or brush-like graft copolymer. These DNA-based amphiphiles self-assemble into micellar nanoparticles with different shapes, including spherical particles, vesicles, rod-like particles, and long cylinders.[90,91] Shape control is achieved based on the same assembly principle as discussed above *via* tuning copolymer composition and architecture of the block copolymers, and solvent conditions. The length of the oligonucleotides used in these DNA amphiphiles typically is on the order of tens to hundreds of base pairs. Incorporation of longer chains, including functional DNA sequences or plasmid DNA, has not been reported. Use of this strategy for the delivery of siRNA or antisense oligonucleotides, however, may be of interest for the field.

Self-assembly through complimentary base-pairing. Recent studies have also reported the generation of complex nanostructures through complementary base-pairing of DNA molecules and other short stranded oligonucleotides.[92] Because of the self-recognition of complementary DNA strands, a multitude of complex two- and three-dimensional assemblies can be rationally designed, ranging from dendritic structures, cubes, polyhedrons, and nanotubes.[92–97] Concerns exist over the stability of DNA nanostructures against nuclease degradation, although studies have shown that the nanostructures exhibit less degradation than nucleotides themselves.[98–100] These DNA nanoparticles have also been used for therapeutic delivery applications, including small molecule drugs, antibodies, nucleic acids, and vaccine adjuvants.[92,101–105] Lee *et al.* have developed a DNA tetrahedron, generated through complementary base-pairing of single stranded oligonucleotides, capable of packaging and delivering small interfering RNA (siRNA) to silence genes of interest in tumors.[106] One unique advantage of this method is the ability to precisely control the density and the spatial orientation of ligand placement of targeting ligands independently in the context of improving transfection efficiency. This assembly approach has also been extended to RNA.[107–109] Recently, Afonin *et al.* have employed an *in silico* design strategy to synthesize functional RNA nanoparticles in the form of nanocubes and nanorings.[110] While these assembled structures are capable of packaging multiple siRNA sequences, their utility was hindered by similar factors that affect naked RNA delivery *in vivo*, such as degradation by nucleases, lack of cell uptake, and rapid clearance. To overcome these shortcomings, cationic amphiphiles were used as carriers to effectively deliver the RNA payload. In this approach, the RNA molecules designed to have unique shapes were further condensed into spherically shaped micelles when complexed with an amphiphile.[111]

An alternative strategy to improve the RNA stability is to generate oligomerized RNA sequences. Shopsowitz *et al.* have reported a method to synthesize a RNA microsponges (~500 nm) densely loaded with RNA generated from a circular DNA template.[112] These RNAi microsponges were condensed into complexes and successfully mediated gene knockdown when used with Lipofectamine and linear polyethylenimine (lPEI) as the transfection agents *in vitro* and *in vivo* in a mouse tumor model.[113] While shape control using DNA and RNA as building blocks has been possible, controlling the shapes of nanoparticles following condensation of these species with polycations remains a challenge that continues to be addressed.

Self-assembly of polyelectrolytes. Self-assembly of oppositely charged polyelectrolytes defines a class of nanoparticles called complex core micelles, also referred to as polyion complex micelles.[114] These micelles exhibit a unique core–shell structure, with the polyelectolyte complex forming a stable core surrounded by a neutral, hydrophilic corona. Complex core micelle formation has been reviewed in several papers,[114–116] although shape control of such assemblies has not received significant attention until recently. DNA as a unique polyanion itself has been used as a building block to generate a variety of complex core micelles with different shapes.[117–119] Using PEG-*b*-poly(L-lysine) (PEG-*b*-PLL) copolymers to package the plasmid DNA, Osada *et al.* found that the length of the PLL segment significantly influenced the shape of the micelle.[120] Short PLL blocks led to the formation of rod and toroid-like particles, whereas longer PLL blocks led to spherical shapes. Further tuning of the length of the PLL segment could be used to control the length of the rod-like shapes, with short PLL segments (degree of polymerization of 19) forming rod lengths greater than 200 nm, and longer PLL segments (degree of polymerization of 70) generating rods with lengths of 50–100 nm.[121,122] It appears that the PEG chain crowdedness (*i.e.* PEG chain density on micelle core surface) as a key factor in controlling micelle rod length.[122,123] For shorter PLL segments, a greater amount of polymer is needed to neutralize the DNA charge, resulting in a higher density of PEG on micelle surface. Due to steric repulsion of the PEG chains, the micelles tend to elongate to provide additional surface area for the PEG corona. In a separate study using *N*-(2-hydroxypropyl) methacrylamide (HPMA) as the hydrophilic block, Shi *et al.* showed that the molecular weight of PLL in a HPMA-*b*-PLL copolymer also effectively changed the shape of complex core micelles formed with plasmid DNA.[124] Nanoparticles formed with copolymers containing longer PLL block exhibited higher aspect ratios than that with shorter PLL blocks, which exhibited more spherical shapes.

Interestingly, solvent quality and polarity has been shown to significantly influence the shape control in this complex core assembly. A recent study by Jiang *et al.* has demonstrated the feasibility of shape variation of DNA-polycation nanoparticles using a single PEG-*b*-polyphosphoramidate (PEG-*b*-PPA) block copolymer and plasmid DNA by tuning solvent polarity (Fig. 1c).[125] When polyelectrolyte complexes were formed in water–dimethylformamide (DMF) or dimethyl sulfoxide (DMSO) mixture solvents with different volume ratios, PEG-*b*-PPA/DNA micelles assumed different shapes ranging from worm-like shapes in water to rod-like and spherical shapes in lower polarity solvents. A similar reversible shape transformation process as shown for amphiphilic block copolymers[88] was also observed for these DNA-containing micelles by titrating solvent with water or DMF after the complexation and micelle formation, allowing shape tuning from spheres to rod-like and worm-like shapes, and *vice versa*. More interestingly, this shape tuning technique yielded micellar particles with a high degree of shape uniformity. It is important to point out that despite of the similarity in shape control with amphiphilic block copolymer, the mechanism for micelle assembly and shape control is distinctly different for these complex core micelles. Molecular dynamics simulations revealed that the DNA plasmid serves as both a functional payload and as a shape template as the conformation of DNA in each solvent condition dictated the final shape of the micelle, and that the DNA chain rigidity and solvent-DNA interaction are key factors influencing micelle shape control in this micelle system. In addition, maximization of PEG entropy in the solvent is essential to ensure shape conversion in these micelles, as nanoparticles prepared without the PEG block only exhibited more condensed spherical shapes in all solvents.

It is important to note that this micelle assembly strategy is not limited to block copolymer of PEG and polycations; polycation-*g*-PEG graft copolymers are also able to condense plasmid DNA into micellar nanoparticles with distinct shapes.[126] Compared with block copolymer carriers, graft copolymers offer much wider parameter space for method optimization to control micelle shapes and stability, including for example, PEG graft density and the molecular weight of the PEG grafts.

One common limitation of polyelectrolyte micelles is their stability in physiological medium. One strategy to stabilize the micelles in ionic buffers is to introduce reversible cross-links.[127,128] This method was employed to effectively preserve the size and shape of PEG-*b*-PPA/DNA micelles following solvent exchange to remove organic solvent.[125]

Shape transforming nanoparticles

Nanoparticles with discrete shapes and the capability to transform their shape in response to an external stimulus are particularly attractive, as it is possible to combine different sets of properties into one nanoparticle system. A recent study by Yoo and Mitragotri showed that rod-like PLGA particles generated by the particle stretch method were able to transform their shape to spheres in response to a change of external stimulus including pH, temperature, or chemical, during time scales ranging from minutes to hours (Fig. 2a).[33] Mechanistic studies revealed that a balance between the viscoelastic property of the polymer and the interfacial tension between the polymer and surrounding media were the two main factors influencing shape transformation kinetics. Another study by Chien *et al.* utilized DNA-amphiphile micelles to demonstrate controllable shape transformation (Fig. 2b).[91] The DNA brush component of the micelle contained a sequence specific cleavage site, and upon treatment with an enzyme specific for this sequence, the micelles transformed from 25 nm spheres to micron-length cylinders. On the other hand, this shape transition could be reversed by addition of a single strand DNA sequence complementary to the DNA remaining in the micelle, leading to the reformation of 25 nm spheres. Surprising, such a shape transformation process can also be achieved for micellar nanoparticles with a complex core prepared from plasmid DNA and PEG-polycation copolymer. A recent study by Williford *et al.* reported the worm-like micelles that were prepared by complexation between plasmid DNA and lPEI-*g*-PEG with a 2 mol% PEG (MW10 kDa) grafted to lPEI (MW17 kDa) through di-

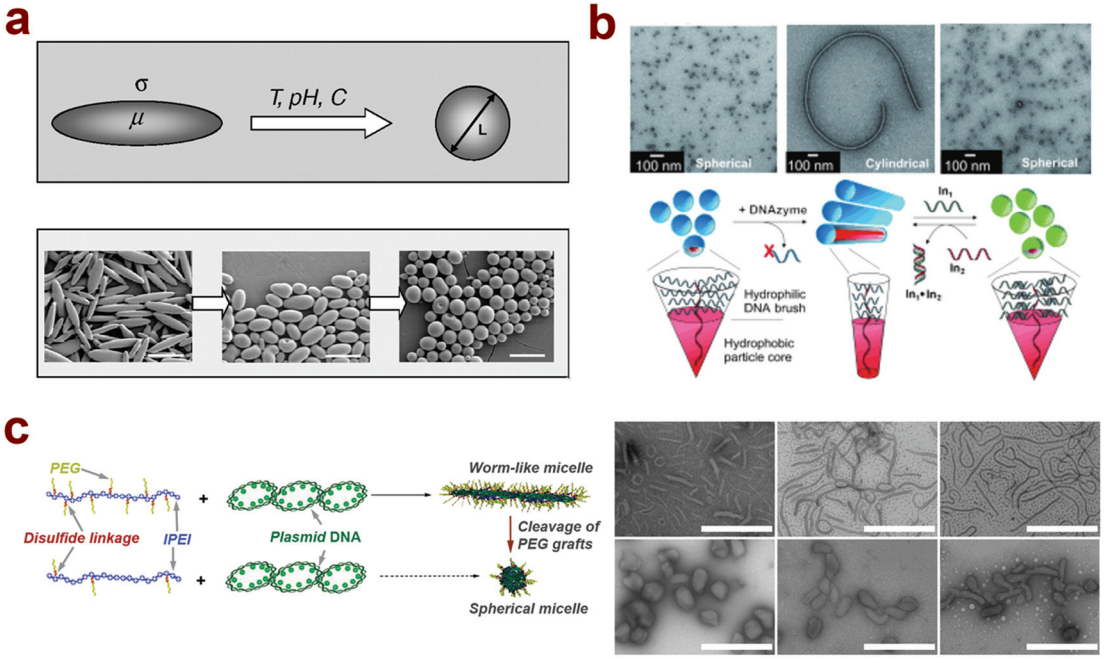

Fig. 2 Several recent studies have developed polymeric nanoparticles capable of shape transformation in response to external stimuli. (A) PLGA polymer particles can transform their shape from rod-like to spherical on time scales ranging from minutes to hours in response to external triggers such as various chemicals, pH changes, and temperature changes;[33] (B) Self-assembled DNA brush polymer micelles undergo shape transformation from spherical to cylindrical particles upon enzymatic cleavage of a fraction of the brush segment, which can be reversed by re-introducing a similar DNA segment through complementary base pairing;[91] (reprinted with permission, ©2010 Wiley-VCH Verlag GmbH & Co. KGaA, Weinheim) (C) Shape transformation of polymer/DNA micelles can be achieved through cleavage of a fraction of the PEG chains on the micelle surface, leading to a transition from worm-like shapes to more condensed spherical and short rod shapes.[126] (Reproduced by permission of The Royal Society of Chemistry.)

sulfide linkages. When these micellar nanoparticles were subjected to a reducing environment such as that in cytosol and cell nuclei, the PEG chains could be cleaved, which triggered the shape transformation from worm-like particles to more condensed spherical and short rod shapes (Fig. 2c).[126] Zeta potential measurements confirmed the cleavage of PEG grafts, highlighting the importance of PEG for controlling and transforming the shape of PEG-polycation/DNA nanoparticles.

Comparative analyses of different methods

While several different methods have been developed to generate nanoparticles with controlled shapes, certain considerations must be given to best utilize these materials for therapeutic delivery applications. Lithography-based methods have significant advantages in the generation of highly monodisperse particles, but limitations can exist in the range of shapes possible with the need to design molds for particle preparation. Drug loading capacity must continue to be studied, particularly for biologics such as siRNA. Membrane stretching provides a robust method for generating a range of aspect ratios over a large size range, from hundreds of nanometers to tens of microns. This method, however, limits the materials choice, as the polymer must be heated above the glass transition temperature during the stretching process. The heating process may also hinder the potential cargo for therapeutic delivery. Finally, self-assembly methods require no complex particle manufacturing processes, relying solely on intermolecular forces to generate complex shapes. The self-assembly process, however, has not been well-studied, and few mechanistic studies have been performed to identify the key driving forces for shape control. Molecular dynamics simulation may be an attractive tool for researchers to better understand the mechanisms that drive shape control of self-assembled polymeric nanoparticles. Stability of nanoparticles generated through each method must also continue to be optimized in physiological media for delivery applications. For example, self-assembled micelles may require additional core crosslinking strategies to preserve the size and shape under *in vivo* conditions. Membrane-stretched particles, comprised of PLA or PLGA, may require some surface conjugation strategies to minimize serum protein adsorption. DNA nanostructures must be designed to minimize susceptibility to nucleases in serum. Finally, the choice of shape control method may be determined by both the materials choice and the payload being delivered. Each method, although versatile for a range of materials and cargos, has specific set of design constraints and optimal conditions that may be tailored for a specific therapeutic molecule and application (see Table 1).

Effect of nanoparticle shape on their biological activities

With the development of several methods for precise control of nanoparticle shape, it has been possible to interrogate the role of shape in nanoparticle-mediated drug and gene delivery. Studies have highlighted the role of shape at each step of the

Table 1 Design constraints and preparation parameters in shape control for different nanoparticle preparation methods

Nanoparticle preparation method		Shapes prepared	Range of aspect ratio	Representative materials used	Cargos
Lithography	PRINT	Rods, cylinders, cubes, filamentous[14,15,18,19]	1–60 (ref. 18,19)	Polyethylene glycol, poly(lactic acid), poly(lactic acid-*co*-glycolic acid), proteins[15,20,21,24]	Small molecule drugs, contrast agents, siRNA[17,21,25]
	S-FIL	Disks, rods, squares, triangles[28–30]	1–8 (ref. 28,29)	Polyethylene glycol[28,29]	Antibodies, nucleic acids, small molecule drugs[28,30]
Membrane stretching		Rods, disks, ellipsoids, pills, barrels, bullets, lenses[32,33,35]	1.5–15 (ref. 32,37,38)	Polystyrene, poly(lactic acid-*co*-glycolic acid)[33,35,38]	Antibodies, small molecule drugs[32,35,38]
Self assembly	Amphiphilic copolymers	Spheres, rods, filamentous, vesicles, toroids, disks[43–45,65,88]	1–>100 (ref.44,65,88)	Polyethylene-*block*-polyethylene glycol, polycaprolactone-*block*-polyethylene glycol, poly(lactic acid-*co*-glycolic acid)-polyethylene glycol, poly(lactic acid)-*block*-polyethylene glycol, polystyrene-*block*-poly(acrylic acid)[39,42,44,47,65,88]	Hydrophobic drugs loaded in the core[65,66,129]
	Nucleic acid base-pairing	Cages, polyhedrons, nanotubes[92,95,96,106]	1–7 (ref, 92,95,106)	Single-stranded DNA[92,97]	Imaging agents, small molecule drugs, siRNA, proteins[102–106]
	Complex core micelles	Spheres, rods, worms[120–122,125,126]	1–30 (ref. 122,125,126)	Polyphosphoramidate-*block*-polyethylene glycol, linear polyethylenimine-*graft*-polyethylene glycol, poly(glutamic acid)-*block*-polyethylene glycol, polylysine-*block*-polyethylene glycol[5,115,116,125,126]	Nucleic acids[5,116,125]

delivery process, including extending nanoparticle circulation time, enhancing tissue-specific delivery, transport and retention, and influencing cellular uptake and intracellular trafficking. The following sections will provide a brief overview on the effect of nanoparticle shape at different delivery steps.

Shape effect on systemic circulation of nanoparticles

Based on the observation that flexible and long worm-like micelles (>1 μm) became elongated under shear in flow condition, which may prevent significant interaction with macrophages in circulation, Geng *et al.* tested the effect of shape on self-assembled nanoparticle circulation time following systemic injection by comparing 3.5-μm long filomicelles with 200 nm spherical micellar nanoparticles.[65] They showed that a significant fraction of both the non-degradable polyethylene-*b*-PEG filomicelles and the degradable PCL-*b*-PEG micelles circulated for up to one week in rodents after i.v. injection, whereas spherical nanoparticles were cleared within 2 days. The circulation half-life decreased as the initial length of the micelle decreased. The extended circulation time of filomicelles was primarily attributed to their ability to reduce binding and clearance by circulating macrophages, in contrast to spherical particles. More efficient delivery of paclitaxel using these filomicelles was demonstrated in a mouse lung cancer model compared to free paclitaxel. At the same dose of paclitaxel, filomicelles showed significant tumor size decrease with about half the amount of free paclitaxel. Furthermore, the animals were able to tolerate a higher dose of the drug, which could potentially translate to higher degree of tumor killing. Tockary *et al.* reported a study comparing circulation time of a series of rod-like PEG-*b*-PLL/DNA micellar nanoparticles with different lengths (Fig. 3a).[122] From blood circulation profile analysis, nanoparticles with longer rod lengths of 162 nm had a greater percentage of particles remaining in circulation compared to shorter, 70 nm rods. For instance, at 3 minutes post-injection, approximately 60% of the longer rods remained in circulation compared with only 30% of the shorter rods. While these numbers do not show such a striking differences in nanoparticle circulation time as the previous study, it is possible that the differences arise from the fact that these particles are much shorter than the micron-sized filomicelles. These results still highlight the potential benefit of elongated particles in providing extended circulation time.

Nanoparticle shape may also play a role in margination *i.e.* drifting of a particle from the center of the vessel close to the vessel wall.[130] Nanoparticle margination dynamics may be important in binding to the endothelium and escaping leaky vasculature in tumor tissue. Theoretical analysis indicates that spherical particles under flow conditions tend to follow a streamline parallel to a vessel wall, whereas non-spherical ellipsoidal particles exhibit more complex rotational and translation trajectories, drifting from one side of the vessel to the other during flow.[131,132] Using a detailed model of particle dynamics in microcirculation where low shear rates are present, elongated, discoidal particles display the greatest ability to marginate; however, the lateral velocity of the particle depends significantly on its Stokes number, which is influenced by the size and the density of the material.[133] Additionally, when comparing a nanosphere and nanorod under identical shear conditions, the binding probability was three-fold higher for the nanorod.[132] A study looking specifically at the effect of shear rate on the margination of non-spherical, micron-sized silica particles found that for the ranges tested, discoidal shapes marginated the most, followed by quasi-hemispherical and spheri-

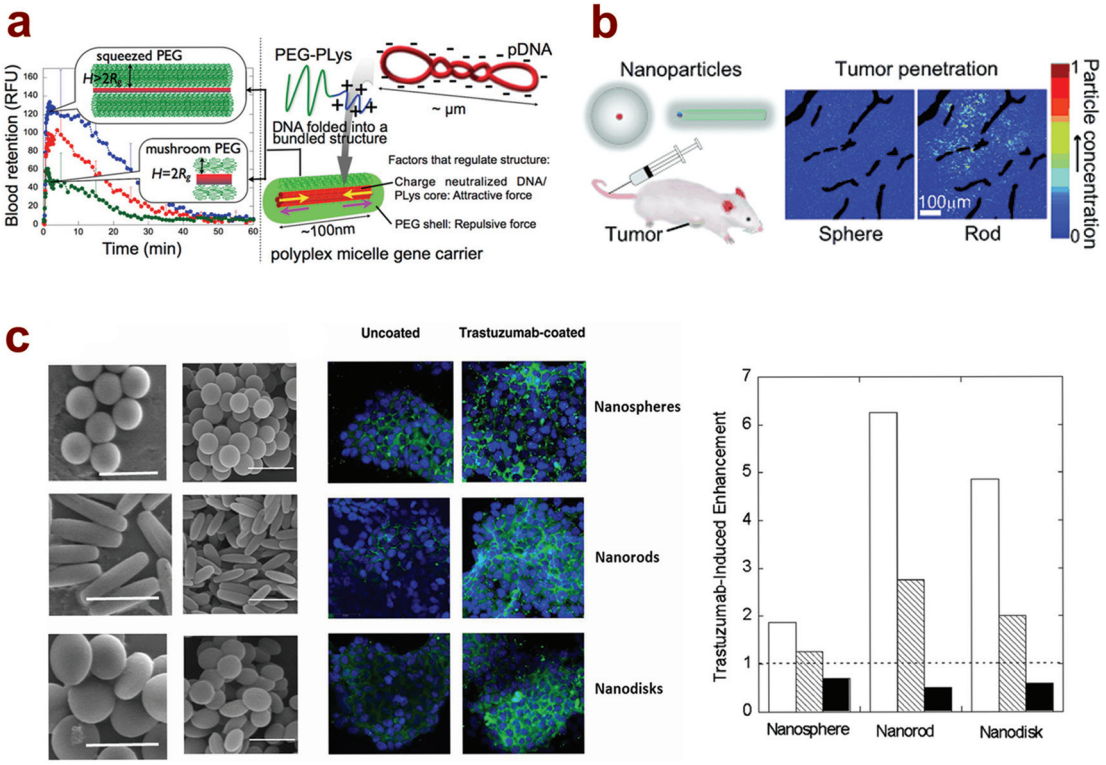

Fig. 3 Nanoparticle shape influences the biological response both *in vitro* and *in vivo* for drug and gene delivery applications. (A) Nanoparticle shape is influenced by the crowdedness of the PEG layer on the surface of polymer/DNA micelles. Dense PEG layer leads to the formation of longer rod shapes that, upon systemic administration *via* tail vein injection, leads to extended circulation compared to shorter, rod shaped micelles;[122] (reprinted with permission, ©2013 American Chemical Society) (B) Greater tumor penetration is observed following i.v. injection of spherical and rod-shaped silica-quantum dot nanoparticles;[137] (reprinted with permission, ©2011 Wiley-VCH Verlag GmbH & Co. KGaA, Weinheim) (C) Scanning electron microscopy images of polystyrene nanospheres, nanorods, and nanodisks, as well as fluorescent microscopy images of *in vitro* cellular uptake of shaped nanoparticles (green) in BT-474 breast cancer cells (blue) comparing uncoated and antibody (trastuzumab)-coated particles. Graph shows that trastuzumab coating enhancement is greatest for nanorods, followed by nanodisks and nanospheres in both BT-474 cells (white bars) and SK-BR-3 cells (dashed bars). No enhancement was observed for any shape in MDA-MB-231 cells (black bars).[35]

cal particles.[134] *In vitro* studies on effect of nanoparticle shape under flow condition using microfluidic flow chamber experiments, also using the silica-based particles,[134] confirmed that spherical particles exhibit significantly lower sedimentation and binding to the walls of the chamber compared to hemispherical and discoidal particles. It will be interesting to see if the results hold for shaped, polymeric nanoparticles as well.

Shape effect on tissue binding and distribution of nanoparticles

Nanoparticle shape has been shown to significantly influence tissue binding and distribution *in vivo*. Using the membrane-stretched PS nanoparticles surface-conjugated with antibodies against ICAM-1 and transferrin for lung and brain targeting, respectively, Kolhar *et al.* demonstrated that anti-ICAM-1-conjugated rods (500 nm length × 125 nm diameter) yielded twice the accumulation in lungs compared to 200 nm spherical particles.[38] Lung to liver accumulation was also 1.7-fold higher for the rods, compared with 0.7 for the spheres, showing that rod-shaped particles improved tissue-specific binding. Similarly for anti-transferrin-conjugated nanoparticles, rod-shaped particles showed a nearly 7-fold higher accumulation in brain compared to spherical particles. *In vitro* studies using a synthetic microvascular network model complemented the *in vivo* results, showing higher binding to the walls of the chamber for the rod-shaped, antibody-conjugated particles, compared with antibody-conjugated spherical particles. Additional studies incorporating bifurcation junctions into the microvascular networks found that particles accumulated more at the branching sites compared to the straight segments, which may have application in certain disease states.[135] Another study by Shuvaev *et al.* using PEG-*b*-polyethylene filomicelles decorated with endothelium-targeting antibodies also showed combined advantages of extended circulation time and improved tissue binding for these worm-like particles, highlighting the importance of nanoparticle shape for improving transport and targeting capabilities.[136]

In addition to tissue targeting, nanoparticle shape has the potential to influence their penetration and distribution once particles transport from the vessels to the tissue. Chu *et al.* reported that PLGA particles formulated by the PRINT method exhibited significantly different tissue distribution of the encapsulated drug, docetaxel, in a particle shape-dependent manner.[17] Rod-like particles (80 nm diameter × 320 nm length) delivered a higher concentration of docetaxel in the

tumor tissue and lower spleen and liver deposition, compared with cube particles (200 nm × 200 nm). Such an improved delivery with rod-like particles was correlated with better permeation or diffusion of these particles in the tumor tissue and a reduction in clearance by macrophages. These results are consistent with a recent study by Chauhan *et al.* using silica nanoparticles and nanorods containing a quantum dot core (Fig. 3b). Tumor tissue distribution for the rod-like nanoparticles (15 nm × 54 nm) was greater than the 35 nm spherical particles, as a result of enhanced penetration and diffusion property for the rods in tissue or gel-like medium.[137]

While the literature is not as extensive for gene therapy applications, several studies have begun to focus on the effect of DNA nanoparticle shape on *in vivo* gene delivery efficiency. Dirisala *et al.,* using self-assembled PEG-*b*-PLL/DNA nanoparticles carrying plasmid DNA encoding anti-angiogenic proteins for pancreatic cancer delivery, identified a critical rod length of 200 nm that is capable of mediating efficient transfection efficiency both *in vitro* and *in vivo*.[121] Above a 200 nm length, rod-shaped nanoparticles showed lower cell uptake in BxPC3 cells and minimal antitumor effect in mice following i.v. injection, even though these nanoparticles displayed extended circulation time. Rods shorter than 200 nm, on the other hand, exhibited significant antitumor response through reduction in tumor volume as well as decreased tumor vascular density upon treatment. Jiang *et al.* used retrograde intrabiliary infusion to deliver shaped, PEG-*b*-PPA/DNA micelles to the rat liver.[125] In this study, worm-like particles (20 nm diameter × 581 nm length) mediated 126-fold higher transfection efficiency than rod-like particles (30 nm diameter × 130 nm length), and 1680-fold higher expression than the spherical particles with an average diameter of 40 nm.

Shape effect on cellular uptake of nanoparticles

The shape effect of nanoparticles has been most extensively characterized at the cellular level. A study by Gratton *et al.* using cationic PEG particles prepared by the PRINT method found that longer rod particles (150 nm diameter × 450 nm length) had faster internalization rates in HeLa cells compared to short rods (200 nm diameter × 200 nm length).[18] As the particles were positively charged, it is likely that the higher aspect ratio particles were able to experience multivalent interactions with the cells, leading to faster uptake. Results for hyaluronic acid (HA)-coated PLGA PRINT particles also showed similar trends: 320 nm × 80 nm rod particles showed nearly 10-fold higher uptake than 200 nm × 200 nm short rods in BT-20 triple negative breast cancer cells.[27] Agarwal *et al.* similarly studied the uptake of hydrogel nanorod and nanodisc particles in several epithelial and endothelial cell lines.[29] In all cell types, the nanodiscs are internalized more than the nanorods. From the results, the authors proposed three key factors that dictate cell uptake *in vitro*: contact force between the particle and the cell surface, sedimentation, and strain energy needed for membrane deformation to uptake the particles. The strain energy, in particular, is hypothesized to be the reason for the increased uptake of nanodiscs compared to nanorods, as more energy is needed to engulf the elongated rod-shaped particles. Polystyrene rods with a size of 367 nm × 126 nm, prepared by the membrane stretching method, displayed higher specific uptake and lower nonspecific uptake compared to 200 nm spherical and disk-shaped (236 nm diameter × 88 nm thickness) nanoparticles in three breast cancer cell lines following surface conjugation of trastuzumab, a HER2-targeted antibody (Fig. 3c).[35] On the other hand, a study comparing cellular uptake of spherical, short cylinder, and long cylinder, PAA-*b*-PS block copolymer nanoparticles conjugated with TAT cell adhesion peptide found that spherical particles exhibited the highest amount of uptake in Chinese hamster ovary cells.[78] The results suggest that it may be difficult for the micron-length cylindrical particles to be internalized by the cell; in addition, particle uptake was compared at the same molar concentration of polymer, meaning that there was a higher number of spherical particles compared to worm-like particles, which may affect the measurements. It is also possible that uptake of different shapes will vary significantly depending on material choice or cell type being investigated.

Several studies have also begun to investigate shape-dependent uptake and intracellular trafficking of DNA-containing nanoparticles. Shi *et al.*, using HPMA-*b*-PLL copolymers to condense DNA, compared cellular uptake, intracellular trafficking, and transfection efficiency for 25 nm × 74 nm oblong complex core micelles and 18 nm × 102 nm rod-like micelles.[124] The transfection efficiency for the oblong micelles was 42-fold higher than the rod-like micelles with a higher aspect ratio. Mechanistic studies showed that cellular uptake for the more condensed particles was approximately 4-fold higher, whereas the rod-like particles, after internalization, tended to accumulate more in endosomal/lysosomal compartments. Other factors, such as charge density, DNA unpacking, and intracellular trafficking kinetics, did not differ significantly for the two nanoparticles, suggesting that shape-dependent cellular uptake may be a determining factor in the observed transfection efficiency differences. Our recent studies also showed that nanoparticle shape may similarly influence cell uptake and transfection efficiency.[125,126] In addition, as polymer/DNA micelles undergoing shape transformation from worm-like to condensed spherical and short rod shapes, a significant increase in *in vitro* transfection efficiency was observed, whereas control particles without shape transformation did not increase transfection efficiency.[126] However, it is important to note that in this study shape transformation occurred concomitantly with PEG cleavage, therefore both shape transformation and increase in nanoparticle surface charge may contribute to the improved transfection results.

Significant discoveries have been made on shape-dependent uptake of microparticles and nanoparticles in phagocytic cells. Using high aspect ratio disc and worm-like particles, results highlight that shape, but not necessarily size, dictates the degree of particle internalization by macrophages.[36,37] For example, for 14 μm × 3 μm ellipsoidal particles, when the macrophage attaches to the end of the particle, it can be effectively internalized within 3 min.[36] When it attaches to the flat

side of the particle, however, no internalization was observed for the duration of the 110 min study. Extending from these observations, a follow-up study compared macrophage internalization of 1–3 μm spherical particles with fiber-like particles stretched from the same set of spherical particles to an aspect ratio of 22.5.[37] The fiber-like particles displayed almost no internalization, whereas approximately half of the spherical particles that attached to the macrophages were internalized. This study highlights the ability to use shape as sole factor to generate a particle that can effectively evade phagocytosis. As another example highlighting the utility of shape to influence macrophage uptake, PLGA particles capable of shape transformation from elliptical disks with an aspect ratio of 5 to spherical particles were compared to control particles unable to transform their shape.[33] When incubated *in vitro* with macrophages, particles were internalized quickly upon shape transformation to near-spherical shapes. In contrast, cells could not phagocytose elliptical disks without shape transformation.

Conclusions

Using the methods presented here, it has been shown that precise shape control can be achieved for polymeric nanoparticles, obtaining a range of nanoparticle shapes including spherical and cylindrical particles, all the way to micron sized, high aspect ratio rod and filamentous particles. Methods are amenable to a wide range of polymeric systems, both non-degradable and degradable, and can deliver cargo ranging from chemotherapeutics, nucleic acids, and contrast agents. Applications of these shape-controlled nanoparticles *in vitro* and *in vivo* has revealed shape-dependent nanoparticle transport properties, allowing particle shape optimization to extend circulation time following systemic injection, improve tissue penetration and distribution, enhance binding to target cells and tissues, and direct cellular uptake and intracellular trafficking behavior. While these findings highlight the promise of shape control for improving the delivery efficiency of polymeric nanoparticles, significant challenges remain to be addressed. As shape is one of the fundamental attributes of nanoparticles, along with size, surface chemistry, charge, surface energetics, *etc*., it may be difficult to isolate the specific shape effect from other parameters on biological transport properties and bioactivities of the nanoparticles. New strategies are needed to independently control nanoparticle shape and other parameters in order to identify shape as the sole governing factor. Further evaluation of the shape in a biological context is also necessary; it is possible that, upon exposure to the complex biological environment, the shape factor could be masked by serum proteins or biological media. Finally, reproducibility, uniformity, and scalability must continue to be addressed in order to identify key formulations for potential clinical development. These considerations aside, it is clear that nanoparticle shape holds great potential as an additional design parameter for improving therapeutic delivery. The continued development of new methods and materials for such shape control provides for an exciting future for nanomedicine.

Acknowledgements

We would like to acknowledge funding support provided by NIH grants R21EB015152, R21EB013274, and U54CA151838, as well as the Defense Threat Reduction Agency Grant W81XWH-13-2-0037.

References

1 M. E. Davis, Z. Chen and D. M. Shin, *Nat. Rev. Drug Discovery*, 2008, **7**, 771–782.
2 S. Parveen, R. Misra and S. K. Sahoo, *Nanomedicine*, 2012, **8**, 147–166.
3 J. J. Shi, A. R. Votruba, O. C. Farokhzad and R. Langer, *Nano Lett.*, 2010, **10**, 3223–3230.
4 M. Perfezou, A. Turner and A. Merkoci, *Chem. Soc. Rev.*, 2012, **41**, 2606–2622.
5 D. W. Pack, A. S. Hoffman, S. Pun and P. S. Stayton, *Nat. Rev. Drug Discovery*, 2005, **4**, 581–593.
6 D. Peer, J. M. Karp, S. Hong, O. C. FaroKHzad, R. Margalit and R. Langer, *Nat. Nanotechnol.*, 2007, **2**, 751–760.
7 J. M. Williford, J. Wu, Y. Ren, M. M. Archang, K. W. Leong and H. Q. Mao, *Annu. Rev. Biomed. Eng.*, 2014, **16**, 347–370.
8 D. S. Pisal, M. P. Kosloski and S. V. Balu-Iyer, *J. Pharm. Sci.*, 2010, **99**, 2557–2575.
9 S. M. Janib, A. S. Moses and J. A. MacKay, *Adv. Drug Delivery Rev.*, 2010, **62**, 1052–1063.
10 Y. H. Bae and K. Park, *J. Controlled Release*, 2011, **153**, 198–205.
11 K. Park, *ACS Nano*, 2013, **7**, 7442–7447.
12 S. Baron, *Medical Microbiology*, University of Texas Medical Branch at Galveston, Galveston, Tex., 4th edn., 1996.
13 P. R. Murray, E. J. Baron, M. A. Pfaller, F. C. Tenover and Y. RH and American Society for Microbiology., *Manual of Clinical Microbiology*, ASM Press, Washington, D.C., 7th edn., 1999.
14 J. Xu, D. H. Wong, J. D. Byrne, K. Chen, C. Bowerman and J. M. DeSimone, *Angew. Chem., Int. Ed. Engl.*, 2013, **52**, 6580–6589.
15 J. P. Rolland, B. W. Maynor, L. E. Euliss, A. E. Exner, G. M. Denison and J. M. DeSimone, *J. Am. Chem. Soc.*, 2005, **127**, 10096–10100.
16 S. E. Gratton, P. D. Pohlhaus, J. Lee, J. Guo, M. J. Cho and J. M. Desimone, *J. Controlled Release*, 2007, **121**, 10–18.
17 K. S. Chu, W. Hasan, S. Rawal, M. D. Walsh, E. M. Enlow, J. C. Luft, A. S. Bridges, J. L. Kuijer, M. E. Napier, W. C. Zamboni and J. M. DeSimone, *Nanomedicine*, 2013, **9**, 686–693.

18 S. E. A. Gratton, P. A. Ropp, P. D. Pohlhaus, J. C. Luft, V. J. Madden, M. E. Napier and J. M. DeSimone, *Proc. Natl. Acad. Sci. U. S. A.*, 2008, **105**, 11613–11618.
19 F. R. Kersey, T. J. Merkel, J. L. Perry, M. E. Napier and J. M. DeSimone, *Langmuir*, 2012, **28**, 8773–8781.
20 S. S. Dunn, S. Tian, S. Blake, J. Wang, A. L. Galloway, A. Murphy, P. D. Pohlhaus, J. P. Rolland, M. E. Napier and J. M. DeSimone, *J. Am. Chem. Soc.*, 2012, **134**, 7423–7430.
21 W. Hasan, K. Chu, A. Gullapalli, S. S. Dunn, E. M. Enlow, J. C. Luft, S. Tian, M. E. Napier, P. D. Pohlhaus, J. P. Rolland and J. M. DeSimone, *Nano Lett.*, 2012, **12**, 287–292.
22 E. M. Enlow, J. C. Luft, M. E. Napier and J. M. DeSimone, *Nano Lett.*, 2011, **11**, 808–813.
23 J. Y. Kelly and J. M. DeSimone, *J. Am. Chem. Soc.*, 2008, **130**, 5438–5439.
24 J. Xu, J. Wang, J. C. Luft, S. Tian, G. Owens, Jr., A. A. Pandya, P. Berglund, P. Pohlhaus, B. W. Maynor, J. Smith, B. Hubby, M. E. Napier and J. M. DeSimone, *J. Am. Chem. Soc.*, 2012, **134**, 8774–8777.
25 J. Nunes, K. P. Herlihy, L. Mair, R. Superfine and J. M. DeSimone, *Nano Lett.*, 2010, **10**, 1113–1119.
26 H. Zhang, J. K. Nunes, S. E. A. Gratton, K. P. Herlihy, P. D. Pohlhaus and J. M. DeSimone, *New J. Phys.*, 2009, 11.
27 S. W. Morton, K. P. Herlihy, K. E. Shopsowitz, Z. J. Deng, K. S. Chu, C. J. Bowerman, J. M. Desimone and P. T. Hammond, *Adv. Mater.*, 2013, **25**, 4707–4713.
28 L. C. Glangchai, M. Caldorera-Moore, L. Shi and K. Roy, *J. Controlled Release*, 2008, **125**, 263–272.
29 R. Agarwal, V. Singh, P. Jurney, L. Shi, S. V. Sreenivasan and K. Roy, *Proc. Natl. Acad. Sci. U. S. A.*, 2013, **110**, 17247–17252.
30 R. Agarwal, V. Singh, P. Jurney, L. Shi, S. V. Sreenivasan and K. Roy, *ACS Nano*, 2012, **6**, 2524–2531.
31 M. Caldorera-Moore, M. K. Kang, Z. Moore, V. Singh, S. V. Sreenivasan, L. Shi, R. Huang and K. Roy, *Soft Matter*, 2011, **7**, 2879–2887.
32 J. A. Champion, Y. K. Katare and S. Mitragotri, *Proc. Natl. Acad. Sci. U. S. A.*, 2007, **104**, 11901–11904.
33 J.-W. Yoo and S. Mitragotri, *Proc. Natl. Acad. Sci. U. S. A.*, 2010, **107**, 11205–11210.
34 J. W. Yoo, N. Doshi and S. Mitragotri, *Macromol. Rapid Commun.*, 2010, **31**, 142–148.
35 S. Barua, J. W. Yoo, P. Kolhar, A. Wakankar, Y. R. Gokarn and S. Mitragotri, *Proc. Natl. Acad. Sci. U. S. A.*, 2013, **110**, 3270–3275.
36 J. A. Champion and S. Mitragotri, *Proc. Natl. Acad. Sci. U. S. A.*, 2006, **103**, 4930–4934.
37 J. A. Champion and S. Mitragotri, *Pharm. Res.*, 2009, **26**, 244–249.
38 P. Kolhar, A. C. Anselmo, V. Gupta, K. Pant, B. Prabhakarpandian, E. Ruoslahti and S. Mitragotri, *Proc. Natl. Acad. Sci. U. S. A.*, 2013, **110**, 10753–10758.
39 J. K. Kim, S. Y. Yang, Y. Lee and Y. Kim, *Prog. Polym. Sci.*, 2010, **35**, 1325–1349.
40 B. K. Kuila and M. Stamm, *J. Mater. Chem.*, 2010, **20**, 6086–6094.
41 M. C. Orilall and U. Wiesner, *Chem. Soc. Rev.*, 2011, **40**, 520–535.
42 C. Park, J. Yoon and E. L. Thomas, *Polymer*, 2003, **44**, 7779–7779.
43 H. G. Cui, Z. Y. Chen, S. Zhong, K. L. Wooley and D. J. Pochan, *Science*, 2007, **317**, 647–650.
44 R. C. Hayward and D. J. Pochan, *Macromolecules*, 2010, **43**, 3577–3584.
45 S. J. Holder and N. A. J. M. Sommerdijk, *Polym. Chem.*, 2011, **2**, 1018–1028.
46 P. Broz, S. Driamov, J. Ziegler, N. Ben-Haim, S. Marsch, W. Meier and P. Hunziker, *Nano Lett.*, 2006, **6**, 2349–2353.
47 Z. L. Tyrrell, Y. Q. Shen and M. Radosz, *Prog. Polym. Sci.*, 2010, **35**, 1128–1143.
48 S. M. D'Addio and R. K. Prud'homme, *Adv. Drug Delivery Rev.*, 2011, **63**, 417–426.
49 P. M. Valencia, O. C. Farokhzad, R. Karnik and R. Langer, *Nat. Nanotechnol.*, 2012, **7**, 623–629.
50 C. W. Wang, D. Sinton and M. G. Moffitt, *ACS Nano*, 2013, **7**, 1424–1436.
51 C. W. Wang, D. Sinton and M. G. Moffitt, *J. Am. Chem. Soc.*, 2011, **133**, 18853–18864.
52 C. W. Wang, A. Bains, D. Sinton and M. G. Moffitt, *Langmuir*, 2012, **28**, 15756–15761.
53 H. Y. Luo, J. L. Santos and M. Herrera-Alonso, *Chem. Commun.*, 2014, **50**, 536–538.
54 J. Thiele, D. Steinhauser, T. Pfohl and S. Forster, *Langmuir*, 2010, **26**, 6860–6863.
55 Y. Bae, S. Fukushima, A. Harada and K. Kataoka, *Angew. Chem., Int. Ed. Engl.*, 2003, **42**, 4640–4643.
56 R. Tong and J. J. Cheng, *Angew. Chem., Int. Ed. Engl.*, 2008, **47**, 4830–4834.
57 R. Tong and J. J. Cheng, *J. Am. Chem. Soc.*, 2009, **131**, 4744–4754.
58 R. Tong and J. J. Cheng, *Bioconjugate Chem.*, 2010, **21**, 111–121.
59 H. C. Yen, H. Cabral, P. Mi, K. Toh, Y. Matsumoto, X. Liu, H. Koori, A. Kim, K. Miyazaki, Y. Miura, N. Nishiyama and K. Kataoka, *ACS Nano*, 2014, **8**, 11591–11602.
60 Y. Yu, C. K. Chen, W. C. Law, J. Mok, J. Zou, P. N. Prasad and C. Cheng, *Mol. Pharm.*, 2013, **10**, 867–874.
61 Y. E. Aguirre-Chagala, J. L. Santos, Y. Huang and M. Herrera-Alonso, *ACS Macro Lett.*, 2014, **3**, 1249–1253.
62 S. Y. Zhang, J. Zou, M. Elsabahy, A. Karwa, A. Li, D. A. Moore, R. B. Dorshow and K. L. Wooley, *Chem. Sci.*, 2013, **4**, 2122–2126.
63 J. Zou, F. W. Zhang, S. Y. Zhang, S. F. Pollack, M. Elsabahy, J. W. Fan and K. L. Wooley, *Adv. Healthc. Mater.*, 2014, **3**, 441–448.
64 X. L. Hu, J. M. Hu, J. Tian, Z. S. Ge, G. Y. Zhang, K. F. Luo and S. Y. Liu, *J. Am. Chem. Soc.*, 2013, **135**, 17617–17629.
65 Y. Geng, P. Dalhaimer, S. Cai, R. Tsai, M. Tewari, T. Minko and D. E. Discher, *Nat. Nanotechnol.*, 2007, **2**, 249–255.

66 S. Kim, Y. Shi, J. Y. Kim, K. Park and J. X. Cheng, *Expert Opin. Drug Delivery*, 2010, **7**, 49–62.
67 C. J. Rijcken, C. J. Snel, R. M. Schiffelers, C. F. van Nostrum and W. E. Hennink, *Biomaterials*, 2007, **28**, 5581–5593.
68 M. Talelli, M. Iman, A. K. Varkouhi, C. J. F. Rijcken, R. M. Schiffelers, T. Etrych, K. Ulbrich, C. F. van Nostrum, T. Lammers, G. Storm and W. E. Hennink, *Biomaterials*, 2010, **31**, 7797–7804.
69 X. L. Zhang, K. Liu, Y. X. Huang, J. N. Xu, J. Li, X. C. Ma and S. Li, *Bioconjugate Chem.*, 2014, **25**, 1689–1696.
70 R. K. O'Reilly, C. J. Hawker and K. L. Wooley, *Chem. Soc. Rev.*, 2006, **35**, 1068–1083.
71 A. M. Nystrom and K. L. Wooley, *Acc. Chem. Res.*, 2011, **44**, 969–978.
72 J. Jin, M. M. Zhang, Q. Q. Xiong, P. C. Sun and H. Y. Zhao, *Soft Matter*, 2012, **8**, 11809–11816.
73 Y. Li, W. Xiao, K. Xiao, L. Berti, J. Luo, H. P. Tseng, G. Fung and K. S. Lam, *Angew. Chem., Int. Ed. Engl.*, 2012, **51**, 2864–2869.
74 H. Wang, L. Tang, C. L. Tu, Z. Y. Song, Q. Yin, L. C. Yin, Z. H. Zhang and J. J. Cheng, *Biomacromolecules*, 2013, **14**, 3706–3712.
75 X. T. Shuai, T. Merdan, A. K. Schaper, F. Xi and T. Kissel, *Bioconjugate Chem.*, 2004, **15**, 441–448.
76 A. M. Nystrom and K. L. Wooley, *Tetrahedron*, 2008, **64**, 8543–8552.
77 H. Fang, K. Zhang, G. Shen, K. L. Woolley and J. S. A. Taylor, *Mol. Pharm.*, 2009, **6**, 615–626.
78 K. Zhang, H. F. Fang, Z. Y. Chen, J. S. A. Taylor and K. L. Wooley, *Bioconjugate Chem.*, 2008, **19**, 1880–1887.
79 P. Zhao, L. X. Liu, X. Q. Feng, C. Wang, X. T. Shuai and Y. M. Chen, *Macromol. Rapid Commun.*, 2012, **33**, 1351–1355.
80 J. Guo, H. Hong, G. Chen, S. Shi, T. R. Nayak, C. P. Theuer, T. E. Barnhart, W. Cai and S. Gong, *ACS Appl. Mater. Interfaces*, 2014, **6**, 21769–21779.
81 M. A. Sowers, J. R. McCombs, Y. Wang, J. T. Paletta, S. W. Morton, E. C. Dreaden, M. D. Boska, M. F. Ottaviani, P. T. Hammond, A. Rajca and J. A. Johnson, *Nat. Commun.*, 2014, **5**, 5460.
82 H. I. Lee, J. Pietrasik, S. S. Sheiko and K. Matyjaszewski, *Prog. Polym. Sci.*, 2010, **35**, 24–44.
83 S. S. Sheiko, B. S. Sumerlin and K. Matyjaszewski, *Prog. Polym. Sci.*, 2008, **33**, 759–785.
84 J. A. Johnson, Y. Y. Lu, A. O. Burts, Y. H. Lim, M. G. Finn, J. T. Koberstein, N. J. Turro, D. A. Tirrell and R. H. Grubbs, *J. Am. Chem. Soc.*, 2011, **133**, 559–566.
85 J. A. Johnson, Y. Y. Lu, A. O. Burts, Y. Xia, A. C. Durrell, D. A. Tirrell and R. H. Grubbs, *Macromolecules*, 2010, **43**, 10326–10335.
86 J. Zou, G. Jafr, E. Themistou, Y. Yap, Z. A. Wintrob, P. Alexandridis, A. C. Ceacareanu and C. Cheng, *Chem. Commun.*, 2011, **47**, 4493–4495.
87 H. W. Shen and A. Eisenberg, *J. Phys. Chem. B*, 1999, **103**, 9473–9487.
88 A. Choucair and A. Eisenberg, *Eur. Phys. J. E: Soft Matter Biol. Phys.*, 2003, **10**, 37–44.
89 M. Kwak and A. Herrmann, *Chem. Soc. Rev.*, 2011, **40**, 5745–5755.
90 F. E. Alemdaroglu, N. C. Alemdaroglu, P. Langguth and A. Herrmann, *Macromol. Rapid Commun.*, 2008, **29**, 326–329.
91 M. P. Chien, A. M. Rush, M. P. Thompson and N. C. Gianneschi, *Angew. Chem., Int. Ed. Engl.*, 2010, **49**, 5076–5080.
92 J. Li, C. Fan, H. Pei, J. Shi and Q. Huang, *Adv. Mater.*, 2013, **25**, 4386–4396.
93 R. P. Goodman, M. Heilemann, S. Doose, C. M. Erben, A. N. Kapanidis and A. J. Turberfield, *Nat. Nanotechnol.*, 2008, **3**, 93–96.
94 F. A. Aldaye, P. K. Lo, P. Karam, C. K. McLaughlin, G. Cosa and H. F. Sleiman, *Nat. Nanotechnol.*, 2009, **4**, 349–352.
95 H. Qian, C. Tian, J. Yu, F. Guo, M. S. Zheng, W. Jiang, Q. F. Dong and C. Mao, *Small*, 2014, **10**, 855–858.
96 C. Zhang, X. Li, C. Tian, G. Yu, Y. Li, W. Jiang and C. Mao, *ACS Nano*, 2014, **8**, 1130–1135.
97 T. Torring, N. V. Voigt, J. Nangreave, H. Yan and K. V. Gothelf, *Chem. Soc. Rev.*, 2011, **40**, 5636–5646.
98 J. Hahn, S. F. J. Wickham, W. M. Shih and S. D. Perrault, *ACS Nano*, 2014, **8**, 8765–8775.
99 J.-W. Keum and H. Bermudez, *Chem. Commun.*, 2009, 7036–7038.
100 Q. Mei, X. Wei, F. Su, Y. Liu, C. Youngbull, R. Johnson, S. Lindsay, H. Yan and D. Meldrum, *Nano Lett.*, 2011, **11**, 1477–1482.
101 Y. X. Zhao, A. Shaw, X. Zeng, E. Benson, A. M. Nystrom and B. Hogberg, *ACS Nano*, 2012, **6**, 8684–8691.
102 S. Ko, H. Liu, Y. Chen and C. Mao, *Biomacromolecules*, 2008, **9**, 3039–3043.
103 S. M. Douglas, I. Bachelet and G. M. Church, *Science*, 2012, **335**, 831–834.
104 X. Liu, Y. Xu, T. Yu, C. Clifford, Y. Liu, H. Yan and Y. Chang, *Nano Lett.*, 2012, **12**, 4254–4259.
105 R. Crawford, C. M. Erben, J. Periz, L. M. Hall, T. Brown, A. J. Turberfield and A. N. Kapanidis, *Angew. Chem., Int. Ed. Engl.*, 2013, **52**, 2284–2288.
106 H. Lee, A. K. Lytton-Jean, Y. Chen, K. T. Love, A. I. Park, E. D. Karagiannis, A. Sehgal, W. Querbes, C. S. Zurenko, M. Jayaraman, C. G. Peng, K. Charisse, A. Borodovsky, M. Manoharan, J. S. Donahoe, J. Truelove, M. Nahrendorf, R. Langer and D. G. Anderson, *Nat. Nanotechnol.*, 2012, **7**, 389–393.
107 W. W. Grabow and L. Jaeger, *Acc. Chem. Res.*, 2014, **47**, 1871–1880.
108 D. Shu, W. D. Moll, Z. Deng, C. Mao and P. Guo, *Nano Lett.*, 2004, **4**, 1717–1723.
109 H. Ohno, T. Kobayashi, R. Kabata, K. Endo, T. Iwasa, S. H. Yoshimura, K. Takeyasu, T. Inoue and H. Saito, *Nat. Nanotechnol.*, 2011, **6**, 116–120.
110 K. A. Afonin, W. K. Kasprzak, E. Bindewald, M. Kireeva, M. Viard, M. Kashlev and B. A. Shapiro, *Acc. Chem. Res.*, 2014, **47**, 1731–1741.

111 T. Kim, K. A. Afonin, M. Viard, A. Y. Koyfman, S. Sparks, E. Heldman, S. Grinberg, C. Linder, R. P. Blumenthal and B. A. Shapiro, *Mol. Ther. Nucleic Acids*, 2013, **2**, e80.
112 K. E. Shopsowitz, Y. H. Roh, Z. J. Deng, S. W. Morton and P. T. Hammond, *Small*, 2014, **10**, 1623–1633.
113 J. B. Lee, J. Hong, D. K. Bonner, Z. Poon and P. T. Hammond, *Nat. Mater.*, 2012, **11**, 316–322.
114 I. K. Voets, A. de Keizer and M. A. Cohen Stuart, *Adv. Colloid Interface Sci.*, 2009, **147–148**, 300–318.
115 K. Kataoka, A. Harada and Y. Nagasaki, *Adv. Drug Delivery Rev.*, 2001, **47**, 113–131.
116 K. Osada, R. J. Christie and K. Kataoka, *J. R. Soc., Interface*, 2009, **6**(Suppl 3), S325–S339.
117 J. H. Chen and N. C. Seeman, *Nature*, 1991, **350**, 631–633.
118 R. P. Goodman, I. A. Schaap, C. F. Tardin, C. M. Erben, R. M. Berry, C. F. Schmidt and A. J. Turberfield, *Science*, 2005, **310**, 1661–1665.
119 Y. He, T. Ye, M. Su, C. Zhang, A. E. Ribbe, W. Jiang and C. Mao, *Nature*, 2008, **452**, 198–201.
120 K. Osada, T. Shiotani, T. A. Tockary, D. Kobayashi, H. Oshima, S. Ikeda, R. J. Christie, K. Itaka and K. Kataoka, *Biomaterials*, 2012, **33**, 325–332.
121 A. Dirisala, K. Osada, Q. Chen, T. A. Tockary, K. Machitani, S. Osawa, X. Liu, T. Ishii, K. Miyata, M. Oba, S. Uchida, K. Itaka and K. Kataoka, *Biomaterials*, 2014, **35**, 5359–5368.
122 T. A. Tockary, K. Osada, Q. Chen, K. Machitani, A. Dirisala, S. Uchida, T. Nomoto, K. Toh, Y. Matsumoto, K. Itaka, K. Nitta, K. Nagayama and K. Kataoka, *Macromolecules*, 2013, **46**, 6585–6592.
123 K. Osada, *Polym. J.*, 2014, **46**, 469–475.
124 J. Shi, J. L. Choi, B. Chou, R. N. Johnson, J. G. Schellinger and S. H. Pun, *ACS Nano*, 2013, **7**, 10612–10620.
125 X. Jiang, W. Qu, D. Pan, Y. Ren, J.-M. Williford, H. Cui, E. Luijten and H.-Q. Mao, *Adv. Mater.*, 2013, **25**, 227–232.
126 J.-M. Williford, Y. Ren, K. Huang, D. Pan and H.-Q. Mao, *J. Mater. Chem. B: Mater. Biol. Med.*, 2014, **2**, 8106–8109.
127 X. Jiang, Y. Zheng, H. H. Chen, K. W. Leong, T. H. Wang and H. Q. Mao, *Adv. Mater.*, 2010, **22**, 2556–2560.
128 J. Li, X. Yu, Y. Wang, Y. Yuan, H. Xiao, D. Cheng and X. Shuai, *Adv. Mater.*, 2014, **26**, 8217–8224.
129 S. M. D'Addio and R. K. Prud'homme, *Adv. Drug Delivery Rev.*, 2011, **63**, 417–426.
130 P. Decuzzi, R. Pasqualini, W. Arap and M. Ferrari, *Pharm. Res.*, 2009, **26**, 235–243.
131 P. Decuzzi, S. Lee, B. Bhushan and M. Ferrari, *Ann. Biomed. Eng.*, 2005, **33**, 179–190.
132 S. Shah, Y. L. Liu, W. Hu and J. M. Gao, *J. Nanosci. Nanotechnol.*, 2011, **11**, 919–928.
133 S. Y. Lee, M. Ferrari and P. Decuzzi, *Nanotechnology*, 2009, **20**, 495101.
134 F. Gentile, C. Chiappini, D. Fine, R. C. Bhavane, M. S. Peluccio, M. M. Cheng, X. Liu, M. Ferrari and P. Decuzzi, *J. Biomech.*, 2008, **41**, 2312–2318.
135 N. Doshi, B. Prabhakarpandian, A. Rea-Ramsey, K. Pant, S. Sundaram and S. Mitragotri, *J. Controlled Release*, 2010, **146**, 196–200.
136 V. V. Shuvaev, M. A. Ilies, E. Simone, S. Zaitsev, Y. Kim, S. Cai, A. Mahmud, T. Dziubla, S. Muro, D. E. Discher and V. R. Muzykantov, *ACS Nano*, 2011, **5**, 6991–6999.
137 V. P. Chauhan, Z. Popovic, O. Chen, J. Cui, D. Fukumura, M. G. Bawendi and R. K. Jain, *Angew. Chem., Int. Ed. Engl.*, 2011, **50**, 11417–11420.

Review in Advance first posted online on June 2 , 2014. (Changes may still occur before final publication online and in print.)

Recent Advances in Nanoparticle-Mediated siRNA Delivery

John-Michael Williford,[1,2] Juan Wu,[3] Yong Ren,[3] Maani M. Archang,[3] Kam W. Leong,[5] and Hai-Quan Mao[2,3,4]

[1]Department of Biomedical Engineering, Johns Hopkins School of Medicine, Baltimore, Maryland 21205

[2]Institute for NanoBioTechnology, [3]Department of Materials Science and Engineering, Johns Hopkins University, Baltimore, Maryland 21218; email: hmao@jhu.edu

[4]Translational Tissue Engineering Center, Johns Hopkins School of Medicine, Baltimore, Maryland 21287

[5]Department of Biomedical Engineering, Duke University, Durham, North Carolina 27708; email: kam.leong@duke.edu

Annu. Rev. Biomed. Eng. 2014. 16:347–70

The *Annual Review of Biomedical Engineering* is online at bioeng.annualreviews.org

This article's doi: 10.1146/annurev-bioeng-071813-105119

Keywords

siRNA delivery, nanoparticle, gene therapy, stability, intracellular trafficking

Abstract

Inhibiting specific gene expression by short interfering RNA (siRNA) offers a new therapeutic strategy to tackle many diseases, including cancer, metabolic disorders, and viral infections, at the molecular level. The macromolecular and polar nature of siRNA hinders its cellular access to exert its effect. Nanoparticulate delivery systems can promote efficient intracellular delivery. Despite showing promise in many preclinical studies and potential in some clinical trials, siRNA has poor delivery efficiency, which continues to demand innovations, from carrier design to formulation, in order to overcome transport barriers. Previous findings for optimal plasmid DNA delivery cannot be generalized to siRNA delivery owing to significant discrepancy in size and subtle differences in chain flexibility between the two types of nucleic acids. In this review, we highlight the recent advances in improving the stability of siRNA nanoparticles, understanding their intracellular trafficking and release mechanisms, and applying judiciously the promising formulations to disease models.

Contents

1. RNAi THERAPEUTICS

Since its initial discovery by Mello, Fire, and colleagues (1), RNA interference (RNAi) has shown great therapeutic potential as a posttranslation gene regulation process for a range of disease, including cancer, genetic disorders, autoimmune diseases, and viral infections (2–4). The development of exogenously produced 21–23 base pair, double-stranded short interfering RNAs (siRNAs) allows for sequence-specific messenger RNA (mRNA) degradation following incorporation into the RNA-induced silencing complex (RISC) in the cytosol (5). However, owing to the high negative charge density and relatively large size of the siRNA molecules, naked siRNA molecules are not able to efficiently enter cells to knock down the mRNA target (6). Furthermore, rapid degradation of siRNA by serum nucleases followed by renal clearance occurs upon its injection into the bloodstream (3, 7). The in vivo application of RNAi has thus been hindered by poor delivery efficiency to the action site of the target cells. Improving delivery strategies remains the critical challenge for realization of the tremendous potential of RNAi therapeutics.

2. DELIVERY METHODS FOR siRNA THERAPEUTICS

2.1. RNA Structural Modifications and Molecular Conjugates

Incorporation of several structural modifications has helped to improve siRNA stability against nuclease degradation. For example, 2′-*O*-methyl modifications, incorporation of alternative 2′-sugar modifications, and introduction of 3′-phosphorothioate linkages have all led to decreased endonuclease degradation. 2′-fluoro modification has also improved stability while maintaining the function of siRNA (8, 9). Structurally modified molecules still suffer from several drawbacks, including limited targeting capability as well as a need for high doses to reach therapeutic concentrations (10). The siRNA conjugates (e.g., cholesterol-conjugated siRNA and RGD peptide–conjugated siRNA) have also been a popular delivery strategy. A recent study by Huang et al. (11) highlighted the effect of conjugation on the biodistribution of siRNA in mice. Injection of

siRNA alone led to rapid accumulation of siRNA in the kidney and intestine, and the authors concluded that intestinal elimination occurred following hepatic processing and secretion, as bile duct ligation led to a near background level of siRNA in the intestine. By contrast, conjugation of RGD or cholesterol to the siRNA led to greater accumulation of siRNA in the liver.

2.2. Lipid-Based Nanoparticle Delivery Systems

Nanoparticles have been widely used to improve siRNA's delivery efficiency both in vitro and in vivo. The most common nanoparticle delivery systems are lipid based. A number of commercially available lipid formulations have been used as siRNA delivery agents, including Lipofectamine 2000 (LF2000) (12), Lipofectamine RNAiMAX (13), 1,2-dioleoyl-3-trimethylammonium-propane (DOTAP) (14), RNAiFect (14), TransIT-TKO (15), and TransIT-siQUEST (15). The majority of siRNA nanoparticles in Phase I clinical trials are lipid based as well (16). A major drawback of lipid-mediated delivery of siRNA arises from an innate immune response often observed after particle administration (17). Studies have shown that liposomes can activate the complement system (18). DOTAP, a common cationic lipid, elicited a severe interferon response, as well as an upregulation of signal transducer and activator of transcription 1 (STAT1), a downstream signaling molecule (14). To reduce the inflammatory response, strategies such as PEGylation, the coating of a particle surface with a layer of poly(ethylene glycol) (PEG), have been widely employed (19, 20). In an alternative approach, Abrams et al. (21) showed that treatment with the anti-inflammatory drug dexamethasone significantly reduced the acute inflammation responses mediated by lipid nanoparticles while maintaining a similar level of siRNA knockdown efficiency.

Lipid nanoparticles typically accumulate in the liver, even without any liver-specific targeting moieties (22–25). For example, a single dose of PEGylated, cholesterol-based lipid particles containing luciferase siRNA yielded a peak gene knockdown of 90% in the liver that persisted for up to 10 days (23). Another lipid-based system composed of cationic lipids with tertiary amines and hydrophobic linoleyl groups (termed TRENL3) also displayed hepatocyte-specific delivery (22). Several recent studies have reported screening of a large library of lipid-based materials to identify the optimal lipid particle compositions for gene silencing. Using a lipid nanoparticle library, Whitehead et al. (26) demonstrated that when comparing parameters for predicting in vivo efficacy of the delivery system, only siRNA entrapment efficiency was partially predictive, whereas surface charge and particle size showed no clear correlation. Another report, by Jayaraman et al. (27), highlighted the importance of the lipid pK_a in its knockdown efficiency in vivo by showing that lipids with pK_a between 6.2 and 6.5 showed the highest knockdown efficiency; an optimized lipid nanoparticle system based on the optimal pK_a mediated 50% gene silencing at a dose as low as 5 μg/kg using a Factor VII siRNA knockdown mouse model. In a follow-up study, Alabi et al. (28) used a multiparametric approach to identify the structure-function-activity relationship for lipid nanoparticle–mediated siRNA delivery in vivo. Their analysis confirmed that pK_a of the cationic lipid has the best correlation with gene silencing of the lipid nanoparticles. However, analyzing a combination of parameters, such as extracellular stability, intracellular stability, uptake, hemolysis, and in vitro knockdown, can be used to better predict in vivo efficacy than examining solely the in vitro knockdown efficiency.

2.3. Polymer-Based Nanoparticle Delivery Systems

Polymer-based systems have also been widely studied for siRNA delivery (29), although many of the polymer carriers were first designed for plasmid DNA delivery. This has led to some reports on inconsistencies in carrier effectiveness when these carriers were extended to siRNA delivery. One of the most commonly used polymers is polyethyleneimine (PEI) in both the linear and

branched forms (30–32). Branched PEI (bPEI) suffers from significant toxicity caused by inflammatory responses and is often subjected to rapid macrophage uptake and clearance (33–35). Linear PEI (lPEI)/siRNA nanoparticles, by contrast, exhibit a better compatibility profile when injected systemically. According to a study by Bonnet et al. (36), no significant increase of proinflammatory cytokines or liver enzymes was observed following lPEI/siRNA nanoparticle administration. A major limitation of PEI/siRNA nanoparticles for in vivo gene knockdown is their poor colloidal stability in salt- and serum-containing media (37, 38). The positively charged nanoparticles tend to rapidly aggregate upon intravenous injection as shown by in situ real-time confocal microscopy (38). Conjugation of PEG chains to these nanoparticles has been explored as a strategy to address this issue (39–41). PEGylated PEI/siRNA nanoparticles exhibited a markedly reduced tendency to aggregate (38). Merkel et al. (42) showed that PEGylation of bPEI/siRNA nanoparticles resulted in a lower amount of liver deposit following intravenous injection. However, the PEGylated nanoparticles showed lower complex stability—they tended to dissociate upon passage through the liver, making them less suitable for systemic injection. In addition, these PEGylated bPEI/siRNA nanoparticles did not elicit a significant degree of complement activation, in contrast to bPEI/siRNA nanoparticles, which induced a moderate level of complement activation in vitro (33). However, it must be cautioned that when tested in a swine model, nanoparticles formed with both bPEI and PEG-bPEI elicited complement activation–related pseudoallergy, as indicated by cardiopulmonary reactions. Among different polymers, use of PEG-grafted bPEI with 20-kDa PEG yielded the least complement activation. In a rodent model for gene knockdown in the lung, PEI/siRNA and PEG-PEI/siRNA nanoparticles were injected intratracheally (43). Both PEG-PEI nanoparticles and PEI particles with hydrophobic fatty acid modifications invoked inflammatory cytokines and elevated levels of IgM in the bronchoalveolar fluid, although PEG-PEI particles showed reduced cytotoxicity. The fatty acid–modified PEI particles showed the greatest knockdown efficiency in leukocytes and alveolar macrophages, highlighting the need for further study to balance improved knockdown efficiency, low cytotoxicity, and reduced immunostimulatory activities for the successful in vivo application of PEI-based carriers.

Although PEI-based polymers constitute a large fraction of polymer-mediated siRNA delivery systems, several new polymers have been developed to address the issues of biodegradability, biocompatibility, and stability. Polycationic micelles have been extensively studied by the Kataoka group (44–47), among others, for successful siRNA delivery in vitro and in vivo. Poly(β-amino ester)s, another important class of polycations owing to their hydrolytic degradability, high transfection efficiency, and low toxicity, have been employed for siRNA delivery (48–51). Using a library of polymers containing different backbone, side-chain, and end-cap building blocks, a number of carriers have been screened to assess their knockdown efficiency in glioblastoma cells in vitro (52). The most efficient carriers mediated over 90% knockdown for up to 15 days while maintaining high cell viability. High levels of gene knockdown were also achieved following low-dose siRNA treatments of only 5 nM.

3. OVERCOMING THE MAJOR BARRIERS FOR siRNA DELIVERY

Many of the materials used for nanoparticle-mediated siRNA delivery, particularly the polycations, were originally developed for plasmid DNA delivery systems. However, there is increasing awareness that the optimal carrier design for binding DNA may differ from that for RNA (53). Although the anionic phosphodiester backbone in both DNA and RNA can interact electrostatically with polycations, the persistence length (the length scale over which the macromolecule behaves like a rigid rod) of double-stranded (ds)DNA is shorter than that of dsRNA—~50 nm versus ~70 nm—rendering dsRNA a stiffer molecule. This is accompanied by a large difference in the

relative sizes of siRNA (typically 21–23 base pairs) and plasmid DNA (usually several thousands of base pairs), which explains the lower degree of multivalent binding and lower condensation ability of siRNA compared with DNA plasmids. Furthermore, siRNA molecules are more susceptible to nuclease degradation than circular plasmids are, so a stable delivery system is imperative for effective in vivo delivery. Finally, the site of action for siRNA knockdown is in the cytoplasm rather than the nucleus as in plasmid DNA, which may result in different intracellular unpacking profiles for optimal performance. It is therefore unsurprising that carriers originally developed for DNA have yielded mixed results when applied to siRNA delivery. Over the past several years, a number of key strategies have been designed with these differences in mind to improve the efficacy of nanoparticle-based siRNA delivery.

3.1. Improving siRNA Packaging Ability and Complex Stability

As mentioned above, PEI has been a popular material for siRNA delivery. However, to form stable nanoparticles, many previous studies used a very high N/P ratio, which is the molar ratio of amines in the polymer backbone to phosphates in the nucleic acid. High N/P ratios lead to a large excess of polycations, often causing high levels of toxicity (32, 54). A recent study by Zheng et al. (55) noted that these high N/P ratios might not be optimal for efficient nanoparticle formation. Using a combination of experimental and molecular dynamics simulations, their study found that stable nanoparticles were formed at a high N/P ratio of 20 as well as at a low N/P ratio of 2. When comparing knockdown levels, N/P ratios of 2 and 20 mediated similar knockdown efficiency, but cytotoxicity was negligible at the low N/P ratio compared with around 25% at the higher N/P ratio of 20, highlighting the potential utility of low N/P ratios for polycation-mediated siRNA delivery.

3.1.1. Increasing nanoparticle stability by introducing hydrophobic component. Hydrophobic modifications of PEI have shown improved particle stability. Modification of 600-Da PEI with alkyl chains of 8 and 13 carbons led to the formation of stable nanoparticles, whereas unmodified PEI did not form particles under the same conditions (56). This result was further confirmed by gene silencing studies, in which the alkyl-modified PEI showed greater than 80% gene knockdown, whereas unmodified PEI did not mediate any gene silencing. It is important to note that the hydrophobic modifications did increase the toxicity significantly, especially at N/P ratios greater than 12, possibly owing to the enhanced ability for membrane disruption. Work by Schroeder et al. (57) used lipid-modified 600-Da PEI in a similar study. When modified with a 16-carbon lipid, up to 80% silencing could be achieved with the highest lipid modification, whereas the unmodified PEI mediated no significant knockdown. The lipid-modified PEI did not affect cell viability. The study also found that binding affinity between the polymer and siRNA decreased with the addition of lipid conjugation. The decrease in binding affinity led to a subsequent increase in knockdown efficiency, highlighting the important balance between particle stability and siRNA release, a result that was corroborated by Han et al. (58) using a different polycation-based siRNA delivery system. Extending their work in vivo, these authors found that the particles with balanced binding affinities showed 70% knockdown in tumor-bearing mice as well as a complete halting of tumor growth after 20 days. Zheng et al. (59) demonstrated efficient gene silencing in vitro and enhanced particle stability in vivo using a PEI-*graft*-polycaprolactone-*block*-PEG (PEI-*g*-PCL-*b*-PEG) copolymers. PCL here serves as the biodegradable hydrophobic component to stabilize the complex core of the micelles. Particles with the highest grafting degrees mediated 75% knockdown in human ovarian cancer SKOV3 cells compared with 50% knockdown for PEI alone. Following intravenous injection, these copolymer/siRNA nanoparticles circulated longer than PEI/siRNA. Lee et al. (60) incorporated poly(D,L-lactic acid-*coglycolic* acid) (PLGA) as the

hydrophobic moiety to stabilize PEI/siRNA micelle nanoparticles with an average diameter of 30 nm. These nanoparticles mediated up to 60% gene silencing in vitro, whereas lPEI/siRNA particles showed no knockdown of gene expression.

3.1.2. Enhancing complex stability by introducing a core-shell structure. A different stabilization strategy, reported by Bui et al. (61), aimed at developing a virus-mimicking core-shell structure. To form the core, siRNA was condensed with PEI, upon which a glycoprotein-mimicking amphiphilic block copolymer hyaluronan-*block*-poly(γ-benzyl L-glutamate) (HA-*b*-PBLG) was coated. The coating was achieved by assembling HA-*b*-PBLG onto the PEI/siRNA core in dimethyl sulfoxide (DMSO), followed by dialysis in water, forming a viral capsid–like shell, as shown in **Figure 1*a***. These modified particles had double the knockdown efficiency of PEI/siRNA complexes. Lipid-polymer hybrid materials have also gained attention in recent years. Using a soft-lithography fabrication technique, Hasan et al. (62) prepared rod-shaped PLGA nanoparticles and coated them with cationic DOTAP:DOPE lipids. The particles were used to condense siRNA with 46% encapsulation efficiency, leading to ∼80% knockdown in three different prostate cancer cell lines. Using a different PEG-*b*-poly(D,L-lactide)/siRNA nanoparticle formulation assembled with a cationic lipid at 90% encapsulation efficiency, the authors reported that 50% knockdown efficiency was achieved in an orthotopic liver tumor model (63). Using a nanoporous silica core coated with a cationic lipid bilayer, Ashley et al. (64) demonstrated a delivery system that can be used for a number of different therapeutics including siRNA. These nanoparticles can encapsulate nearly 1,000 times more siRNA than can liposomes of similar size and made of the same lipid components. Finally, Jiang et al. (65) prepared iron oxide nanoparticles coated with a lipid-like material for delivery of both DNA and siRNA, offering a platform amenable to magnetically guided targeting and the potential for MRI imaging. Magnetic field was also used to enhance gene knockdown efficiency; up to 90% knockdown was achieved using these nanoparticles in presence of magnet at 3 ng/well siRNA, as compared with 50% knockdown without magnetic field.

3.1.3. Enhancing complex stability by covalent and physical cross-links. Strategies to improve the stability of siRNA nanoparticles have also focused significantly on the use of cross-linking as well as on the incorporation of assisting molecules. The Wagner group (66–68) developed a series of oligo(ethane amino) amides using solid-phase peptide synthesis methods to generate carriers with i-shape, T-shape, and U-shape configurations, depending on the building blocks used. Incorporation of cysteines into the oligomers was particularly beneficial for stabilizing the particles through the formation of disulfide bonds (67). Shim & Kwon (32) studied the effect of linear PEI modification with an acid-degradable ketal group. Compared with unmodified lPEI, ketalized lPEI displayed greater gene silencing with similar or decreased toxicity, even at N/P ratios of 40 and above. This increase in knockdown was attributed to a greater release of siRNA into the cytoplasm owing to the presence of the degradable ketal groups. In a similar study, Shim & Kwon (69) prepared a linear polyspermine for siRNA delivery through cross-linking with both ketalized and nonketalized diacrylates. The ketalized polyspermine showed the highest gene silencing owing to the enhanced intracellular release of siRNA. Fröhlich et al. (70) prepared siRNA nanoparticles using an oligoethylenimine-based polymer that was cross-linked using an amine-reactive cross-linker, dithiobis(succinimidyl propionate) (DSP). Cross-linked nanoparticles exhibited higher stability and, thus, greater cell uptake and knockdown efficiency (80% versus 40%) compared with nanoparticles without DSP. Matsumoto et al. (71) prepared a PEG-*b*-poly(L-lysine) (PLL) copolymer with a disulfide-cross-linked core by thiolating the PLL segment with 2-iminothiolane. Compared with un-cross-linked nanoparticles, the thiolated particles achieved 100-fold higher knockdown efficiency owing to increased nanoparticle stability

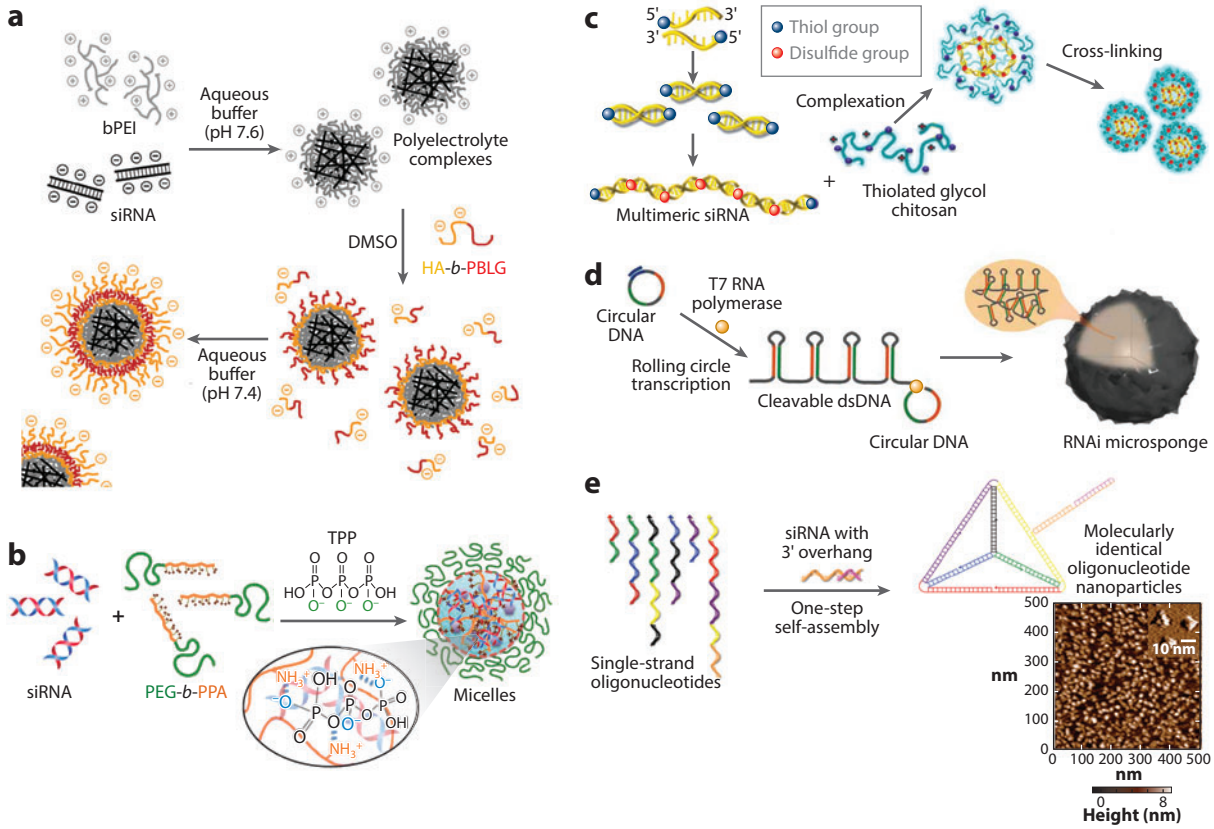

Figure 1

Example strategies for enhancing the stability of siRNA nanoparticles. (*a*) Design of core-shell particles by self-assembling HA-*b*-PBLG polymer coating around a bPEI/siRNA core. (Panel adapted with permission from 61; ©2012 American Chemical Society.) (*b*) Stabilization of PEG-*b*-PPA/siRNA nanoparticles through ionic cross-linking by TPP (73). (*c*) Formation of nanoparticles by condensing oligomeric siRNA and thiolated glycol chitosan. (Panel adapted with permission from 76; ©2012 WILEY-VCH Verlag GmbH & Co. KGaA, Weinheim.) (*d*) Generation of self-assembled RNAi microsponges using rolling circle transcription, forming multiple tandem hairpin structures from antisense-sense strand binding. Once delivered to cytosol, the hairpins can be cleaved by Dicer, thus releasing individual siRNA molecules. [Panel adapted by permission from Macmillan Publishers Ltd.: *Nature Materials* (79), ©2012.] (*e*) Generation of self-assembled tetrahedron oligonucleotide nanoparticles for site-specific siRNA hybridization, with an atomic force microscopy image showing monodispersed nucleic acid nanoparticles on mica. [Panel adapted by permission Macmillan Publishers Ltd.: *Nature Nanotechnology* (80), ©2012.] Abbreviations: bPEI, branched polyethyleneimine; DMSO, dimethyl sulfoxide; ds, double-stranded; HA-*b*-PBLG, hyaluronan-*block*-poly(γ-benzyl L-glutamate); PEG-*b*-PPA, poly(ethylene glycol)-*block*-polyphosphoramidate; RNAi, RNA interference; siRNA, short interfering RNA; TPP, sodium triphosphate.

in physiological medium. Hong et al. (72) also used a disulfide cross-linking strategy to form lPEI/siRNA nanogels. By using lPEI and siRNA both modified with disulfide, the authors found that nanoparticle stability was maintained after challenge with an excess amount of polyanions. Under reducing conditions similar to those in the cytoplasm, siRNA was efficiently released. These cross-linked nanoparticles improved knockdown efficiency from undetectable levels to over 70% in a melanoma cell line. Moving beyond covalent cross-linking strategies, a report by Nakanishi et al. (73) used an ionic cross-linking agent, sodium triphosphate (TPP), to improve the stability of PEG-*block*-polyphosphoramidate (PPA)/siRNA micellar nanoparticles (**Figure 1*b***). Without TPP, particle formation was not detected under the tested conditions. TPP

incorporation led to the formation of stable, discrete, and uniform 80–100-nm nanoparticles that were able to achieve up to 80% knockdown efficiency with no significant loss in cell viability.

3.1.4. Enhancing complex stability by using multimeric siRNA. Whereas all of the above-described studies focused on ways to alter the structure of the carrier, several studies have explored modifications of the siRNA cargo to improve its compaction ability and particle stability. One popular strategy for siRNA modification is to generate multimeric siRNA molecules that have higher molecular weights (74). Upon complexation with lPEI, the multimeric siRNAs formed much smaller (80-nm) and more condensed nanoparticles, compared with the 464-nm particles formed by monomeric siRNA. Multimeric lPEI/siRNA nanoparticles had up to 60% knockdown efficiency, whereas unmodified siRNA particles only showed ∼20% knockdown. Similarly, Lee et al. further improved efficiency with multimeric siRNAs linked via disulfide bonds (75). Using this polymeric siRNA, the authors formed nanoparticles with thiolated glycol chitosan, as shown in **Figure 1*c*** (76). When these nanoparticles were injected systemically into tumor-bearing mice, significant amounts of them accumulated in the tumor tissue, leading to a reduction in tumor growth. Liao et al. (77) used a more controlled conjugation scheme that connects two siRNA molecules through a PEG linkage. This dimerized siRNA led to improved siRNA enzymatic stability, higher gene silencing, and longer duration of knockdown compared with monomeric siRNA. This strategy also allows for simultaneous dual-target knockdown via conjugation of two separate siRNA sequences. Hong et al. (78) reported the formation of siRNA microgels with controllable porosity through the use of a Y-shaped or linear cross-linking agent. Condensation with lPEI led to the formation of particles with sizes ranging from 99 to 215 nm for Y-shaped and linear siRNA molecules, respectively. Up to 60% knockdown efficiency was achieved, compared with negligible knockdown efficiency for particles prepared with monomeric siRNA. Lee et al. (79) reported a unique approach for multimeric siRNA synthesis: As shown in **Figure 1*d***, rolling circle transcription leads to the formation of RNAi microsponges, composed completely of cleavable hairpin RNA strands that can be processed by the enzyme DICER into siRNA molecules. The authors estimated that each microsponge could hold as many as 102,000 siRNA molecules, although DICER cleavage efficiency was only around 21%. Because the microsponges were more than 2 μm in diameter, PEI was used to condense the sponges into 200-nm particles. At a concentration of 980 fM, PEI/siRNA microsponges were able to reduce gene expression by nearly 60%, using approximately three orders of magnitude less carrier than standard nanoparticle/siRNA delivery vehicles require. Another interesting approach reported by Lee et al. (80) takes advantage of complementary DNA strand binding to form self-assembled nucleic acid nanoparticles (**Figure 1*e***). The particles form a tetrahedral structure, and siRNA can be linked to the nanoparticle through complementary binding of a 3′-overhanging end. Because they are self-assembled from defined DNA sequences, the particles show a high degree of uniformity with a diameter of around 28 nm. Particle circulation half-life was increased 4-fold over siRNA alone, and 50% gene knockdown was achieved following intravenous injection of a 2.5 mg/kg siRNA dose in KB tumor–bearing mice.

3.2. Increasing Cellular Entry

Cellular uptake of nanoparticles for siRNA delivery is a roadblock preventing the successful translation of RNAi therapeutics. Because many of the nanoparticles carry a positive surface charge, nonspecific interaction and binding occur with the negatively charged cell membrane. However, as mentioned above, positively charged particles tend to aggregate in serum-containing media and biological fluid, necessitating a masking of the positive charge through PEGylation. PEGylated nanoparticles, though offering greater stability, often display impaired cell binding and uptake

(81). For this reason, strategies to improve binding and uptake through the shedding of the PEG layer under specific stimuli have been developed.

One such study, reported by Kim et al. (82), used a block copolymer of PEG and a polyaspartamide derivative linked together by disulfide bonds. When exposed to reducing conditions, such as those in the cytoplasm and in the tumor microenvironment, the PEG chains were cleaved, leading to an increased surface charge as a result of the loss of PEG shielding. In addition, this carrier showed improved knockdown efficiency both in vitro and in vivo in pancreatic cancer cells and subcutaneous tumor xenograft, respectively. A second study, by Yang et al. (83) and highlighted in **Figure 2*a***, used a pH-sensitive linker that allowed shedding of the PEG chains upon small changes in local pH, such as those in the tumor microenvironment, where pH can fall to ~6.5. The authors prepared a particle with a polycationic core coated with an anionic polymer linked to PEG. At a pH of 6.5, the anionic polymer became positively charged, causing the PEG to dissociate, as confirmed by surface-charge measurements. Cell uptake, gene knockdown, and tumor growth were all significantly better for the particles with sheddable PEG coronas, compared with the nonsheddable controls. In a third study, a lipid-based nanoparticle vehicle was prepared with a matrix metalloproteinase (MMP)-cleavable PEG coating, as the tumor microenvironment is rich in MMPs (84). The cleavable particles showed improved gene silencing, cellular uptake, and endosomal escape compared with noncleavable controls. In addition, higher tumor accumulation and gene silencing were observed in vivo for the cleavable particles.

Beyond the removal of the PEG layer, additional studies aiming to improve the targeting and cellular uptake of siRNA nanocomplexes rely on the use of cell- and tissue-specific ligands. A number of these studies seek to improve the targeting of nanoparticles to tumor tissue. Common ligands such as RGD, transferrin, and folate have been extensively used for tumor targeting (44, 85, 86). Several additional targeting molecules have also been identified recently. One such molecule is a peptide sequence known as LyP-1 (87). LyP-1 is a cell surface protein that is overexpressed on tumor cells, tumor lymphatics, and tumor-associated macrophages (88). Conjugation of antibody fragments against human epidermal growth factor 2 (Her2)-expressing breast cancer cells to nanocomplexes has also shown benefits in vivo, including enhanced delivery to the tumor tissue as well as a slowing of tumor growth when the nanocomplexes were administered intravenously (89). Liver-specific targeting molecules have also been widely studied for improved nanoparticle-mediated siRNA delivery. Vitamin A–conjugated liposomes have shown enhanced activity against liver fibrosis (90). *N*-acetylgalactosamine-conjugated micellar nanoparticles showed enhanced targeting and gene knockdown efficiency in mouse hepatocytes compared with nontargeted particles (91).

In addition to the use of ligand-targeting strategies, enhanced siRNA nanoparticle uptake can be achieved through the use of cell-penetrating peptides (CPPs) or polymers. Common CPPs include the TAT peptide, derived from HIV virus, and various polyarginine peptides (92). Combination of a CPP with a LyP-1 targeting peptide led to enhanced tumor-specific delivery compared with the use of untargeted controls, highlighting the potential for combination peptides to afford both active targeting and enhanced cellular penetration (**Figure 2*b***) (93). Several groups are currently developing additional cell-penetrating materials. Recent work by Cheng and colleagues (94, 95) involves the development of supramolecular self-assembled nanocomplexes for enhanced intracellular delivery. Although the work currently applies mainly to plasmid DNA, extension of these systems to siRNA delivery is also possible. Incorporation of an α-helical cationic polypeptide into the carrier has allowed for enhanced membrane penetration capabilities, both extracellularly to improve cell uptake and intracellularly to enhance endosomal escape.

One final study (96), albeit not for direct in vivo use, involved the development of a microfluidics-based platform for intracellular delivery of a number of different cargos, including

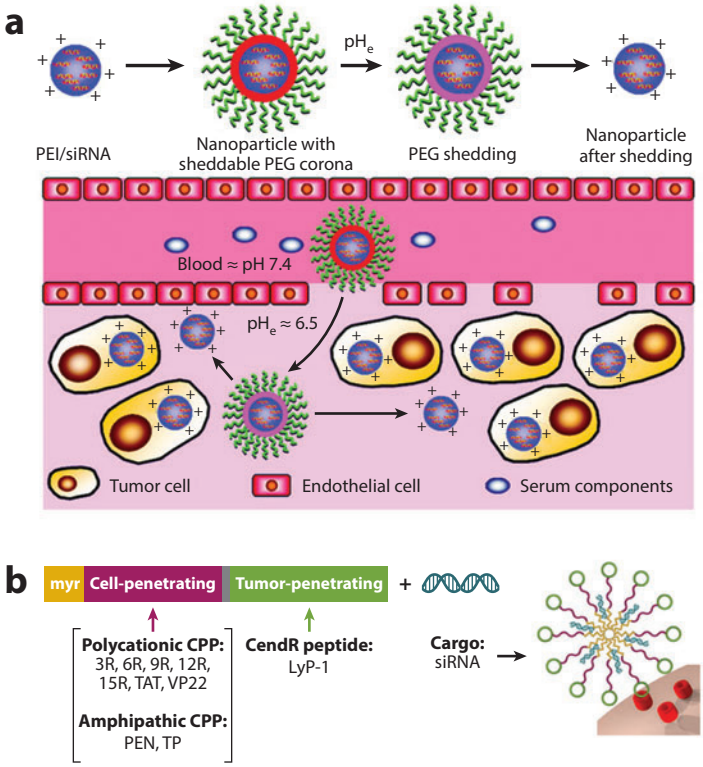

Figure 2

Example strategies for enhancing siRNA nanoparticle cellular uptake. (*a*) PEI/siRNA nanoparticle with a sheddable PEG corona. PEG-coated nanoparticles exhibit higher colloidal stability and reduced protein binding in circulation. When delivered to the tumor tissue, the slightly acidic microenvironment induces cleavage of PEG from the particle surface and reexposes the PEI/siRNA positively charged nanoparticle core, therefore enhancing nanoparticle uptake. (Panel adapted with permission from 83; ©2012 American Chemical Society.) (*b*) Design of a tumor-targeting nanoparticle with CPPs for siRNA delivery. The design includes a LyP-1 domain as a tumor-specific ligand as well as a polycationic CPP and an amphipathic CPP, connected by a 4-glycine spacer, for enhancing cellular entry and endosomal escape. In addition, a subset of peptide carriers is N-myristoylated to enhance membrane affinity and, likely, core stability. (Panel adapted with permission from 93; ©2012 American Chemical Society.) Abbreviations: CendR, C-end rule motif; CPP, cell-penetrating peptide; myr, N-myristoylated subset of peptide carriers; PEG, poly(ethylene glycol); PEI, polyethyleneimine; pH_e, extracellular pH; siRNA, short interfering RNA.

polymers, proteins, nanomaterials, and siRNA. An advantage of this system is that it does not require a nanoparticle carrier to deliver the siRNA. Owing to the constriction of the cells when they pass through channels in the device, rapid cellular deformation leads to the formation of transient pores in the membrane, allowing uptake of siRNA and other materials. An advantage of this system is that it can be used for difficult-to-transfect cells, showing better delivery of transcription factors than that mediated by electroporation or CPPs.

3.3. Improving Intracellular Trafficking

In order to successfully carry out its downstream functions, intact siRNA must be delivered to the cytoplasm after escape from the endocytic compartment. Without endosomal escape, the

siRNA risks being destroyed in the late endosomes and lysosomes, where the pH of the organelles gradually drops to 5 (30).

Quantitative description of the intracellular trafficking and endosomal escape steps has thus far been fairly limited. However, several recent studies have provided more mechanistic understanding of this process, highlighting the major intracellular barriers that limit successful delivery of siRNA therapeutics. One such study using an ionizable lipid nanoparticle delivery system (97) investigated the uptake and transport properties using fluorescent imaging as well as electron microscopy (98). The primary uptake mechanism occurred via clathrin-mediated endocytosis and macropinocytosis, and only a small fraction of siRNA (1–2%) was actually released from the endocytic vesicles. A similar study (99), which also used lipid nanoparticles, found that a large fraction of the siRNA, perhaps as high as 70% of the dose, was transported out of the cell through a recycling pathway mediated by Niemann–Pick disease type C1 (NPC1) within 24 h after nanoparticle uptake, as shown in **Figure 3*a***. Cells deficient for NPC1 showed increased intracellular nanoparticle concentration and higher knockdown efficiency. A separate study by Fichter et al. (100) showed a different intracellular trafficking pattern for Glycofect polymeric nanoparticles leading to their accumulation in both the Golgi and the endoplasmic reticulum (ER), although this accumulation may have been due to the presence of galactose moieties in the carrier. In the same study, a similar accumulation pattern of PEI polyplexes was observed in the Golgi and ER, although to a lesser extent than the Glycofect polyplexes.

One common method for endosomal escape of nanoparticles involves the proton sponge mechanism (101–103). The theory holds that, with the presence of protonatable amines on the nanoparticle carrier, the pH of the endosome can be buffered, protecting the cargo from acid degradation as well as drawing an influx of water into the endosomal compartment, which leads to its swelling and subsequent rupture. The endosomal burst allows for the escape of the contents into the cytoplasm. Recently, additional studies have attempted to better understand the proton sponge mechanism. For example, Banjaminsen et al. (104) developed a nanoparticle pH sensor for measuring the pH in the lysosomal compartment. After treatment with PEI polyplexes and with or without the nanoparticle pH sensor, there was no change in the lysosomal pH. This finding raises the possibility that the proton sponge mechanism is not the dominant method of endosomal escape for PEI polyplexes. Another group (105) further studied endosomal escape of lipoplexes (LF2000) and polyplexes (lPEI) using real-time fluorescence imaging. The authors found that, for polyplexes, only a small fraction of particles—an average of one or two per cell—were able to escape from the endosomes. Complete endosomal rupture was not observed for polyplexes or lipoplexes; endosomal escape of polyplexes occurred as an instantaneous discharge, whereas lipoplexes escaped slowly over time into the cytoplasm. This study once again highlights that endosomal escape is a major barrier for polyplex-mediated siRNA delivery. Efficacy of these systems will continue to be limited until this barrier can be circumvented.

Pharmacological agents can be used to help promote endosomal escape. Coloading siRNA with amphotericin B (AmB), an antifungal drug known to increase membrane permeability, leads to enhanced endosomal release and gene knockdown efficiency, compared with using unloaded controls (106). In addition to the AmB loading, the micelles in this study also contained a pH-sensitive protonation, which led to further enhancement of endosomal escape, possibly through a proton sponge mechanism. In addition to AmB, chloroquine and influenza virus hemagglutinin–based fusogenic peptides have also been used to enhance the endosomal escape of nanoparticle delivery vehicles (107, 108).

Once the carriers escape from the endosomes, the siRNA must also be able to release from the delivery vehicle so that it can enter into the RISC complex to mediate gene knockdown. One popular strategy for cytosolic release of siRNA is the incorporation of a reduction-sensitive

component to the system. Because the cytoplasm is a highly reducing environment, where glutathione concentration is significantly higher (109), site-specific siRNA release can be achieved (**Figure 3*b***). One popular strategy for enhanced siRNA release involves the incorporation of disulfide bonds into a poly(β-amino ester) polymer backbone (110). Such siRNA polyplexes thus maintain stability extracellularly but unpack intracellularly. Similar design concepts can be found in polyplexes involving dextran (111), PLL dendrimers (112), PEG hydrogels (113), PEI (114, 115), and poly(β-amino ester)s (116).

A new siRNA imaging two-probe system has also been developed to better understand the nanoparticle unpacking dynamics after uptake (117). The first probe remains quenched until in a reduction-sensitive environment, after which it is able to fluoresce. The second probe, based

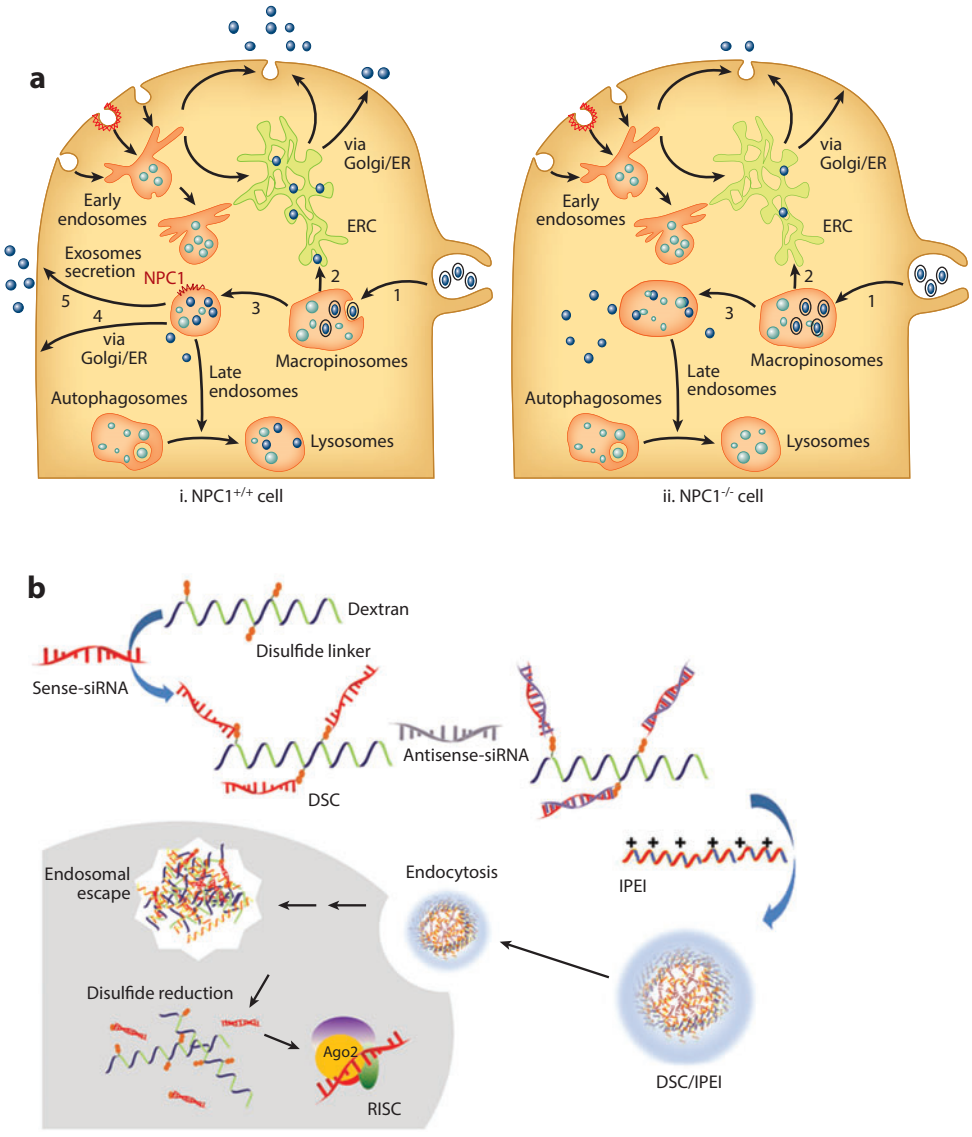

on a Förster resonance energy transfer (FRET), becomes fluorescent when siRNA molecules are in close proximity (117, 118). In both cases, because the siRNA itself is labeled, no labeling of the polymer/nanoparticle carrier is required, which allows for better direct comparison between delivery vehicles. The study showed a slight correlation between particle dissociation constant and gene silencing activity, which suggests that carrier unpacking is important to the success of siRNA delivery.

The vast majority of intracellular trafficking studies rely on qualitative comparison of immunofluorescence images and colocalization of fluorescently labeled siRNA or nanoparticles with different organelles. It is difficult to extract a kinetic description of the multistep processes and to determine the rate-limiting barrier(s). More importantly, the throughput capability of this approach is often low, allowing the analysis of only a small fraction of cells. Further developments of new methodologies are needed to enable quantitative characterization of the intracellular trafficking steps and to allow a more thorough understanding of this process.

In addition to improving the understanding of intracellular trafficking mechanisms, boosting the intracellular stability of siRNA remains a critical challenge for enhancing its therapeutic potential. As mentioned above, a number of siRNA structural modifications have been employed, leading to prolonged siRNA stability in extracellular fluids such as serum. Less attention has been given to the intracellular stability of siRNA, where cytoplasmic nucleases can also cause rapid degradation of the duplex—although when bound to the RISC complex, the molecules persist longer than the unbound strands (119). Although it led to improved extracellular stability, 2′-*O*-methyl-modified siRNA did not show any improvement in the duration of gene knockdown in vitro using a luciferase reporter system (120). Similar results were also observed with additional chemically modified siRNA systems (121). Interestingly, it was observed that further siRNA modification to include a 4′-thioribonucleoside led to 44% gene knockdown at 7 days, whereas siRNA lacking the thio modification mediated negligible knockdown efficiency (122). Analysis using quantitative polymerase chain reaction (PCR) estimated that 20 times more 4′-thioribonucleoside siRNA was present at day 7, highlighting the critical importance of improving both intracellular and extracellular siRNA stability to prolonged gene knockdown.

Figure 3

Barriers to intracellular trafficking and release of siRNA delivered by nanoparticles. (*a*) Transcytosis of cationic LNPs limits effective intracellular delivery of siRNA. LNP trafficking in (i) NPC1+/+ and (ii) NPC1−/− cells. LNPs enter through macropinocytosis (1); a small fraction of LNPs move from macropinosomes to the ERC (2), whereas the majority are directed to late endosomes (3). Late endosomes sort LNPs to lysosomes for degradation or utilize multiple recycling pathways to traffic the lysosomes out of the cell, either through the ER-Golgi route (4) or by direct fusion of late endosomes (containing multivesicular bodies) with the plasma membrane (i.e., exosome secretion) (5). By contrast, the late endosome recycling mechanisms in the NPC1-deficient cell (ii) are impaired, leading both to accumulation of siRNA LNPs in enlarged late endosomes and to sustained escape of siRNA that improves gene silencing. [Panel adapted by permission from Macmillan Publishers Ltd.: *Nature Biotechnology* (99), ©2013.] (*b*) Effective cytosolic release of siRNA may limit the incorporation into RISC. A popular strategy to promote intracellular release of siRNA while maintaining extracellular stability is to introduce reversible disulfide cross-links. In this example, double-stranded siRNAs are conjugated to dextran with disulfide bonds and then form complex nanoparticles with lPEI. Once the nanoparticles are delivered to the reductive environment in the cytosol, the siRNA chains can be released. (Panel adapted from 111, ©2013, with permission from Elsevier.) Abbreviations: DSC, dextran-siRNA conjugate; ER, endoplasmic reticulum; ERC, endocytic recycling compartment; LNPs, lipid nanoparticles; lPEI, linear polyethyleneimine; NPC1 cell, Niemann–Pick type C1 cell; RISC, RNA-induced silencing complex; siRNA, short interfering RNA.

4. NEW DEVELOPMENTS IN DISEASE TREATMENT USING siRNA THERAPEUTICS

Although a number of obstacles to siRNA delivery still exist, several carriers have been developed, characterized, and applied for in vivo studies. Two of the most common applications for siRNA delivery involve hepatic and cancer therapies. In addition, two other routes of administration, oral and topical, demonstrate the vast potential for the development of new siRNA therapeutics.

4.1. Liver-Specific Delivery of siRNA

The liver represents a critical target for siRNA delivery, as it is the site of a number of viral infections, metabolic disorders, and cancer (123–125). One early application of liver-specific siRNA was the treatment of cirrhosis through knockdown of rat protein gp46, the analog to human heat shock protein 47, a main facilitator of collagen secretion and subsequent fibrosis (90). Gene knockdown was achieved by intravenous injection of vitamin A–conjugated liposomes, which provided liver-specific targeting. Following treatment, collagen secretion was reduced and fibrotic areas were significantly smaller, leading to survival rates of 100% at the most frequent dosing times, compared with no survival for control groups. A separate study using a polymer-based system termed Dynamic Polyconjugates—which consists of a poly(vinyl ether) for endosomal lysis, *N*-acetylgalactosamine for hepatocyte targeting, and PEG for shielding—showed ∼80% knockdown of apolipoprotein B (apoB) following intravenous injection of 2.5 mg siRNA/kg body weight (126). Using PEGylated lipoplexes, Akinc et al. (25) demonstrated that greater than 90% of the complexes accumulated in the liver after intravenous injection. Using a Factor VII knockdown model, the authors showed that gene silencing could be achieved for nearly 1 month, with 50% knockdown activity after 3 weeks. In addition, monthly dosing led to similar silencing levels and kinetics, with no evidence of an adaptive immune response. Further studies on this platform showed that other lipoplex formulations could achieve significant knockdown of Factor VII at doses as low as 0.1 mg/kg in mice, though for shorter duration than with the higher dose of 1 mg/kg (24, 26, 127). Furthermore, Love et al. (24) demonstrated the feasibility of combining five unique hepatocyte siRNA sequences into one nanoparticle formulation, which resulted in more than 50% knockdown of each gene target at a dose as low as 0.1 mg/kg per siRNA. Another study using a similar lipoplex showed effective reduction of cholesterol level in both rodents and nonhuman primates. Using an siRNA targeting low-density lipoprotein receptors, the authors observed a 60% decrease in rodent cholesterol concentration and a ∼50% decrease in LDL cholesterol level in primates following systemic administration at a dose of 5 mg/kg (128).

4.2. Tumor-Specific Delivery of siRNA

Cancer treatment remains one of the most widespread applications of siRNA therapeutics. A recent report by Ren et al. (129) described a peptide-based "tumor-penetrating siRNA nanocomplex" targeting a potential ovarian cancer oncogene, *ID4*. These siRNA nanoparticles were shown to selectively target and penetrate deep within the tumor tissue. Following intravenous injection of 5 mg/kg siRNA every 3 days for 25 days, tumor growth slowed by 82% and survival rate increased compared with those of controls and nonsense RNA nanoparticles. In a separate study, a peptide fusion protein, consisting of Her2 single chain–fragmented antibodies (ScFvs) bound to protamine, was complexed with polo-like kinase 1 (PLK1) siRNA for breast cancer suppression (130). The siRNA nanocomplexes significantly slowed $Her2^+$ tumor growth, reduced the number

of detectable metastases, and prolonged survival time following twice-weekly intravenous injection of a 2 mg/kg dose for 4 weeks. These nanoparticles were also used to deliver a cocktail of antitumor siRNA, leading to even better results than with PLK1 siRNA alone. Leuschner et al. (131) showed that lipoplexes could successfully deliver siRNA to inflammatory monocytes. When the lipoplexes were applied to a colorectal cancer model and treated with CCR2 siRNA, a 75% reduction of tumor-associated macrophages was observed. The study also highlighted the utility of this delivery system in a number of other disease models, including treating atherosclerosis and myocardial infarction and prolonging survival of transplanted pancreatic islets.

Liu et al. (132) demonstrated that a cationic micellar nanoparticle, consisting of biodegradable PCL-*block*-poly(2-aminoethylethylene phosphate) and PCL-*block*-PEG, could deliver siRNA against hypoxia-inducible factor-1α, targeting the hypoxic tumor microenvironment. When tested in a mouse prostate cancer model, intravenous administration of 2-mg/kg-siRNA micellar nanoparticles inhibited tumor growth by nearly 60% and induced sensitization to doxorubicin treatment. Codelivery of PLK1 siRNA and paclitaxel with these micellar nanoparticles in a mouse breast cancer xenograft model also showed significant antitumor effect and potentiated the chemotherapeutic effect of paclitaxel, and a 1,000-fold lower dose of paclitaxel with siRNA could achieve the same antitumor effect as paclitaxel alone (133). Codelivery of siRNA and chemotherapeutics has shown synergistic effect in several other systems as well. For example, coencapsulation of siRNA for the oncogene *c-Myc* with gemcitabine monophosphate resulted in a significant decrease in tumor growth using DOTAP-based lipid/calcium phosphate nanoparticles in a non-small-cell lung cancer mouse model (134). With the same delivery system, switching to vascular endothelial growth factor (VEGF) siRNA also improved treatment response, as demonstrated by a reduction in tumor growth and tumor vascular density (135).

For tumor-specific siRNA nanoparticle delivery, it is important to pay attention to the tumor vasculature to maximize the enhanced permeation and retention (EPR) effect. In a recent study, Li et al. (136) showed that enhancing the tumor vascularity by ectopic expression of VEGF led to greater efficiency of siRNA delivery to the tumor tissue (136). This result was corroborated when comparing a highly vascularized with a poorly vascularized tumor model, which showed that siRNA-mediated gene knockdown was 60% in the former versus 15% in the latter.

4.3. Additional Administration Routes for siRNA Nanoparticles

Oral delivery is a convenient and unique route of administration for many therapeutics. In a recent report, Yin et al. (137) used a self-assembled polymeric nanoparticle to orally deliver tumor necrosis factor alpha (TNF-α) siRNA for treatment of inflammatory diseases. Incorporation of a mannose-targeting ligand directed particle uptake to enterocytes and macrophages in the small intestine. Cysteamine was also included to form disulfide bonds with the mucosal glycoproteins, keeping the particles localized. Using a hepatic injury model, siRNA nanoparticle treatment led to an 80% decrease in TNF-α levels in the lung, liver, and spleen, suggesting that the orally administered nanoparticles transported to other tissues following intestinal absorption.

Topical delivery is another convenient but challenging delivery route. Using 13-nm gold nanoparticles as carriers for surface-conjugated siRNA, Zheng et al. (138) showed that topical delivery of siRNA-targeting epidermal growth factor receptor (EGFR) led to decreased EGFR expression in keratinocytes, lowered downstream signaling activation, and decreased epidermal thickness by 40%. The treatment was well tolerated and did not show any gold-nanoparticle accumulation in internal organs, suggesting its potential for treatment of skin lesions, tumors, and genetic disorders.

4.4. Clinical Trials of siRNA Delivery

Coverage of clinical trials involving siRNA/small hairpin (sh)RNA prior to 2010 can be found in a recent excellent review article (139). Davis et al. (140) reported the first direct evidence of an RNAi effect in a Phase I clinical trial when an siRNA against the M2 subunit of ribonucleotide reductase (RRM2) was delivered using a nanoparticulate delivery system comprising a cyclodextrin-based cationic polymer, PEG, and a transferrin ligand. Nanoparticles accumulated in the tumor tissue and mediated a significant reduction of mRNA level for RRM2. Specific cleavage of the target sequence was also confirmed using 5′-RACE analysis. In another recent report, Tabernero et al. (141) studied the delivery of siRNA targeting VEGF and kinesin spindle protein (KSP), using a lipoplex system, for the treatment of patients with advanced cancer and liver metastases. Following intravenous injection of nanoparticles at siRNA doses ranging from 0.4 to 1.5 mg/kg, cleavage of VEGF was detected at the target site, leading to lower mRNA levels and disease control in four patients, including a complete regression in one patient with significant liver metastases. Finally, Coelho et al. (142) examined a lipid nanoparticle formulation for the treatment of transthyretin amyloidosis, a life-threatening condition in which hepatocyte-produced transthyretin amyloid is deposited in other organs and tissues. After delivery of an siRNA against transthyretin, the authors observed a reduction in circulating transthyretin level of up to 86.8% with no significant adverse side effects.

5. CONCLUDING REMARKS

Important progress has been made in designing biomaterials and engineering nanoparticles and in understanding the mechanisms of nanoparticle uptake and intracellular trafficking, as showcased above. Despite the promise shown by nanoparticle-mediated siRNA delivery in many preclinical studies and extensive development in carrier design, outcomes from the initial clinical studies have not been as promising as hoped (143). These initial results highlight the challenges in nanoparticle engineering of overcoming physiological barriers at the systemic, tissue, and cellular levels. More effort is required to understand the interactions between various siRNA nanoparticles and blood components, which is crucial for controlling siRNA nanoparticles' colloidal stability in circulation, and, thus, their trafficking dynamics, and their delivery efficiency to the target tissue (144). Different imaging modalities can be employed to provide quantitative characterization of transport kinetics of siRNA nanoparticles in vivo and in vitro.

Physical and physiological factors that influence nanoparticle transport properties in vivo should be taken into consideration when designing the next generation of nanoparticles. For example, there is an increasing body of evidence indicating that the shape of nanoparticles plays important roles in dictating their biofunctionality, including their systemic trafficking (145), cellular uptake (146), and tissue diffusion (147). A recent study by Jiang et al. (148) reported a method to condense plasmid DNA into micellar nanoparticles with PEG-*b*-PPA under controlled solvent conditions. The resultant micellar nanoparticles had a core shell structure and tunable shape (**Figure 4**), which allowed the authors to generate a series of micellar nanoparticles with uniform spherical, rod-like, and worm-like morphologies. Using the disulfide cross-linking method, the authors demonstrated that the shape of these nanoparticles markedly influenced DNA delivery efficiency in rat liver. These results highlight the significance of the shape of micelles in influencing their biodistribution and, likely, endocytic uptake. This strategy will likely be a fruitful approach for siRNA formulations.

An aspect of RNAi therapeutics development that has been underappreciated, at least in academic labs, is manufacturing. Bulk mixing remains the norm in synthesizing or formulating siRNA

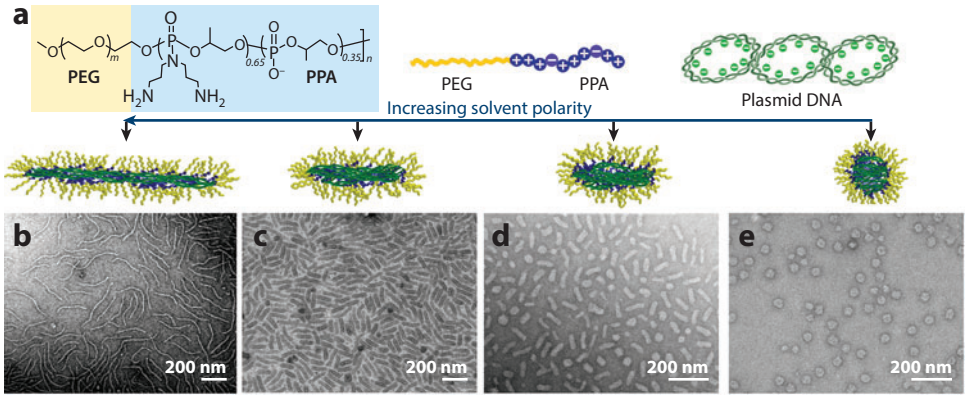

Figure 4

Controlling the shape of polycation-condensed plasmid DNA nanoparticles. (*a*) Condensation of DNA with PEG-*b*-PPA in solvents with various polarity yields nanoparticles of different shapes. (*b–e*) TEM images of PEG_{10K}-*b*-PPA_{4K}/DNA micelles prepared in (*b*) 10%, (*c*) 30%, (*d*) 50%, and (*e*) 70% of DMF/water mixture. Abbreviations: DMF, dimethylformamide; PEG-*b*-PPA, poly(ethylene glycol)-*block*-polyphosphoramidate. (Figure adapted with permission from 148; ©2013 WILEY-VCH Verlag GmbH & Co. KGaA, Weinheim.)

lipoplexes and polyplexes. Although simple, fast, and inexpensive, bulk mixing produces nanoparticles heterogeneous in size, composition, and surface charge. A more concerted effort to develop engineering technologies to manufacture siRNA nanoparticles with better control of these parameters will address a critical barrier to the eventual translation of RNAi therapeutics.

Scientifically, RNAi presents tremendous opportunities in research and therapeutics. Commercially, RNAi therapeutics has gone through its ups and downs. Haussecker (143) in his commentary on RNAi therapeutics commercialization categorizes its current development in the recovery phase, with it having emerged from the discovery, boom, and backlash phases. He also likens the technology development of RNAi therapy to that of gene therapy. If that is the case, the future for science and development of RNAi therapeutics is bright because gene therapy is enjoying a revival. A pervasive theme in the analysis of RNAi business potential is the need for better delivery. Recent advances described in this review suggest that the field will reach that potential.

DISCLOSURE STATEMENT

The authors are not aware of any affiliations, memberships, funding, or financial holdings that might be perceived as affecting the objectivity of this review.

ACKNOWLEDGMENTS

We acknowledge funding support provided by NIH grants EB015152, EB013274-01A1, EB015000, HL109442, AI096395, and U54CA151838, as well as a pilot grant from the Johns Hopkins Institute for NanoBioTechnology.

LITERATURE CITED

1. Fire A, Xu SQ, Montgomery MK, Kostas SA, Driver SE, Mello CC. 1998. Potent and specific genetic interference by double-stranded RNA in *Caenorhabditis elegans*. *Nature* 391:806–11

2. Bumcrot D, Manoharan M, Koteliansky V, Sah DWY. 2006. RNAi therapeutics: a potential new class of pharmaceutical drugs. *Nat. Chem. Biol.* 2:711–19
3. Castanotto D, Rossi JJ. 2009. The promises and pitfalls of RNA-interference-based therapeutics. *Nature* 457:426–33
4. Oh Y-K, Park TG. 2009. siRNA delivery systems for cancer treatment. *Adv. Drug Deliv. Rev.* 61:850–62
5. Wilson RC, Doudna JA. 2013. Molecular mechanisms of RNA interference. *Annu. Rev. Biophys.* 42:217–39
6. Reischl D, Zimmer A. 2009. Drug delivery of siRNA therapeutics: potentials and limits of nanosystems. *Nanomedicine* 5:8–20
7. Krieg AM. 2011. Is RNAi dead? *Mol. Ther.* 19:1001–2
8. Judge AD, Bola G, Lee ACH, MacLachlan I. 2006. Design of noninflammatory synthetic siRNA mediating potent gene silencing in vivo. *Mol. Ther.* 13:494–505
9. Whitehead KA, Langer R, Anderson DG. 2009. Knocking down barriers: advances in siRNA delivery. *Nat. Rev. Drug Discov.* 8:129–38
10. Lee SJ, Son S, Yhee JY, Choi K, Kwon IC, et al. 2012. Structural modification of siRNA for efficient gene silencing. *Biotechnol. Adv.* 31:491–503
11. Huang Y, Hong J, Zheng S, Ding Y, Guo S, et al. 2011. Elimination pathways of systemically delivered siRNA. *Mol. Ther.* 19:381–85
12. Dalby B, Cates S, Harris A, Ohki EC, Tilkins ML, et al. 2004. Advanced transfection with Lipofectamine 2000 reagent: primary neurons, siRNA, and high-throughput applications. *Methods* 33:95–103
13. Zhao M, Yang H, Jiang X, Zhou W, Zhu B, et al. 2008. Lipofectamine RNAiMAX: an efficient siRNA transfection reagent in human embryonic stem cells. *Mol. Biotechnol.* 40:19–26
14. Ma Z, Li J, He FT, Wilson A, Pitt B, Li S. 2005. Cationic lipids enhance siRNA-mediated interferon response in mice. *Biochem. Biophys. Res. Commun.* 330:755–59
15. Palliser D, Chowdhury D, Wang QY, Lee SJ, Bronson RT, et al. 2006. An siRNA-based microbicide protects mice from lethal herpes simplex virus 2 infection. *Nature* 439:89–94
16. Forbes DC, Peppas NA. 2012. Oral delivery of small RNA and DNA. *J. Control. Release* 162:438–45
17. Sakurai H, Kawabata K, Sakurai F, Nakagawa S, Mizuguchi H. 2008. Innate immune response induced by gene delivery vectors. *Int. J. Pharm.* 354:9–15
18. Szebeni J. 2005. Complement activation-related pseudoallergy: a new class of drug-induced acute immune toxicity. *Toxicology* 216:106–21
19. Akinc A, Zumbuehl A, Goldberg M, Leshchiner ES, Busini V, et al. 2008. A combinatorial library of lipid-like materials for delivery of RNAi therapeutics. *Nat. Biotechnol.* 26:561–69
20. Chono S, Li S-D, Conwell CC, Huang L. 2008. An efficient and low immunostimulatory nanoparticle formulation for systemic siRNA delivery to the tumor. *J. Control. Release* 131:64–69
21. Abrams MT, Koser ML, Seitzer J, Williams SC, DiPietro MA, et al. 2010. Evaluation of efficacy, biodistribution, and inflammation for a potent siRNA nanoparticle: effect of dexamethasone co-treatment. *Mol. Ther.* 18:171–80
22. Yu B, Hsu SH, Zhou C, Wang X, Terp MC, et al. 2012. Lipid nanoparticles for hepatic delivery of small interfering RNA. *Biomaterials* 33:5924–34
23. Tao W, Davide JP, Cai M, Zhang GJ, South VJ, et al. 2010. Noninvasive imaging of lipid nanoparticle-mediated systemic delivery of small-interfering RNA to the liver. *Mol. Ther.* 18:1657–66
24. Love KT, Mahon KP, Levins CG, Whitehead KA, Querbes W, et al. 2010. Lipid-like materials for low-dose, in vivo gene silencing. *Proc. Natl. Acad. Sci. USA* 107:1864–69
25. Akinc A, Goldberg M, Qin J, Dorkin JR, Gamba-Vitalo C, et al. 2009. Development of lipidoid-siRNA formulations for systemic delivery to the liver. *Mol. Ther.* 17:872–79
26. Whitehead KA, Sahay G, Li GZ, Love KT, Alabi CA, et al. 2011. Synergistic silencing: combinations of lipid-like materials for efficacious siRNA delivery. *Mol. Ther.* 19:1688–94
27. Jayaraman M, Ansell SM, Mui BL, Tam YK, Chen J, et al. 2012. Maximizing the potency of siRNA lipid nanoparticles for hepatic gene silencing in vivo. *Angew. Chem. Int. Ed. Engl.* 51:8529–33
28. Alabi CA, Love KT, Sahay G, Yin H, Luly KM, et al. 2013. Multiparametric approach for the evaluation of lipid nanoparticles for siRNA delivery. *Proc. Natl. Acad. Sci. USA* 110:12881–86

29. Howard KA. 2009. Delivery of RNA interference therapeutics using polycation-based nanoparticles. *Adv. Drug Deliv. Rev.* 61:710–20
30. Dominska M, Dykxhoorn DM. 2010. Breaking down the barriers: siRNA delivery and endosome escape. *J. Cell Sci.* 123:1183–89
31. Grayson ACR, Doody AM, Putnam D. 2006. Biophysical and structural characterization of polyethylenimine-mediated siRNA delivery in vitro. *Pharm. Res.* 23:1868–76
32. Shim MS, Kwon YJ. 2009. Acid-responsive linear polyethylenimine for efficient, specific, and biocompatible siRNA delivery. *Bioconjug. Chem.* 20:488–99
33. Merkel OM, Urbanics R, Bedocs P, Rozsnyay Z, Rosivall L, et al. 2011. In vitro and in vivo complement activation and related anaphylactic effects associated with polyethylenimine and polyethylenimine-graft-poly(ethylene glycol) block copolymers. *Biomaterials* 32:4936–42
34. Owens DE, Peppas NA. 2006. Opsonization, biodistribution, and pharmacokinetics of polymeric nanoparticles. *Int. J. Pharm.* 307:93–102
35. Zintchenko A, Philipp A, Dehshahri A, Wagner E. 2008. Simple modifications of branched PEI lead to highly efficient siRNA carriers with low toxicity. *Bioconjug. Chem.* 19:1448–55
36. Bonnet ME, Erbacher P, Bolcato-Bellemin AL. 2008. Systemic delivery of DNA or siRNA mediated by linear polyethylenimine (L-PEI) does not induce an inflammatory response. *Pharm. Res.* 25:2972–82
37. Dash PR, Read ML, Fisher KD, Howard KA, Wolfert M, et al. 2000. Decreased binding to proteins and cells of polymeric gene delivery vectors surface modified with a multivalent hydrophilic polymer and retargeting through attachment of transferrin. *J. Biol. Chem.* 275:3793–802
38. Nomoto T, Matsumoto Y, Miyata K, Oba M, Fukushima S, et al. 2011. In situ quantitative monitoring of polyplexes and polyplex micelles in the blood circulation using intravital real-time confocal laser scanning microscopy. *J. Control. Release* 151:104–9
39. Mao S, Neu M, Germershaus O, Merkel O, Sitterberg J, et al. 2006. Influence of polyethylene glycol chain length on the physicochemical and biological properties of poly(ethylene imine)-graft-poly(ethylene glycol) block copolymer/SiRNA polyplexes. *Bioconjug. Chem.* 17:1209–18
40. Petersen H, Fechner PM, Martin AL, Kunath K, Stolnik S, et al. 2002. Polyethylenimine-graft-poly(ethylene glycol) copolymers: influence of copolymer block structure on DNA complexation and biological activities as gene delivery system. *Bioconjug. Chem.* 13:845–54
41. Sutton D, Kim S, Shuai X, Leskov K, Marques JT, et al. 2006. Efficient suppression of secretory clusterin levels by polymer-siRNA nanocomplexes enhances ionizing radiation lethality in human MCF-7 breast cancer cells in vitro. *Int. J. Nanomed.* 1:155–62
42. Merkel OM, Librizzi D, Pfestroff A, Schurrat T, Buyens K, et al. 2009. Stability of siRNA polyplexes from poly(ethylenimine) and poly(ethylenimine)-g-poly(ethylene glycol) under in vivo conditions: effects on pharmacokinetics and biodistribution measured by fluorescence fluctuation spectroscopy and single photon emission computed tomography (SPECT) imaging. *J. Control. Release* 138:148–59
43. Beyerle A, Braun A, Banerjee A, Ercal N, Eickelberg O, et al. 2011. Inflammatory responses to pulmonary application of PEI-based siRNA nanocarriers in mice. *Biomaterials* 32:8694–701
44. Christie RJ, Matsumoto Y, Miyata K, Nomoto T, Fukushima S, et al. 2012. Targeted polymeric micelles for siRNA treatment of experimental cancer by intravenous injection. *ACS Nano* 6:5174–89
45. Christie RJ, Miyata K, Matsumoto Y, Nomoto T, Menasco D, et al. 2011. Effect of polymer structure on micelles formed between siRNA and cationic block copolymer comprising thiols and amidines. *Biomacromolecules* 12:3174–85
46. Naito M, Ishii T, Matsumoto A, Miyata K, Miyahara Y, Kataoka K. 2012. A phenylboronate-functionalized polyion complex micelle for ATP-triggered release of siRNA. *Angew. Chem. Int. Ed. Engl.* 51:10751–55
47. Suma T, Miyata K, Ishii T, Uchida S, Uchida H, et al. 2012. Enhanced stability and gene silencing ability of siRNA-loaded polyion complexes formulated from polyaspartamide derivatives with a repetitive array of amino groups in the side chain. *Biomaterials* 33:2770–79
48. Green JJ, Langer R, Anderson DG. 2008. A combinatorial polymer library approach yields insight into nonviral gene delivery. *Acc. Chem. Res.* 41:749–59
49. Green JJ, Zugates GT, Langer R, Anderson DG. 2009. Poly(β-amino esters): procedures for synthesis and gene delivery. *Methods Mol. Biol.* 480:53–63

50. Tzeng SY, Guerrero-Cazares H, Martinez EE, Sunshine JC, Quinones-Hinojosa A, Green JJ. 2011. Non-viral gene delivery nanoparticles based on poly(β-amino esters) for treatment of glioblastoma. *Biomaterials* 32:5402–10
51. Tzeng SY, Hung BP, Grayson WL, Green JJ. 2012. Cystamine-terminated poly(beta-amino ester)s for siRNA delivery to human mesenchymal stem cells and enhancement of osteogenic differentiation. *Biomaterials* 33:8142–51
52. Tzeng SY, Green JJ. 2013. Subtle changes to polymer structure and degradation mechanism enable highly effective nanoparticles for siRNA and DNA delivery to human brain cancer. *Adv. Healthc. Mater.* 2:468–80
53. Gary DJ, Puri N, Won Y-Y. 2007. Polymer-based siRNA delivery: perspectives on the fundamental and phenomenological distinctions from polymer-based DNA delivery. *J. Control. Release* 121:64–73
54. Fischer D, Li YX, Ahlemeyer B, Krieglstein J, Kissel T. 2003. In vitro cytotoxicity testing of polycations: influence of polymer structure on cell viability and hemolysis. *Biomaterials* 24:1121–31
55. Zheng M, Pavan GM, Neeb M, Schaper AK, Danani A, et al. 2012. Targeting the blind spot of polycationic nanocarrier-based siRNA delivery. *ACS Nano* 6:9447–54
56. Guo G, Zhou L, Chen Z, Chi W, Yang X, et al. 2013. Alkane-modified low-molecular-weight polyethylenimine with enhanced gene silencing for siRNA delivery. *Int. J. Pharm.* 450:44–52
57. Schroeder A, Dahlman JE, Sahay G, Love KT, Jiang S, et al. 2012. Alkane-modified short polyethyleneimine for siRNA delivery. *J. Control. Release* 160:172–76
58. Han L, Tang C, Yin C. 2013. Effect of binding affinity for siRNA on the in vivo antitumor efficacy of polyplexes. *Biomaterials* 34:5317–27
59. Zheng M, Librizzi D, Kılıç A, Liu Y, Renz H, et al. 2012. Enhancing in vivo circulation and siRNA delivery with biodegradable polyethylenimine-graft-polycaprolactone-block-poly(ethylene glycol) copolymers. *Biomaterials* 33:6551–58
60. Lee SH, Mok H, Lee Y, Park TG. 2011. Self-assembled siRNA-PLGA conjugate micelles for gene silencing. *J. Control. Release* 152:152–58
61. Bui L, Abbou S, Ibarboure E, Guidolin N, Staedel C, et al. 2012. Encapsidation of RNA-polyelectrolyte complexes with amphiphilic block copolymers: toward a new self-assembly route. *J. Am. Chem. Soc.* 134:20189–96
62. Hasan W, Chu K, Gullapalli A, Dunn SS, Enlow EM, et al. 2012. Delivery of multiple siRNAs using lipid-coated PLGA nanoparticles for treatment of prostate cancer. *Nano Lett.* 12:287–92
63. Yang XZ, Dou S, Sun TM, Mao CQ, Wang HX, Wang J. 2011. Systemic delivery of siRNA with cationic lipid assisted PEG-PLA nanoparticles for cancer therapy. *J. Control. Release* 156:203–11
64. Ashley CE, Carnes EC, Phillips GK, Padilla D, Durfee PN, et al. 2011. The targeted delivery of multicomponent cargos to cancer cells by nanoporous particle-supported lipid bilayers. *Nat. Mater.* 10:389–97
65. Jiang S, Eltoukhy AA, Love KT, Langer R, Anderson DG. 2013. Lipidoid-coated iron oxide nanoparticles for efficient DNA and siRNA delivery. *Nano Lett.* 13:1059–64
66. Fröhlich T, Edinger D, Kläger R, Troiber C, Salcher E, et al. 2012. Structure–activity relationships of siRNA carriers based on sequence-defined oligo (ethane amino) amides. *J. Control. Release* 160:532–41
67. Salcher EE, Kos P, Fröhlich T, Badgujar N, Scheible M, Wagner E. 2012. Sequence-defined four-arm oligo(ethanamino)amides for pDNA and siRNA delivery: impact of building blocks on efficacy. *J. Control. Release* 164:380–86
68. Schaffert D, Troiber C, Salcher EE, Fröhlich T, Martin I, et al. 2011. Solid-phase synthesis of sequence-defined T-, i-, and U-shape polymers for pDNA and siRNA delivery. *Angew. Chem. Int. Ed. Engl.* 50:8986–89
69. Shim MS, Kwon YJ. 2011. Dual mode polyspermine with tunable degradability for plasmid DNA and siRNA delivery. *Biomaterials* 32:4009–20
70. Fröhlich T, Edinger D, Russ V, Wagner E. 2012. Stabilization of polyplexes via polymer crosslinking for efficient siRNA delivery. *Eur. J. Pharm. Sci.* 47:914–20
71. Matsumoto S, Christie RJ, Nishiyama N, Miyata K, Ishii A, et al. 2009. Environment-responsive block copolymer micelles with a disulfide cross-linked core for enhanced siRNA delivery. *Biomacromolecules* 10:119–27

72. Hong CA, Kim JS, Lee SH, Kong WH, Park TG, et al. 2013. Reductively dissociable siRNA-polymer hybrid nanogels for efficient targeted gene silencing. *Adv. Funct. Mater.* 23:316–22
73. Nakanishi M, Patil R, Ren Y, Shyam R, Wong P, Mao H-Q. 2011. Enhanced stability and knockdown efficiency of poly(ethylene glycol)-*b*-polyphosphoramidate/siRNA micellar nanoparticles by co-condensation with sodium triphosphate. *Pharm. Res.* 28:1723–32
74. Mok H, Lee SH, Park JW, Park TG. 2010. Multimeric small interfering ribonucleic acid for highly efficient sequence-specific gene silencing. *Nat. Mater.* 9:272–78
75. Lee S-Y, Huh MS, Lee S, Lee SJ, Chung H, et al. 2010. Stability and cellular uptake of polymerized siRNA (poly-siRNA)/polyethylenimine (PEI) complexes for efficient gene silencing. *J. Control. Release* 141:339–46
76. Lee SJ, Huh MS, Lee SY, Min S, Lee S, et al. 2012. Tumor-homing poly-siRNA/glycol chitosan self-cross-linked nanoparticles for systemic siRNA delivery in cancer treatment. *Angew. Chem. Int. Ed. Engl.* 51:7203–7
77. Liao Z-X, Hsiao C-W, Ho Y-C, Chen H-L, Sung H-W. 2013. Disulfide bond-conjugated dual PEGylated siRNAs for prolonged multiple gene silencing. *Biomaterials* 34:6930–37
78. Hong CA, Lee SH, Kim JS, Park JW, Bae KH, et al. 2011. Gene silencing by siRNA microhydrogels via polymeric nanoscale condensation. *J. Am. Chem. Soc.* 133:13914–17
79. Lee JB, Hong J, Bonner DK, Poon Z, Hammond PT. 2012. Self-assembled RNA interference microsponges for efficient siRNA delivery. *Nat. Mater.* 11:316–22
80. Lee H, Lytton-Jean AK, Chen Y, Love KT, Park AI, et al. 2012. Molecularly self-assembled nucleic acid nanoparticles for targeted in vivo siRNA delivery. *Nat. Nanotechnol.* 7:389–93
81. Mishra S, Webster P, Davis ME. 2004. PEGylation significantly affects cellular uptake and intracellular trafficking of non-viral gene delivery particles. *Eur. J. Cell Biol.* 83:97–111
82. Kim HJ, Oba M, Pittella F, Nomoto T, Cabral H, et al. 2012. PEG-detachable cationic polyaspartamide derivatives bearing stearoyl moieties for systemic siRNA delivery toward subcutaneous BxPC3 pancreatic tumor. *J. Drug Target.* 20:33–42
83. Yang XZ, Du JZ, Dou S, Mao CQ, Long HY, Wang J. 2012. Sheddable ternary nanoparticles for tumor acidity-targeted siRNA delivery. *ACS Nano* 6:771–81
84. Hatakeyama H, Akita H, Ito E, Hayashi Y, Oishi M, et al. 2011. Systemic delivery of siRNA to tumors using a lipid nanoparticle containing a tumor-specific cleavable PEG-lipid. *Biomaterials* 32:4306–16
85. Dohmen C, Fröhlich T, Lächelt U, Röhl I, Vornlocher HP, et al. 2012. Defined folate-PEG-siRNA conjugates for receptor-specific gene silencing. *Mol. Ther. Nucleic Acids* 1:e7
86. Bartlett DW, Su H, Hildebrandt IJ, Weber WA, Davis ME. 2007. Impact of tumor-specific targeting on the biodistribution and efficacy of siRNA nanoparticles measured by multimodality in vivo imaging. *Proc. Natl. Acad. Sci. USA* 104:15549–54
87. Van Asbeck AH, Beyerle A, McNeill H, Bovee-Geurts PH, Lindberg S, et al. 2013. Molecular parameters of siRNA–cell penetrating peptide nanocomplexes for efficient cellular delivery. *ACS Nano* 7:3797–807
88. Laakkonen P, Porkka K, Hoffman JA, Ruoslahti E. 2002. A tumor-homing peptide with a targeting specificity related to lymphatic vessels. *Nat. Med.* 8:751–55
89. Dou S, Yao YD, Yang XZ, Sun TM, Mao CQ, et al. 2012. Anti-Her2 single-chain antibody mediated DNMTs-siRNA delivery for targeted breast cancer therapy. *J. Control. Release* 161:875–83
90. Sato Y, Murase K, Kato J, Kobune M, Sato T, et al. 2008. Resolution of liver cirrhosis using vitamin A-coupled liposomes to deliver siRNA against a collagen-specific chaperone. *Nat. Biotechnol.* 26:431–42
91. Wang HX, Xiong MH, Wang YC, Zhu J, Wang J. 2013. *N*-acetylgalactosamine functionalized mixed micellar nanoparticles for targeted delivery of siRNA to liver. *J. Control. Release* 166:106–14
92. Van den Berg A, Dowdy SF. 2011. Protein transduction domain delivery of therapeutic macromolecules. *Curr. Opin. Biotechnol.* 22:888–93
93. Ren Y, Hauert S, Lo JH, Bhatia SN. 2012. Identification and characterization of receptor-specific peptides for siRNA delivery. *ACS Nano* 6:8620–31
94. Gabrielson NP, Lu H, Yin L, Kim KH, Cheng J. 2012. A cell-penetrating helical polymer for siRNA delivery to mammalian cells. *Mol. Ther.* 20:1599–609

95. Yin L, Song Z, Kim KH, Zheng N, Gabrielson NP, Cheng J. 2013. Non-viral gene delivery via membrane-penetrating, mannose-targeting supramolecular self-assembled nanocomplexes. *Adv. Mater.* 25:3063–70
96. Sharei A, Zoldan J, Adamo A, Sim WY, Cho N, et al. 2013. A vector-free microfluidic platform for intracellular delivery. *Proc. Natl. Acad. Sci. USA* 110:2082–87
97. Akinc A, Querbes W, De S, Qin J, Frank-Kamenetsky M, et al. 2010. Targeted delivery of RNAi therapeutics with endogenous and exogenous ligand-based mechanisms. *Mol. Ther.* 18:1357–64
98. Gilleron J, Querbes W, Zeigerer A, Borodovsky A, Marsico G, et al. 2013. Image-based analysis of lipid nanoparticle-mediated siRNA delivery, intracellular trafficking and endosomal escape. *Nat. Biotechnol.* 31:638–46
99. Sahay G, Querbes W, Alabi C, Eltoukhy A, Sarkar S, et al. 2013. Efficiency of siRNA delivery by lipid nanoparticles is limited by endocytic recycling. *Nat. Biotechnol.* 31:653–58
100. Fichter KM, Ingle NP, McLendon PM, Reineke TM. 2013. Polymeric nucleic acid vehicles exploit active interorganelle trafficking mechanisms. *ACS Nano* 7:347–64
101. Akinc A, Thomas M, Klibanov AM, Langer R. 2005. Exploring polyethylenimine-mediated DNA transfection and the proton sponge hypothesis. *J. Gene Med.* 7:657–63
102. Boussif O, Lezoualch F, Zanta MA, Mergny MD, Scherman D, et al. 1995. A versatile vector for gene and oligonucleotide transfer into cells in culture and in vivo-polyethylenimine. *Proc. Natl. Acad. Sci. USA* 92:7297–301
103. Kichler A, Leborgne C, Coeytaux E, Danos O. 2001. Polyethylenimine-mediated gene delivery: a mechanistic study. *J. Gene Med.* 3:135–44
104. Benjaminsen RV, Mattebjerg MA, Henriksen JR, Moghimi SM, Andresen TL. 2013. The possible "proton sponge" effect of polyethylenimine (PEI) does not include change in lysosomal pH. *Mol. Ther.* 21:149–57
105. ur Rehman Z, Hoekstra D, Zuhorn IS. 2013. Mechanism of polyplex- and lipoplex-mediated delivery of nucleic acids: real-time visualization of transient membrane destabilization without endosomal lysis. *ACS Nano* 7:3767–77
106. Yu H, Zou Y, Wang Y, Huang X, Huang G, et al. 2011. Overcoming endosomal barrier by amphotericin B-loaded dual pH-responsive PDMA-*b*-PDPA micelleplexes for siRNA delivery. *ACS Nano* 5:9246–55
107. Pouton CW, Lucas P, Thomas BJ, Uduehi AN, Milroy DA, Moss SH. 1998. Polycation-DNA complexes for gene delivery: a comparison of the biopharmaceutical properties of cationic polypeptides and cationic lipids. *J. Control. Release* 53:289–99
108. Wagner E, Plank C, Zatloukal K, Cotten M, Birnstiel ML. 1992. Influenza virus hemagglutinin HA-2 N-terminal fusogenic peptides augment gene transfer by transferrin-polylysine-DNA complexes: toward a synthetic virus-like gene-transfer vehicle. *Proc. Natl. Acad. Sci. USA* 89:7934–38
109. Griffith OW. 1999. Biologic and pharmacologic regulation of mammalian glutathione synthesis. *Free Radic. Biol. Med.* 27:922–35
110. Kozielski KL, Tzeng SY, Green JJ. 2013. A bioreducible linear poly(β-amino ester) for siRNA delivery. *Chem. Commun.* (*Camb.*) 49:5319–21
111. Kim JS, Oh MH, Park JY, Park TG, Nam YS. 2013. Protein-resistant, reductively dissociable polyplexes for in vivo systemic delivery and tumor-targeting of siRNA. *Biomaterials* 34:2370–79
112. Baigude H, Su J, McCarroll J, Rana TM. 2013. In vivo delivery of RNAi by reducible interfering nanoparticles (iNOPs). *ACS Med. Chem. Lett.* 4:720–23
113. Dunn SS, Tian S, Blake S, Wang J, Galloway AL, et al. 2012. Reductively responsive siRNA-conjugated hydrogel nanoparticles for gene silencing. *J. Am. Chem. Soc.* 134:7423–30
114. Park K, Hong SW, Hur W, Lee M-Y, Yang J-A, et al. 2011. Target specific systemic delivery of TGF-β siRNA/(PEI-SS)-g-HA complex for the treatment of liver cirrhosis. *Biomaterials* 32:4951–58
115. Park K, Lee M-Y, Kim KS, Hahn SK. 2010. Target specific tumor treatment by VEGF siRNA complexed with reducible polyethyleneimine-hyaluronic acid conjugate. *Biomaterials* 31:5258–65
116. Kozielski KL, Tzeng SY, Green JJ. 2013. siRNA nanomedicine: the promise of bioreducible materials. *Expert Rev. Med. Devices* 10:7–10
117. Alabi CA, Sahay G, Langer R, Anderson DG. 2013. Development of siRNA-probes for studying intracellular trafficking of siRNA nanoparticles. *Integr. Biol.* (*Camb.*) 5:224–30

118. Alabi CA, Love KT, Sahay G, Stutzman T, Young WT, et al. 2012. FRET-labeled siRNA probes for tracking assembly and disassembly of siRNA nanocomplexes. *ACS Nano* 6:6133–41
119. Shin S, Kwon HM, Yoon KS, Kim DE, Hah SS. 2011. FRET-based probing to gain direct information on siRNA sustainability in live cells: asymmetric degradation of siRNA strands. *Mol. Biosyst.* 7:2110–13
120. Collingwood MA, Rose SD, Huang L, Hillier C, Amarzguioui M, et al. 2008. Chemical modification patterns compatible with high potency dicer-substrate small interfering RNAs. *Oligonucleotides* 18:187–200
121. Bartlett DW, Davis ME. 2007. Effect of siRNA nuclease stability on the in vitro and in vivo kinetics of siRNA-mediated gene silencing. *Biotechnol. Bioeng.* 97:909–21
122. Takahashi M, Nagai C, Hatakeyama H, Minakawa N, Harashima H, Matsuda A. 2012. Intracellular stability of 2′-OMe-4′-thioribonucleoside modified siRNA leads to long-term RNAi effect. *Nucleic Acids Res.* 40:5787–93
123. Li L, Wang H, Ong ZY, Xu K, Ee PLR, et al. 2010. Polymer- and lipid-based nanoparticle therapeutics for the treatment of liver diseases. *Nano Today* 5:296–312
124. Pecot CV, Calin GA, Coleman RL, Lopez-Berestein G, Sood AK. 2011. RNA interference in the clinic: challenges and future directions. *Nat. Rev. Cancer* 11:59–67
125. Wisse E, Jacobs F, Topal B, Frederik P, De Geest B. 2008. The size of endothelial fenestrae in human liver sinusoids: implications for hepatocyte-directed gene transfer. *Gene Ther.* 15:1193–99
126. Rozema DB, Lewis DL, Wakefield DH, Wong SC, Klein JJ, et al. 2007. Dynamic PolyConjugates for targeted in vivo delivery of siRNA to hepatocytes. *Proc. Natl. Acad. Sci. USA* 104:12982–87
127. Siegwart DJ, Whitehead KA, Nuhn L, Sahay G, Cheng H, et al. 2011. Combinatorial synthesis of chemically diverse core-shell nanoparticles for intracellular delivery. *Proc. Natl. Acad. Sci. USA* 108:12996–3001
128. Frank-Kamenetsky M, Grefhorst A, Anderson NN, Racie TS, Bramlage B, et al. 2008. Therapeutic RNAi targeting PCSK9 acutely lowers plasma cholesterol in rodents and LDL cholesterol in nonhuman primates. *Proc. Natl. Acad. Sci. USA* 105:11915–20
129. Ren Y, Cheung HW, Von Maltzhan G, Agrawal A, Cowley GS, et al. 2012. Targeted tumor-penetrating siRNA nanocomplexes for credentialing the ovarian cancer oncogene *ID4*. *Sci. Transl. Med.* 4:147ra112
130. Yao YD, Sun TM, Huang SY, Dou S, Lin L, et al. 2012. Targeted delivery of PLK1-siRNA by ScFv suppresses Her2+ breast cancer growth and metastasis. *Sci. Transl. Med.* 4:130ra48
131. Leuschner F, Dutta P, Gorbatov R, Novobrantseva TI, Donahoe JS, et al. 2011. Therapeutic siRNA silencing in inflammatory monocytes in mice. *Nat. Biotechnol.* 29:1005–10
132. Liu XQ, Xiong MH, Shu XT, Tang RZ, Wang J. 2012. Therapeutic delivery of siRNA silencing HIF-1 alpha with micellar nanoparticles inhibits hypoxic tumor growth. *Mol. Pharm.* 9:2863–74
133. Sun TM, Du JZ, Yao YD, Mao CQ, Dou S, et al. 2011. Simultaneous delivery of siRNA and paclitaxel via a "two-in-one" micelleplex promotes synergistic tumor suppression. *ACS Nano* 5:1483–94
134. Zhang Y, Peng L, Mumper RJ, Huang L. 2013. Combinational delivery of c-myc siRNA and nucleoside analogs in a single, synthetic nanocarrier for targeted cancer therapy. *Biomaterials* 34:8459–68
135. Zhang Y, Schwerbrock NM, Rogers AB, Kim WY, Huang L. 2013. Codelivery of VEGF siRNA and gemcitabine monophosphate in a single nanoparticle formulation for effective treatment of NSCLC. *Mol. Ther.* 21:1559–69
136. Li L, Wang R, Wilcox D, Zhao X, Song J, et al. 2012. Tumor vasculature is a key determinant for the efficiency of nanoparticle-mediated siRNA delivery. *Gene Ther.* 19:775–80
137. Yin L, Song Z, Qu Q, Kim KH, Zheng N, et al. 2013. Supramolecular self-assembled nanoparticles mediate oral delivery of therapeutic TNF-α siRNA against systemic inflammation. *Angew. Chem. Int. Ed. Engl.* 52:5757–61
138. Zheng D, Giljohann DA, Chen DL, Massich MD, Wang XQ, et al. 2012. Topical delivery of siRNA-based spherical nucleic acid nanoparticle conjugates for gene regulation. *Proc. Natl. Acad. Sci. USA* 109:11975–80
139. Burnett JC, Rossi JJ, Tiemann K. 2011. Current progress of siRNA/shRNA therapeutics in clinical trials. *Biotechnol. J.* 6:1130–46
140. Davis ME, Zuckerman JE, Choi CH, Seligson D, Tolcher A, et al. 2010. Evidence of RNAi in humans from systemically administered siRNA via targeted nanoparticles. *Nature* 464:1067–70

141. Tabernero J, Shapiro GI, LoRusso PM, Cervantes A, Schwartz GK, et al. 2013. First-in-humans trial of an RNA interference therapeutic targeting VEGF and KSP in cancer patients with liver involvement. *Cancer Discov.* 3:406–17
142. Coelho T, Adams D, Silva A, Lozeron P, Hawkins PN, et al. 2013. Safety and efficacy of RNAi therapy for transthyretin amyloidosis. *N. Engl. J. Med.* 369:819–29
143. Haussecker D. 2012. The business of RNAi therapeutics in 2012. *Mol. Ther. Nucleic Acids* 1:e8
144. Tenzer S, Docter D, Kuharev J, Musyanovych A, Fetz V, et al. 2013. Rapid formation of plasma protein corona critically affects nanoparticle pathophysiology. *Nat. Nanotechnol.* 8:772–81
145. Geng Y, Dalhaimer P, Cai S, Tsai R, Tewari M, et al. 2007. Shape effects of filaments versus spherical particles in flow and drug delivery. *Nat. Nanotechnol.* 2:249–55
146. Chithrani BD, Ghazani AA, Chan WC. 2006. Determining the size and shape dependence of gold nanoparticle uptake into mammalian cells. *Nano Lett.* 6:662–68
147. Chauhan VP, Popović Z, Chen O, Cui J, Fukumura D, et al. 2011. Fluorescent nanorods and nanospheres for real-time in vivo probing of nanoparticle shape-dependent tumor penetration. *Angew. Chem. Int. Ed. Engl.* 50:11417–20
148. Jiang X, Qu W, Pan D, Ren Y, Williford JM, et al. 2013. Plasmid-templated shape control of condensed DNA-block copolymer nanoparticles. *Adv. Mater.* 25:227–32

Electronic Acknowledgement Receipt

EFS ID:	19082338
Application Number:	62000838
International Application Number:	
Confirmation Number:	6635
Title of Invention:	SHAPE-CONTROLLED siRNA NANOPARTICLES FOR IN VIVO DELIVERY OF RNA THERAPEUTICS
First Named Inventor/Applicant Name:	HAI-QUAN MAO
Customer Number:	101943
Filer:	Jeffrey Childers./Amy Martin
Filer Authorized By:	Jeffrey Childers.
Attorney Docket Number:	111232-00283.P13032-01
Receipt Date:	20-MAY-2014
Filing Date:	
Time Stamp:	16:48:32
Application Type:	Provisional

Payment information:

Submitted with Payment	yes
Payment Type	Electronic Funds Transfer
Payment was successfully received in RAM	$130
RAM confirmation Number	3572
Deposit Account	
Authorized User	

File Listing:

Document Number	Document Description	File Name	File Size(Bytes)/ Message Digest	Multi Part /.zip	Pages (if appl.)

Doc Code: **TR.PROV**
Document Description: Provisional Cover Sheet (SB16)

PTO/SB/16 (11-08)
Approved for use through 05/31/2015. OMB 0651-0032
U.S. Patent and Trademark Office: U.S. DEPARTMENT OF COMMERCE
Under the Paperwork Reduction Act of 1995, no persons are required to respond to a collection of information unless it displays a valid OMB control number

Provisional Application for Patent Cover Sheet

This is a request for filing a PROVISIONAL APPLICATION FOR PATENT under 37 CFR 1.53(c)

Inventor(s)

Inventor 1 — Remove

Given Name	Middle Name	Family Name	City	State	Country
HAI-QUAN		MAO	BALTIMORE	MD	US

Inventor 2 — Remove

Given Name	Middle Name	Family Name	City	State	Country
PHILIP	C.	WONG	LUTHERVILLE	MD	US

Inventor 3 — Remove

Given Name	Middle Name	Family Name	City	State	Country
RISHAB		SHYAM	BALTIMORE	MD	US

Inventor 4 — Remove

Given Name	Middle Name	Family Name	City	State	Country
YONG		REN	PARKVILLE	MD	US

All Inventors Must Be Listed – Additional Inventor Information blocks may be generated within this form by selecting the **Add** button. — Add

Title of Invention	SHAPE-CONTROLLED siRNA NANOPARTICLES FOR IN VIVO DELIVERY OF RNA THERAPEUTICS
Attorney Docket Number (if applicable)	111232-00283.P13032-01

Correspondence Address

Direct all correspondence to (select one):

◉ The address corresponding to Customer Number	○ Firm or Individual Name
Customer Number	101943

The invention was made by an agency of the United States Government or under a contract with an agency of the United States Government.

- ○ No.
- ○ Yes, the invention was made by an agency of the United States Government. The U.S. Government agency name is:
- ◉ Yes, the invention was under a contract with an agency of the United States Government. The name of the U.S. Government agency and Government contract number are:

Doc Code: **TR.PROV**

Document Description: Provisional Cover Sheet (SB16)

NIH-R21EB015152/DTRA-W81XWH-I0-2-0053/R01NS041438

SHAPE-CONTROLLED siRNA NANOPARTICLES FOR *IN VIVO* DELIVERY OF RNA THERAPEUTICS

FEDERALLY SPONSORED RESEARCH OR DEVELOPMENT

This invention was made with government support under R21EB015152 awarded by the National Institutes of Health (NIH), W81XWH-l0-2-0053 awarded by the U.S. Army Defense Threat Reduction Agency (DTRA), and R01NS041438 awarded by the National Institute of Neurological Disorders and Stroke (NINDS). The government has certain rights in the invention.

BACKGROUND

Identifying parameters that mediate efficient delivery of siRNA via nanoparticles to the central nervous system (CNS) can have important therapeutic implications for treating CNS-related diseases, such as Alzheimer's Disease, a progressive degenerative brain disorder characterized pathologically by the accumulation of amyloid-ß (Aß) species and neurofibrillary tangles. ß-site APP cleaving enzyme 1 (BACE1), a key enzyme required for the generation of Aß from the amyloid-ß precursor protein (APP), is a well-validated therapeutic target amenable to the RNA interference therapeutic strategy.

Considerable progress has been made toward developing RNA interference as a therapeutic strategy (Alvarez-Erviti et al., 2011). Efficient delivery and knockdown of suitable targets in an *in vivo* context has been challenging, however. The development of siRNA loaded nanoparticles has demonstrated their capability for packaging and delivery in *in vitro* and *in vivo* models (Lee et al., 2012; Jensen et al., 2013). Various polycationic carriers have the capability to package and deliver siRNA in the form of nanoparticles, although their *in vivo* transfection efficiency has been disappointing.

Studies have shown that the shape of the nanoparticles can play a key role toward improving delivery efficiency (Jiang et al., 2013). The effort to build a viable *in vivo* siRNA delivery method will involve the need to understand the effect of varying shape on payload delivery, while maintaining the integrity of the nanoparticle complex until it reaches its site of delivery. Thus far, controlling the shape of these siRNA nanoparticles, however, has been inaccessible.

SUMMARY

In some aspects, the presently disclosed subject matter provides a method for preparing a shape-controlled siRNA nanoparticle, the method comprising: providing a copolymer solution comprising a block copolymer or a graft copolymer of a water soluble, non-charged polymer and a polycation in a first solvent, wherein the water soluble, non-charged polymer and the polycation each have a structure and a molecular weight; and mixing the copolymer solution with a solution of siRNA at a predetermined siRNA to copolymer ratio and pH in a second solvent to form a shape-controlled siRNA nanoparticle, wherein the siRNA has a predetermined number of base pairs and the first and second solvent can be the same or different; and wherein the shape-controlled siRNA nanoparticle has a shape controlled by one or more of the: structure of the water soluble, non-charged polymer; molecular weight of the water soluble, non-charged polymer; structure of the polycation; molecular weight of the polycation; number of base pairs of the siRNA; ratio of siRNA to copolymer; pH; first solvent comprising the copolymer solution and/or the second solvent comprising the siRNA solution, and, if the copolymer is a graft copolymer, a graft density thereof.

In particular aspects, the water soluble, non-charged polymer comprises polyethylene glycol (PEG) and the polycation is linear polyethylenimine (LPEI).

In other aspects, the presently disclosed subject matter provides a method for treating a disease or condition, the method comprising administering to a subject in need of treatment thereof, a shape-controlled siRNA nanoparticle described hereinabove, or a pharmaceutical composition thereof, in an amount effective for treating the disease or condition.

In particular aspects, the disease is a neurological disease. In yet more particular aspects, the neurological disease is selected from the group consisting of Amyotrophic lateral sclerosis (ALS), frontotemporal dementia (FTD), Parkinson's disease, Alzheimer's disease, Huntington's disease, and dementia with Lewy Bodies.

Certain aspects of the presently disclosed subject matter having been stated hereinabove, which are addressed in whole or in part by the presently disclosed subject matter, other aspects will become evident as the description proceeds when taken in connection with the accompanying Examples and Figures as best described herein below.

THAT WHICH IS CLAIMED:

1. A method for preparing a shape-controlled siRNA nanoparticle, the method comprising:

providing a copolymer solution comprising a block copolymer or a graft copolymer of a water soluble, non-charged polymer and a polycation in a first solvent, wherein the water soluble, non-charged polymer and the polycation each have a structure and a molecular weight; and

mixing the copolymer solution with a solution of siRNA at a predetermined siRNA to copolymer ratio and pH in a second solvent to form a shape-controlled siRNA nanoparticle, wherein the siRNA has a predetermined number of base pairs and the first and second solvent can be the same or different; and

wherein the shape-controlled siRNA nanoparticle has a shape controlled by one or more of the: structure of the water soluble, non-charged polymer; molecular weight of the water soluble, non-charged polymer; structure of the polycation; molecular weight of the polycation; number of base pairs of the siRNA; ratio of siRNA to copolymer; pH; first solvent comprising the copolymer solution and/or the second solvent comprising the siRNA solution, and, if the copolymer is a graft copolymer, a graft density thereof.

2. The method of claim 1, wherein the water soluble, non-charged polymer comprises polyethylene glycol (PEG).

3. The method of claim 2, wherein the PEG has a molecular weight ranging from about 500 Da to about 20 kDa.

4. The method of claim 3, wherein the PEG has a molecular weight of about 10 kDa.

5. The method of claim 2, wherein the copolymer is a graft copolymer and the PEG has a graft density ranging from about 0.1% to about 20%.

6. The method of claim 5, wherein the PEG has a graft density selected from the group consisting of a 2% graft density, a 4% graft density, and an 8% graft

density.

7. The method of claim 6, wherein the 2% graft density results in a worm-shaped siRNA nanoparticle, the 4% graft density of the PEG results in a rod-shaped siRNA nanoparticle, and the 8% graft density of PEG results in a spherically-shaped siRNA nanoparticle.

8. The method of claim 1, wherein the polycation is selected from the group consisting of linear polyethylenimine (LPEI), poly-lysine, poly-arginine, poly-histidine, chitosan, branched PEI, a poly (beta-aminoester), a polyphosphoester, polyphosphoramidate (PPA), and PEG-*b*-polyphosphoramidate (PEG-PPA).

9. The method of claim 8, wherein the polycation is LPEI.

10. The method of claim 9, wherein the LPEI has a molecular weight ranging from about 2 kDa to about 50 kDa.

11. The method of claim 10, wherein the LPEI has a molecular weight of about 17 kDa.

12. The method of claim 1, wherein the siRNA has about 25 base pairs.

13. The method of claim 1, wherein the siRNA decreases the expression of ß-site APP cleaving enzyme 1 (BACE1) and/or amyloid-ß precursor protein (APP).

14. The method of claim 1, wherein the siRNA comprises a siRNA sequence selected from the group consisting of SEQ ID NO: 1, 2, 3, 4, 5, and 6.

15. The method of claim 1, wherein the ratio of siRNA to copolymer is measured as copolymer nitrogen to siRNA phosphate (N/P ratio) and has a range from about 0.1 to about 20.

16. The method of claim 15, wherein the N/P ratio is less than about 10.

17. The method of claim 1, wherein the pH has a range from about 1 to about 7.5.

18. The method of claim 1, wherein the first and/or second solvent is water or in a mixture comprising water and a water-miscible solvent selected from the group consisting of dimethylformamide (DMF), dimethyl sulfoxide (DMSO), dioxane, and tetrahydrofuran (THF).

19. The method of claim 18, wherein the water-miscible solvent is 70% DMF.

20. The method of claim 19, further comprising removing the water-miscible solvent from the siRNA nanoparticle.

21. The method of claim 20, further comprising crosslinking the siRNA nanoparticle.

22. The method of claim 1, wherein the shape of the siRNA nanoparticle is selected from the group consisting of worm-shaped, spherically-shaped, and rod-shaped.

23. A siRNA nanoparticle prepared by the method of claim 1.

24. A method for treating a disease or condition, the method comprising administering to a subject in need of treatment thereof, a shape-controlled siRNA nanoparticle of claim 1, or a pharmaceutical composition thereof, in an amount effective for treating the disease or condition.

25. The method of claim 24, comprising administering the shape-controlled siRNA nanoparticle to the brain and/or spinal cord of the subject.

26. The method of claim 24, wherein the disease or condition comprises a neurodegenerative disease.

27. The method of claim 26, wherein the neurodegenerative disease is selected from the group consisting of Amyotrophic lateral sclerosis (ALS), frontotemporal dementia (FTD), Parkinson's disease, Alzheimer's disease, Huntington's disease, and dementia with Lewy Bodies.

28. The method of claim 26, further comprising the knockdown of one or more genes.

29. The method of claim 26, wherein the siRNA decreases the expression of β-site APP cleaving enzyme 1 (BACE1) and/or amyloid-β precursor protein (APP).

30. The method of claim 29, wherein the siRNA comprises is a siRNA sequence selected from the group consisting of SEQ ID NO: 1, 2, 3, 4, 5, and 6.